

2014

# Lung Alveolar and Tissue Analysis Under Mechanical Ventilation

Trenicka Rolle

*Virginia Commonwealth University*

Follow this and additional works at: <http://scholarscompass.vcu.edu/etd>

 Part of the [Engineering Commons](#)

© The Author

---

Downloaded from

<http://scholarscompass.vcu.edu/etd/3398>

This Thesis is brought to you for free and open access by the Graduate School at VCU Scholars Compass. It has been accepted for inclusion in Theses and Dissertations by an authorized administrator of VCU Scholars Compass. For more information, please contact [libcompass@vcu.edu](mailto:libcompass@vcu.edu).

Trenicka K. Rolle School of Engineering  
Virginia Commonwealth University

This is to certify that the thesis prepared by Trenicka K. Rolle entitled LUNG ALVEOLAR AND TISSUE ANALYSIS UNDER MECHANICAL VENTILATION has been approved by his or her committee as satisfactory completion of the thesis or dissertation requirement for the degree of Master of Science

---

Charles P. Cartin, Ph.D., Committee Chair, School of Engineering

---

Daren Chen, Ph.D., Mechanical Engineering, School of Engineering

---

Rebecca L. Heise, Ph.D., Biomedical Engineering, School of Engineering

---

Angela Reynolds, Ph.D., Mathematics and Applied Mathematics, College of Humanities and Sciences

---

Gary Tepper, Ph.D., Chair, Mechanical and Nuclear Engineering, School of Engineering

---

Barbara Boyan, Ph.D., Dean, School of Engineering

---

Dr. F. Douglas Boudinot, Dean of the School of Graduate Studies

[Click here and type the Month, Day and Year this page was signed.]

© Trenicka K. Rolle, 2014

All Rights Reserved

LUNG ALVEOLAR AND TISSUE ANALYSIS UNDER MECHANICAL  
VENTILATION

Thesis submitted in partial fulfillment of the requirements for the degree of Master of  
Science at Virginia Commonwealth University.

by

TRENICKA K ROLLE  
BACHELOR OF SCIENCE, VIRGINIA COMMONWELATH UNIVERSITY, 2011  
MASTER OF SCIENCE, VIRGINIA COMMONWEALTH UNIVERSITY, 2014

Director: DR. KARLA MOSSI  
DIRECTOR OF GRADUATE STUDIES, MECHANICAL AND NUCLEAR  
ENGINEERING

Advisor: DR. CHARLES P. CARTIN  
ASSISTANT PROFESSOR, MECHANICAL AND NUCLEAR ENGINEERING

Virginia Commonwealth University  
Richmond, Virginia  
May 2014

## Acknowledgement

I can only begin this acknowledgement by first thanking God for giving me the opportunity to be who and where I am today. There are so many people that have been instrumental in helping me to complete this degree that this has been a team effort.

I would like to acknowledge my former advisor Dr. Ramana Pidaparti who first gave me the opportunity to attend graduate school and work on this project. I also would like to acknowledge my committee for being willing and able to aid me in completing another leg of my academic pursuits. I especially would like to thank Dr. Angela Reynolds and Dr. Rebecca Heise for always checking in and meeting with the group to discuss progress and goals, it truly meant a lot to me to have your guidance and structure. I truly thank Dr. Cartin and Dr. Chen for being a part of this process, your advising is surely appreciated. I definitely have to thank the graduate program director, Dr. Karla Mossi for being always ready and willing to help, she has been my saving grace in many situations.

I would not have made it this far without the love and support of my mother and grandmother who have been my number one supporters and motivators from the moment I entered college. Their words of encouragement, prayers and provision has sustained me while here at VCU. In addition my family as a whole has been extremely supportive of my academic pursuits and have never ceased to make me aware of how proud they are of me. I am eternally grateful to have been blessed with such a wonderful family.

I would be remised if I did not mention my church family who have been my family away from the Bahamas. I have never in my life met such wonderful people who are willing to go the distance and offer such spiritual, emotional and financial support. My ReJOYce family has made this degree, this journey and overall my life so much better and words cannot express my gratitude to all of them. My roommates Stephanie and Danielle have been the wind beneath my wings at times and I can't tell them enough how much I appreciate their love and concern for me always. I must acknowledge my significant other Maurice for his love and support throughout these years. He has consistently been my diary and shoulder to lean on when graduate school seemed more than I could handle and I couldn't see the light at the end of the tunnel. I am overjoyed that I've had him in my life.

I cannot forget to mention the friends I've made while in graduate school, Omolulu, Enerel, John, Ariel, Toun, Firdaweke, Naveen, Naren, Keith, Sanjah and Krishna. They have all made being a graduate student exciting and easier to bear. The late nights and sometimes all-nighters in the engineering labs and at the James Cabell library will be memories that I'll take with me and never forget. My time here at VCU has been unforgettable and I wouldn't trade it for the world. I have grown in so many ways and the experiences I've encountered on this journey have been life changing to say the least. Best wishes to everyone, God bless.

## Table of Contents

	Page
Acknowledgements.....	ii
List of Tables .....	vii
List of Figures .....	viii
Chapter	
1 Introduction.....	1
1.1 Background .....	1
1.2 Mechanical Ventilation Overview.....	3
1.3 Review of Literature.....	9
1.4 Thesis Objectives .....	21
2 Lung Alveolar Analysis .....	24
2.1 Methods .....	24
2.1.1 Airflow Equations .....	26
2.1.2 Alveolar Wall Equations .....	27
2.1.3 Computational Simulation.....	28
2.1.4 Finite Element Meshes and Boundary Conditions .....	29
2.1.5 Material Parameters.....	35
2.1.6 Mechanical Ventilation Parameters.....	35
2.1.7 Normal Lung with Structural Changes.....	36
2.1.8 Normal Lung with Mechanical Property Changes .....	38



2.2	Results .....	39
2.2.1	Fluid pressures and velocities.....	39
2.2.2	Structural displacements and stresses.....	46
2.3	Discussion .....	61
3	Alveolar Tissue Analysis .....	61
3.1	Introduction .....	61
3.2	Methods .....	62
3.3	Results .....	66
3.3.1	Total Displacements .....	66
3.3.2	Mechanical Stresses .....	66
3.4	Discussion .....	76
4	Comprehensive Modeling.....	78
4.1	Introduction .....	78
4.2	Methods .....	79
4.3	Results .....	79
4.3.1	Pressures and Velocities .....	80
4.3.2	Structural Displacements and Stresses .....	83
4.4	Discussion .....	91
5	Conclusions and Future Work .....	94
5.1	Lung Alveolar Analysis .....	94

5.2 Alveolar Tissue Analysis .....	95
5.3 Comprehensive Model Analysis .....	96
5.4 Final Remarks.....	97
References.....	99

List of Tables

	Page
Table 2.1: Description of geometric parameters for the idealized alveolar model .....	26
Table 2.2: Mesh sizes for the normal, NLSC and NLMPC alveolar models.....	30
Table 2.3: Material properties for the NLMPC model at age 70 .....	38
Table 3.1: Dimensions for thickness of alveolar septal layers.....	64
Table 3.2: Material property characteristics for each layer of the tissue model .....	64
Table 3.3: Material property characteristics utilized for the tissue analysis.....	64

## List of Figures

	Page
Figure 1.1: Weibel Model of branching for the respiratory airways. ....	2
Figure 1.2: Standard setup of a patient on a ventilator .....	5
Figure 1.3: Forms of ventilator induced lung injury as a result of moderate and high levels of stress/strain. Where volutrauma and barotrauma result in high airway pressures and volumes. Atelectrauma results in the opening and closing of collapsed airways. Finally, all of the aforementioned can then lead to biotrauma. ....	8
Figure 2.1: Geometric representations of the airway generations based on ICRP [69] tracheobronchial geometry and the idealized three-dimensional model of the alveolar geometry used for fluid-solid interaction analysis with each alveolar sac labeled.....	25
Figure 2.2: Fluid-structure interaction algorithm used to solve the model.....	29
Figure 2.3: Chart of mesh independence study for FSI analysis.....	31
Figure 2.4: 3-D mesh for the normal lung solid (top) and fluid (bottom) model.....	32
Figure 2.5: a. Normal breathing input waveform. b. Ventilator input waveform.....	34
Figure 2.6: a) Diseased lung model with both fluid and solid shown. b) 3-Dimensional meshed fluid and solid models.....	37
Figure 2.7: Contours of velocity magnitudes for the a) ventilator waveform at 2.2s, b) normal breathing waveform at 4.725s, c) ventilator waveform at 2.285s, and d) normal breathing waveform at 5.725s.....	41

Figure 2.8: Contours of pressure magnitude for the a) ventilator waveform at 2.2s, b) normal breathing waveform at 4.725s, c) ventilator waveform at 2.285s, d) normal breathing waveform at 5.625s.....	42
Figure 2.9: Pressure vs. Time transient for the ventilator waveform. Figure on right source [88].....	43
Figure 2.10: Pressure vs. Time transient for the normal breathing waveform. Source for figure [89].....	44
Figure 2.11: Contours of velocity magnitude for the a) diseased lung model at 2.2s, b) aged lung model at 2.2s, c) diseased lung model at 2.285s, d) aged lung at 2.285s.....	45
Figure 2.12: Contours of pressure magnitude for the a) diseased lung model at 2.2s, b) aged lung model at 2.2s, c) diseased lung model at 2.285s, d) aged lung at 2.285s.....	46
Figure 2.13: Contours of total mesh displacement magnitude for the a) ventilator waveform at 2.2s, b) normal breathing waveform at 0.65s, c) ventilator waveform at 2.285s and d) normal breathing at 1.65s.....	48
Figure 2.14: Contours of von Mises stress magnitude for the a) ventilator waveform at 2.2s, b) normal breathing waveform at 4.725s, c) ventilator waveform at 2.285s and d) normal breathing waveform at 5.625s.....	49
Figure 2.15: Contours of first principal stress magnitude for the a) ventilator waveform at 2.2s, b) normal breathing waveform at 4.725s, c) ventilator waveform at 2.285s and d) normal breathing waveform at 5.625s.....	50

Figure 2.16: Contours of second principal stress magnitude for the a) ventilator waveform at 2.2s, b) normal breathing waveform at 4.725s, c) ventilator waveform at 2.285s and d) normal breathing waveform at 5.625s .....	51
Figure 2.17: Contours of third principal stress magnitude for the a) ventilator waveform at 2.2s, b) normal breathing waveform at 4.725s, c) ventilator waveform at 2.285s and d) normal breathing waveform at 5.625s .....	52
Figure 2.18: Comparison plots of normal versus ventilator breath for total mesh displacement (top) and significant stresses (bottom).....	53
Figure 2.19: Contours of total mesh displacement magnitude for the a) NLSC model at 2.2s, b) NLMPC model at 2.2s, c) NLSC model at 2.285s and d) NLMPC model at 2.285s.....	55
Figure 2.20: Contours of von Mises stress magnitude for the a) NLSC model at 2.2s, b) NLMPC model at 2.2s, c) NLSC model at 2.285s and d) NLMPC model at 2.285s.....	56
Figure 2.21: Contours of first principal stress for the a) NLSC model at 2.2s, b) NLMPC model at 2.2s, c) NLSC model at 2.285s and d) NLMPC model at 2.285s .....	57
Figure 2.22: Contours of second principal stress for the a) NLSC model at 2.2s, b) NLMPC model at 2.2s, c) NLSC model at 2.285s and d) NLMPC model at 2.285s.....	58
Figure 2.23: Contours of third principal stress for the a) NLSC model at 2.2s, b) NLMPC model at 2.2s, c) NLSC model at 2.285s, d) NLMPC model at 2.285s.....	59

Figure 2.24: Comparison plots of total displacement (top) and von Mises stress (bottom) between NLSC and NLMPC models.....	60
Figure 3.1: 3-Dimensional model of the alveolar tissue geometry in various views.....	63
Figure 3.2: 3-Dimensional tissue model with hexahedral mesh and applied boundary conditions displayed.....	65
Figure 3.3: Contours of total displacement in each tissue layer endothelial cell layer (top), basement membrane (middle) and epithelial cell layer (bottom) at 0.4s (top) and 2s (bottom).....	67
Figure 3.4: Contours of von Mises stress in each tissue layer endothelial cell layer (top), basement membrane (middle) and epithelial cell layer (bottom)at 0.4s (top) and 2s (bottom).....	69
Figure 3.5: Contours of first principal stress in each tissue layer endothelial cell layer (top), basement membrane (middle) and epithelial cell layer (bottom)at 0.4s (top) and 2s (bottom).....	70
Figure 3.6: Contours of second principal stress in each tissue layer endothelial cell layer (top), basement membrane (middle) and epithelial cell layer (bottom)at 0.4s (top) and 2s (bottom).....	71
Figure 3.7: Contours of third principal stress in each tissue layer endothelial cell layer (top), basement membrane (middle) and epithelial cell layer (bottom)at 0.4s (top) and 2s (bottom).....	72

Figure 3.8: Comparison plot of various stresses during inspiration and expiration.....	73
Figure 4.1: Contours of velocity magnitude for the a) comprehensive lung model at 2.2s, b) normal lung model at 2.2s, c) comprehensive lung model at 2.285s, and d) normal lung model at 2.285s with ventilator waveform.....	81
Figure 4.2: Contours of pressure magnitude for the a) comprehensive lung model at 2.2s, b) normal lung model at 2.2s, c) comprehensive lung model at 2.285s, and d) normal lung model at 2.285s with ventilator waveform.....	82
Figure 4.3: Contours of total mesh displacement magnitude for the a) comprehensive lung model at 2.2s, b) normal lung model at 2.2s, c) comprehensive lung model at 2.285s, and d) normal lung model at 2.285s with ventilator waveform.....	85
Figure 4.4: Contours of von Mises stress magnitude for the a) comprehensive lung model at 2.2s, b) normal lung model at 2.2s, c) comprehensive lung model at 2.285s, and d) normal lung model at 2.285s with ventilator waveform.....	86
Figure 4.5: Contours of first principal stress magnitude for the a) comprehensive lung model at 2.2s, b) normal lung model at 2.2s, c) comprehensive lung model at 2.285s, and d) normal lung model at 2.285s with ventilator waveform.....	87
Figure 4.6: Contours of second principal stress magnitude for the a) comprehensive lung model at 2.2s, b) normal lung model at 2.2s, c) comprehensive lung model at 2.285s, and d) normal lung model at 2.285s with ventilator waveform.....	88



Figure 4.7: Contours of third principal stress magnitude for the a) comprehensive lung model at 2.2s, b) normal lung model at 2.2s, c) comprehensive lung model at 2.285s, and d) normal lung model at 2.285s with ventilator waveform.....	89
Figure 4.8: Comparison plots of the von Mises stress (top) and first principal stress (bottom) for the NLSC, NLMPC and comprehensive lung models. ....	90
Figure 4.9: Comparison plot of intraalveolar pressure during inspiration for the comprehensive, NLMPC and NLSC models.....	92

# Abstract

## LUNG ALVEOLAR AND TISSUE ANALYSIS UNDER MECHANICAL VENTILATION

By Trenicka Rolle, M.S.

A Thesis submitted in partial fulfillment of the requirements for the degree of Master of Science at Virginia Commonwealth University.

Virginia Commonwealth University, 2014

Advisor: Dr. Charles P. Cartin  
Assistant Professor, Department of Mechanical and Nuclear Engineering

Mechanical ventilation has been a major therapy used by physicians in support of surgery as well as for treating patients with reduced lung function. Despite its many positive outcomes and ability to maintain life, in many cases, it has also led to increased injury of the lungs, further exacerbating the diseased state. Numerous studies have investigated the effects of long term ventilation with respect to lungs, however, the connection between the global deformation of the whole organ and the strains reaching the alveolar walls remains unclear. The walls of lung alveoli also called the alveolar septum are characterized as a multilayer

heterogeneous biological tissue. In cases where damage to this parenchymal structure insists, alveolar overdistension occurs. Therefore, damage is most profound at the alveolar level and the deformation as a result of such mechanical forces must be investigated thoroughly. This study investigates a three-dimensional lung alveolar model from generations 22 (alveolar ducts) through 24 (alveoli sacs) in order to estimate the strain/stress levels under mechanical ventilation conditions. Additionally, a multilayer alveolar tissue model was generated to investigate localized damage at the alveolar wall. Using ANSYS, a commercial finite element software package, a fluid-structure interaction analysis (FSI) was performed on both models. Various cases were simulated that included a normal healthy lung, normal lung with structural changes to model disease and normal lung with mechanical property changes to model aging. In the alveolar tissue analysis, strains obtained from the aged lung alveolar analysis were applied as a boundary condition and used to obtain the mechanical forces exerted as a result.

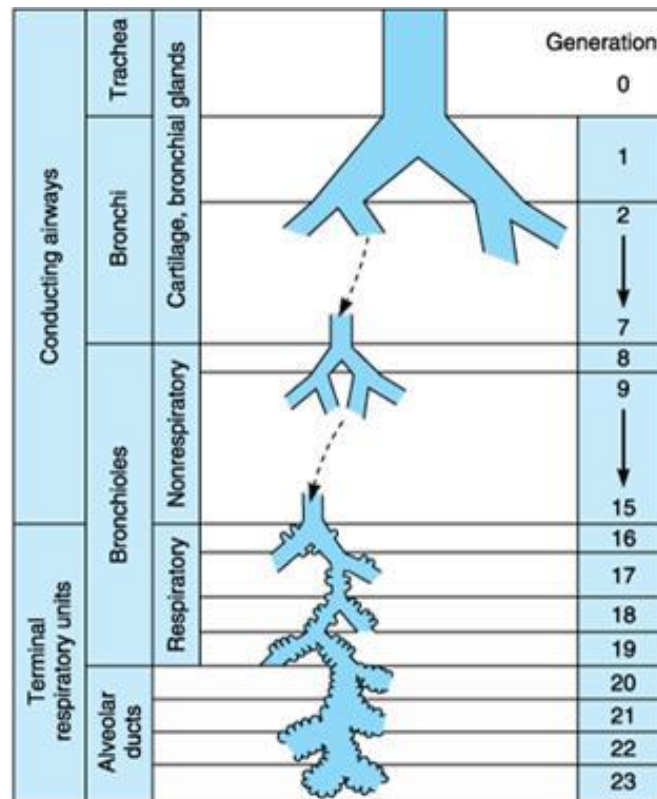
This work seeks to give both a qualitative and quantitative description of the stress/strain fields exerted at the alveolar region of the lungs. Regions of stress/strain concentration will be identified in order to gain perspective on where excess damage may occur. Such damage can lead to overdistension and possible collapse of a single alveolus. Furthermore, such regions of intensified stress/strain are translated to the cellular level and offset a signaling cascade. Hence, this work will provide distributions of mechanical forces across alveolar and tissue models as well as significant quantifications of damaging stresses and strains.

# CHAPTER 1

## Introduction

### 1.1 Background

The human respiratory system is one of the most unique and intricate systems in the human body. Its sophisticated framework houses one of the most complex and vital organs to the function of the entire body, i.e. the lungs. Being suited with the task of gas exchange across the respiratory surface, each aspect of the lungs plays an integral role in ensuring that this process is carried out effectively and efficiently. The primary function of the respiratory system entails the intake of oxygen into the body and the expulsion of carbon dioxide from the body. The lungs, on a smaller scale, possess a tree-like structure and have been classified as a network of branched airways that help to facilitate gas exchange. This network consists of the trachea, bronchi, terminal and respiratory bronchioles, alveolar ducts, and ending with alveoli. This system of branching has been categorized in terms of generations beginning with the trachea at generation 0 (G0) ending at generation 23 (G23) representing the entrance to the alveolar sacs [1]. The alveoli themselves are termed as generation 24 (G24). This model of numbered airways was developed by Weibel who gave an approximation for branching airways under the assumption that there exists a dichotomy in each generation as  $2^N$  [1]. Figure 1.1 depicts the Weibel model for lung classification.



Source: McPhee SJ, Ganong WF: *Pathophysiology of Disease: An Introduction to Clinical Medicine*, 5th Edition: <http://www.accessmedicine.com>

Copyright © The McGraw-Hill Companies, Inc. All rights reserved.

Figure 1.1 Weibel Model of branching for the respiratory airways [66].

Functions of the lung are divided into two main processes, inhalation and exhalation. The combination of these two processes is known as a breath cycle. The total capacity of the lungs is 5.8 liters with a functional reserve capacity of 2.4 liters [2]. The lungs process an air volume of about 0.5 liters per breathing cycle that lasts for 5s under sedentary conditions [3]. Gas exchange across the respiratory surface is made effortlessly as a result of the large surface area of the lungs. Surface area of the lungs extends from less than 10 cm<sup>2</sup> in G0 – G5 to approximately 140 m<sup>2</sup> for alveoli, G24 [3].

Within the respiratory system there exists several essential units that without these the lung would be incapable of performing its function. These functional units are described as lung parenchyma comprising of the respiratory bronchioles, alveolar ducts and alveoli. More specifically, the alveolus is the key unit whose structure is both suited and responsible for gas exchange. Alveolar walls are comprised of a thin permeable wall lined with a thin film of liquid. This thin liquid film along with surfactant, a substance secreted by alveolar type II cells, helps to stabilize the lungs at large volumes keeping alveoli from collapsing. This is also known as parenchymal tethering. Alveoli are grouped together in clusters that form an alveolar sac, which allows for the sharing of structural walls, called the alveolar septum, between adjacent alveolus. As a result, uniform expansion of alveoli during inhalation ensues whilst collapse of individual alveoli are resisted. There are approximately 300 million alveoli comprising the lungs [4]. Specifically dimensions include an average diameter ranging from 100 – 200  $\mu\text{m}$  with most studies utilizing an average spherical diameter of 150  $\mu\text{m}$  [4,5,6,7] and an entrance length of 100  $\mu\text{m}$  [7] which are all consistent with previous lung alveolar studies.

## **1.2 Mechanical Ventilation Overview**

The exchange of carbon dioxide and oxygen via the respiratory system is extremely vital to the maintenance and function of every part of the body. Therefore, without sufficient or limited respiration an individual's life would be at serious risk. For decades on end there have been myriad of diseases and disorders that have threatened lung health. Even more so, the repercussions of such diseases have grave impacts on lung function, particularly in cases

where lung parenchyma become damaged. Damage of any kind to lung parenchyma, sites of gas exchange, drastically reduce lung function. Diseases such as Chronic Obstructive Pulmonary Disease (COPD), pulmonary fibrosis and cystic fibrosis have been the leading cause of deaths among patients with lung disease. Disorders such as Asthma and adult respiratory distress syndrome (ARDS) have also lead to many deaths in patients across the United States. According to a study done by Vital Statistics of the United States, National Center for Health Statistics (NCHS) in 2010 lung disease accounted for 21.6% of the deaths from cardiovascular, lung, and blood disease [8].

Moreover, COPD accounted for 135,000 of lung deaths in 2010 and diseases of the airways accounted for 58.9% of deaths from lung disease [8]. COPD is a disease of the airway and consists of chronic bronchitis and emphysema. Chronic bronchitis involves a long term cough with mucus and emphysema involves the destruction of the lungs over time. There are currently no known cures for such diseases mainly because once the damage has occurred there is no way to reverse it and restore the lungs back to its once healthy state. Nevertheless, treatments are available in order to help patients manage their disease symptoms such as bronchodilators, cardiopulmonary rehabilitation, inhaled steroids, oxygen therapy, and surgery.

In circumstances where the disease process is extremely heightened, a patient may be at risk of respiratory failure. Under these circumstances, mechanical or artificial ventilation has been used as a major life-saving therapeutic instrument in modern intensive care medicine. Figure 1.2 shows the setup for patients on ventilators. In cases where other serious injuries have occurred, while treatment is being administered that may disrupt the

patient's normal breathing, physicians will utilize mechanical ventilation as a tool to maintain patient breathing. The rate of mechanical ventilation is 2.8 per 1000, accounting for approximately 700,000 episodes annually [9].

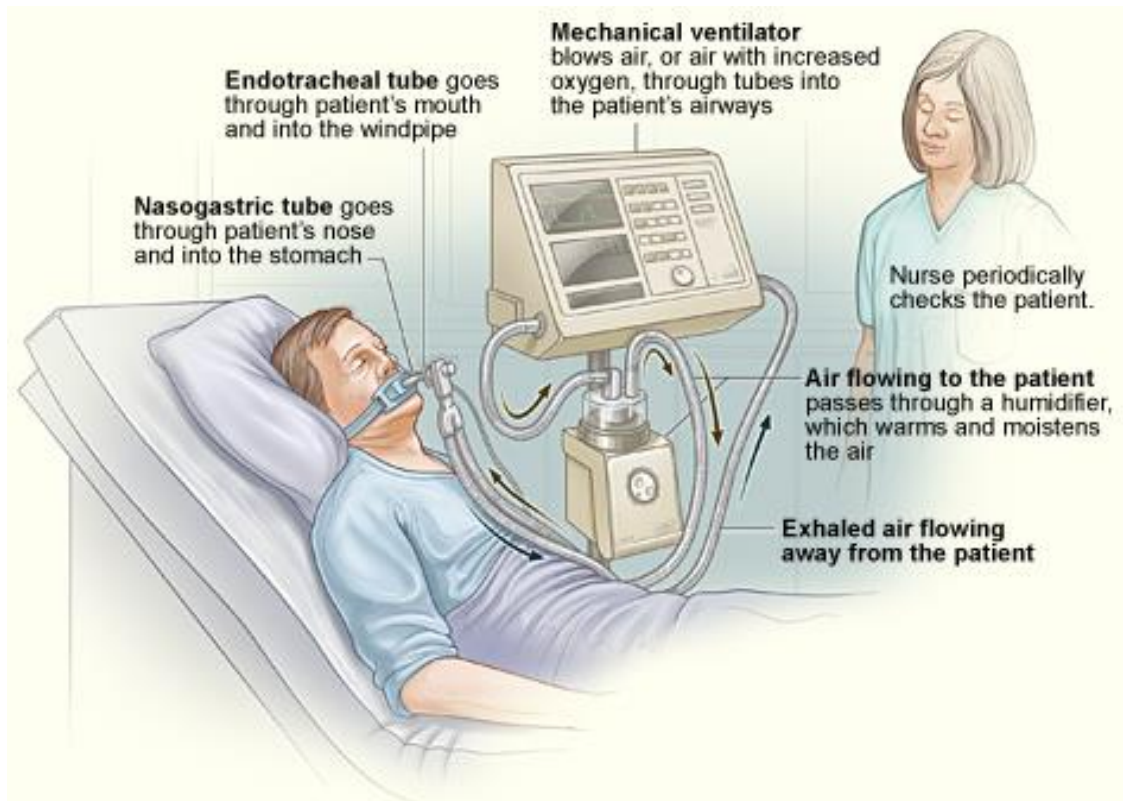


Figure 1.2 Standard setup of a patient on a ventilator [68]

Mechanical ventilation's objectives are to deliver oxygen to the body while removing carbon dioxide from the bloodstream and therefore reducing the work of breathing on the lungs, allowing lung tissue and airways to heal. However, it has also been proven to initiate and even exacerbate significant lung injury and inflammation, particularly in patients with acute respiratory distress syndrome (ARDS) and acute lung injury (ALI) [10]. Mechanisms



of such injury include lung overdistension and repetitive opening and closing of collapsed lung parenchyma, increasing stiffness of lung and therefore making the lung inelastic, a need for higher pressures to reopen the lungs and increased surface tension at the gas-liquid interface [10].

Of equal importance are those conditions associated with mechanical ventilation termed ventilator induced lung injury (VILI) and ventilator associated lung injury (VALI). VILI is a direct effect of mechanical ventilation causing acute lung injury. VALI resembles ARDS and occurs in patients receiving mechanical ventilation. Nevertheless, major differences between VALI and VILI include the fact that VALI may be associated with preexisting lung disease such as ARDS and unlike VILI, cannot be proven that it is caused by mechanical ventilation but is only associated with it [11].

Several methods of MV exist which include synchronized intermittent mandatory ventilation (SIMV) airway pressure release ventilation, volume or pressure controlled inverse ratio ventilation, proportional assisted ventilation, and high frequency ventilation. More of a focus has been placed on pressure controlled ventilation methods such as continuous positive airway pressure (CPAP) and positive end expiration pressure (PEEP), allowing these methods to be the mainstays of ventilation. High frequency ventilation (HFV) was brought about as an alternative solution during the 1970's and 1980's as a means to complications and failures in conventional ventilation. It was proven to cause less circulatory interference, reduce airleaks in bronchopleural fistulae, and create similar or improved gas exchange at lower airway pressures [12]. As promising as HFV was considered to be it still

offered no clear advantages with respect to morbidity and mortality rates of patients [11, 12, 13].

Ventilators transfer a high level of mechanical energy to the airways in order to overcome impedance by the lung. This has been the resulting cause of VILI which has been attributed to barotrauma, volutrauma, atelectrauma and lastly biotrauma [14,15]. The aforementioned conditions create serious implications on lung health and can lead to what is known as multi-system organ failure (MSOF). As a result, a means of improved lung protective therapies is essential. Figure 1.3 illustrates the cascade effect of lung injury due to mechanical ventilation.

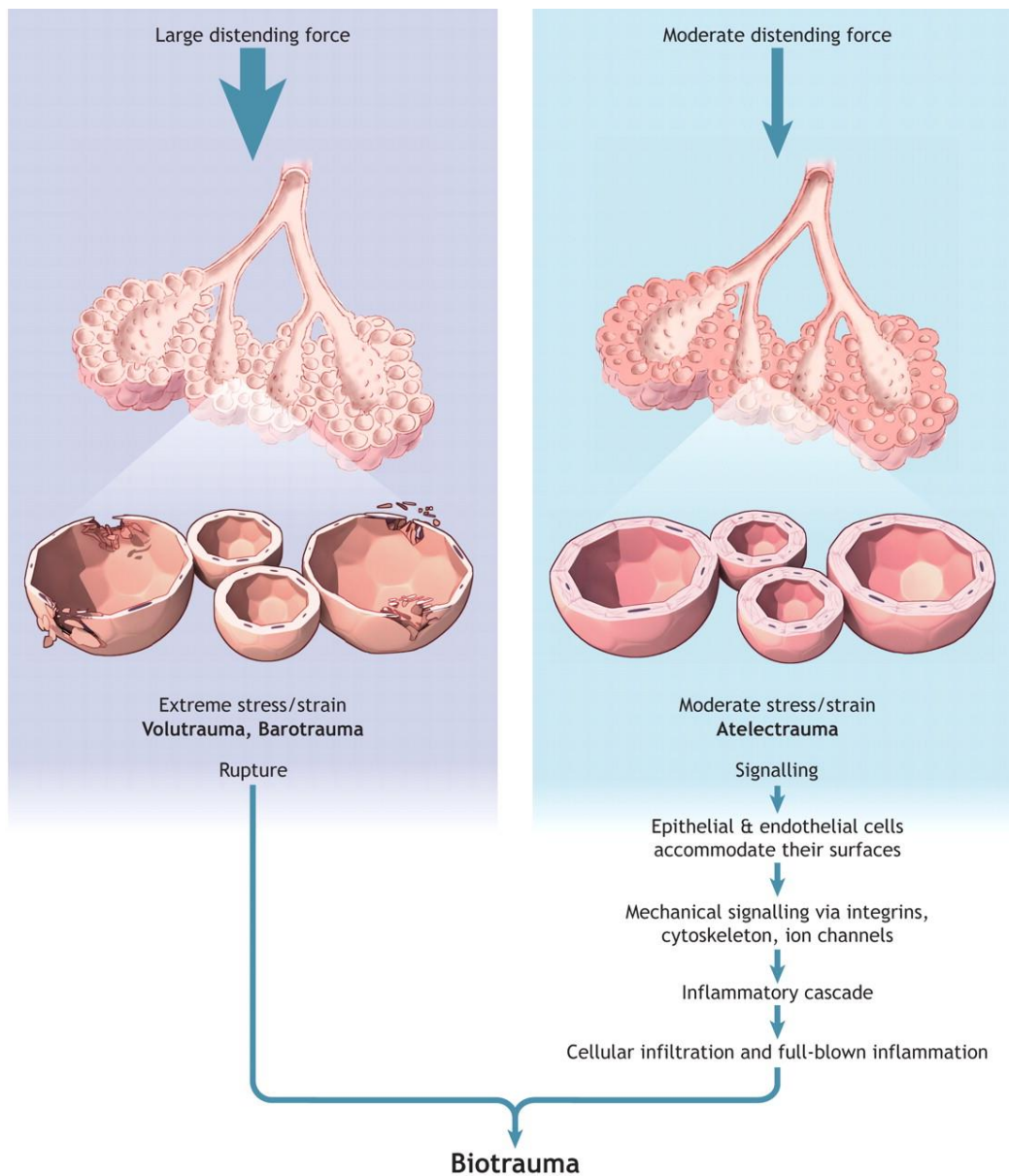


Figure 1.3. Forms of ventilator induced lung injury as a result of moderate and high levels of stress/strain. Where volutrauma and barotrauma result in high airway pressures and volumes. Atelectrauma results in the opening and closing of collapsed airways. Finally, all of the aforementioned can then lead to biotrauma. [67]

### 1.3 Review of Literature

Understanding the role that mechanical ventilation plays in exacerbating lung injury is vital to the development of future protocols and tools to aid in patient breathing. Very few studies have incorporated mechanical ventilation conditions to their studies, but there remains fundamental studies that have given insight into the dynamic behavior of lung alveoli significant to this study. The following provides a review on experimental as well as numerical studies that have resulted in an in depth knowledge on the subject of lung alveoli and their behavior under varying conditions.

Studies investigating the lungs as a whole began with a myriad of work done by Weibel [1] who developed a mathematical model that would classify the geometry of branching airways in a sequence that began with the trachea and terminated at the alveolar sac. Weibel's work gave significant understanding to the morphometry of the lungs and more specifically, lung alveoli, alveolar-capillary frameworks, lung parenchyma and other respiratory models that have become standard for any current and future studies involving the lung [16,17,18,19]. Thereafter, Horsfield *et al.* performed extensive studies using human lung casts that lead to mathematical models defining branching angles and diameters as well as further details on the morphology of the human lung [20,21,22,23].

Ventilation is defined as the flow of air into and out of the lungs. Studies on ventilation of the lungs dates back to the 1960's beginning with extensive work done by Dr. Robert E. Hyatt. Hyatt and Fry [24] who studied pulmonary ventilation in order to ascertain information about the pressure, volume, and gas flow relationships in the lung using experimental data obtained from a human being. Hyatt and Wilcox [25] studied the pressure-

flow relationship in the respiratory tree and more specifically how pressure drops throughout intrathoracic and extrathoracic airways. Using various test subjects Hyatt and Wilcox measured the velocity in the trachea at the centerline and a point approximately 1 mm from the tracheal wall. Isovolume PV curves of the lower airways as well as flow resistance were also obtained and reported. The pressure drops were measured by estimating the convective and frictional contributions seeing that each has an independent significance, where the convective portion is due to convective acceleration. Formulas that measured the instantaneous pressure drop from the trachea to the alveolus were developed and (Equations 1.1a, 1.1b).

$$\Delta P_{C.A.} = \frac{K\rho\bar{v}^2}{2g} \quad (1.1a)$$

$$\Delta P_{A-T} = \Delta P_{(friction)} + \Delta P_{C.A.} \quad (1.1b)$$

Where,  $\rho$  is the gas density,  $v$  is the average gas velocity across the trachea,  $K$  is a constant relative to the spatial integration of the gas velocity over the cross sectional area of the trachea and finally  $g$  represents gravitational acceleration. Flow resistance was evaluated by comparing subjects who are normal with those who have emphysema. Schroter and Sudlow [26] studied flow profiles in the human bronchial tree utilizing 2 generations of bifurcated symmetrical models. These models were rigid and had smooth dry uncorrugated walls. Results yielded flow visualization at a single junction for which the Reynolds number did not exceed 4500. Velocity profile measurements were also obtained using point velocity measurements with a hot wire probe. This was placed downstream in the flow and measurements were taken parallel and normal to the plane of the junction. Their work

deduced that the further away from the trachea both the bronchial diameter and velocity fall. Furthermore, that the bulk flow in the airways is of Stokes type and gaseous diffusion velocities are comparable to those with bulk velocity. Lastly, there exist complex flow patterns during inspiration and expiration with the mechanical mixing of air being present in the system.

Jaeger and Matthys [27] also studied flow patterns within the airways while focusing towards the upper airways. Measurements of intratracheal pressure and flow were performed on six male subjects. Results were plotted diagrams of pressure vs. flow, resistance vs. flow, and pressure vs flow with a logarithmic scale. Stemming from the study were conclusions that flow in the upper airways can be assimilated to that which exists in a Venturi-meter and that the Reynolds' number within the larynx ranges from 10 – 10000. Pedley et al [28,29,30] performed extensive work on predictions of pressure drop and resistance as well as energy losses within the airway by developing a mathematical model that would determine the overall pressure drop in a branched system. Additionally, Pedley et al [31] developed a non-linear theory for the distribution of ventilation in a compartmentalized model of the lung. By injecting a bolus of  $^{133}\text{Xe}$  gas into the model at inspire for a given lung volume. As inspiration continues to total lung capacity (TLC) the regional concentration of  $^{133}\text{Xe}$  were measured. Results from the non-linear model show that the distribution of the said gas to the lower lobes is favored provided that inspiration is slow. However, as inspiratory flow rate increases more of the bolus is distributed to the upper lobes which is indicative of flow reversal. The reversal is directly related to the volume dependence of resistance with the upper airways having a lower resistance resulting from greater expansion.

Olson et al. [32] developed a theoretical analysis in order to predict the fluid flow regime and pressure drop of air inspired into the lung using a model of the average airway in the human lung. Olson et al. theorized that the pressure drop and velocity profile were attributed to anatomical features that included length of bronchus and bronchiole, angle of branching, cross sectional area, upper airways, and elasticity of the tube walls. The lengths of the bronchus and bronchiole account for at least 75% of the total pressure drop and elasticity to have an unknown small effect on pressure drop. The total cross sectional area for flow and resultant average fluid velocity is higher at generation  $n$  compared to that at generation  $n+1$ . Inefficiencies in this study stem from the inaccuracy of the geometry and assumptions that the geometry remains constant throughout inspiration. Olson et al. [33] performed additional studies on elastic cast replicas of the human airway system. The goal was to investigate the fluid dynamic parameters pertinent to aerosol transport and deposition. Five ranges of flow rates were used 0-200 ml/sec, 200-400 ml/sec, 400-600 ml/sec, 600-1000 ml/sec and 1000-2000 ml/sec. Using hot wire anemometers air velocities were measured in the central airways. Profiles of the velocity were then taken at frequent intervals. The static pressure was measured at frequent intervals using wall pressure taps positioned flush with the tube wall. Measurements of velocity indicated that a superimposed fluctuating velocity component was present in the central airways at all flow rates above 200 ml/sec, which indicated turbulence existed in these airways where unstable flows were present at the larynx for a Reynolds numbers below 2000. Surprisingly, such random fluctuations or turbulence still exist in sublobar bronchi that may exhibit a Reynolds number below 100.

More recently, outside the realm of experimental work that has been performed to gain understanding on ventilation inside of the lungs, computational fluid dynamics (CFD) has been a useful tool in the investigation of flow through the respiratory system. Based on computational fluid dynamics, a fluid is defined as a substance that with no fixed shape and has the ability to continuously deform under an applied load. Both liquids and gases are considered to be fluids. Pedley et al. [34] compiled a survey of the gas flow and mixing in pulmonary airways particularly at high frequencies. Results yielded experimental, computational and mathematical studies on the topic. Of interest are the computational studies comprised within this survey which include three-dimensional numerical simulation of inspiratory and expiratory flows in small airways and computational, and experimental models of high frequency oscillations. Results demonstrated that the advancement of gas transport through the airways at high frequency is likely due to coupling of secondary motions caused by airway curvature with the oscillatory longitudinal flow. Limitations to this study lie within the accurate simulation of the phenomena only in idealized geometries as opposed to real lung geometries. Balashazy et al. [35] studied the effects of different CFD models as well as airway bifurcation geometries on resulting air flow fields and particle deposition patterns. The first model was computed by solving the Navier-Stokes and continuity equation in a three-dimensional computational mesh via a finite difference method. The second model is performed by using the FIRE® commercial fluid dynamics program package. Additionally, two bifurcation models were used, which included a narrow bifurcation model and a physiologically realistic bifurcation (PRB) model. The flow results yielded from the models showed that flow in each case were generally similar with flows in



the daughter branches being more symmetric in the second model. In terms of geometry differences, the PRB geometry reduced the magnitude secondary motions in the daughter airways. Wilquem and Degrez [36] investigated a two-dimensional steady inspiratory flow through a three-generation model of the central airways. Simulations for Reynolds number ranging from 200-1200 were performed. Their work demonstrated an existence of separation regions where the number and location of these separation regions were strongly dependent on Reynolds number. Additionally results showed skewed velocity profiles and unbalanced flow distributions between the medial and lateral branches. Other studies utilizing computational fluid dynamics to simulate flow in three-dimensional airway models include those done by Liu et al. [37, 38], Ertbruggen et al. [39] and Harrington et al. [40].

The field of computational fluid dynamics has been extensive in the investigation of airflow throughout the pulmonary system. Nevertheless, these studies do not take into consideration the solid mechanics of a dynamic dilating lung. There remains a plethora of research that sheds light on the mechanical behavior of the lung from a solid mechanics aspect. Such research has incorporated structural models of the lung with defined elastic properties and in many cases hyperelastic properties coupled with finite element analysis. Notwithstanding that a great deal of development took place in order to determine the mechanical properties of the lung early studies by Y.C. Fung gave an in depth mathematical analysis of stress and strain in the lungs [41]. Mentions of previous works and first investigations into this topic of interest are outlined in this study Fung et al. investigated the macroscopic stress distribution in the lungs, with an emphasis on stresses and strains in areas of the lung greater than individual alveoli. He further developed the stress-strain relationship,

a strain-energy function for tissue elasticity as well as a pseudostrain function that incorporated the effects of surface tension stress. The understanding of the mechanical behavior of the lung is greatly attributed to works that involve finite element analysis (FEA) of the lung. The first FEA study performed by Matthews and West [42] gave insight into the mechanical behavior of the lung due to its own weight. In the model they assume an incrementally isotropic lung material with a constant Poisson's ratio of 0.3 if  $\epsilon > 0$  or 0.48 if  $\epsilon < 0$  and an elastic modulus equal to  $0.8 E_0 / (0.8 - \epsilon)$  where,  $E_0$  is a constant and  $\epsilon$  is the mean strain in the element. Dale, Matthews and Schroter [43] developed a mathematical model for the pressure-volume curve of a microscopic element of the lung. Elastic material properties were defined using those of the constituent materials. The analysis focused mainly on a single alveolus and neglects the effects of surface tension. Results demonstrated the pressure-volume characteristics of an alveolar model in the absence of closure. Kowe et al. [44] extended the work of Dale et al. in their study of the elastic and surface tension effects in lung alveolus using FE methods. In this analysis the FINEL finite element package is used and deformations were used to determine the stresses and strains. Plots of the pressure volume curves were presented based on the stress-strain relationship used in the model. Karakaplan et al. [45] presented a mathematical model of lung parenchyma in the form of a strain energy function and includes the effect of surfactant. Using a geometric model that represents the actual morphology, nonlinear elastic properties, inclusion of surface tension and the finite element analysis technique their model is able to analyze and simulate the behavior of lung parenchyma to a greater extent. The predictions of the model were then compared with experimental data and proved to show good agreement. Harding and

Robinson [46] constructed an alveolar sac geometry representing the terminal air unit from generations 19 and below. Using GAMBIT 2.3.16 (a software package of ANSYS) the model was meshed in order to form a finite element model. The model employed the use of moving walls via a user defined function and simulation was set up and executed using FLUENT. Results yielded no recirculation and flow rate ratios (0.18 – 0.36) were within a reasonable range of what had been reported in previous studies (0.057 – 1). Li and Kleinstreuer [47] investigated the air flow pattern in lung alveoli by applying the lattice-Boltzman method to three different shaped alveoli. A moving wall boundary condition was applied to the alveoli as well as a pressure inlet condition. The results of the analysis depicts that the airflow velocity and vertical flows are dependent on geometric structure. On the other hand, the pressure distributions obtained are not as dependent on geometry and so are less influenced. Specifically, they found that flow patterns in the main conducting duct for each model were similar in each case, however the alveolus shape did determine the airflow patterns in terms of vortex characteristics in alveolar cavities. Pressure drop for the three cases of varying geometry were virtually the same and flow within the alveolus is much weaker than in the main duct. By applying a moving wall it was discovered that with wall expansion, airflow moves towards the walls. This results in the streamlines being shifted toward the wall where they terminate as opposed to appearing along the wall surface.

Schroter et al. [48] modeled the mechanical behavior in mammalian lung alveolar ducts utilizing the finite element method. The geometry of the model entailed an assembly of truncated octahedral alveoli that surround an air duct. Effects of surface tension were included within this model, particularly at the gas-liquid interface. Results from the study

included pressure-volume curves that were compared with previous work and experimental data that illustrated plausible comparisons. Gefen and Elad et al. [49] developed a 2-D model of an alveolar sac structure in normal and simulated emphysematic lungs. Using a commercial finite-element software package it was determined that the quasi-steady stress distributions and displacements for the alveolar sac at various lung volumes. Results of this study showed that the deformation at the alveolar wall is not uniform. Moreover, significant stress concentrations are developed near curved regions in normal lungs. Such regions of high stress concentration become most vulnerable in cases of emphysema. Dailey and Ghadiali [7] performed a fluid structure analysis on 2-D hexagonal honeycomb alveolar sac models. They investigated the behavior of a dilute suspension of micron-sized particles with no interactions between particles being accounted for within the study. A simulation was performed to incorporate negative pressure breathing conditions. The applied tissue forces would then deform lung parenchyma creating flow within alveoli. This alveolar flow was then used to calculate the trajectories of particles. Results showed that slightly higher flow rates were found within the central sac except for particles injected within  $1 \mu\text{m}$  of the moving walls where particles would remain entrained in the fluid and not impact walls. Brownian diffusion dominates the transport of smaller particles  $d_p < 0.5 \mu\text{m}$ . On the other hand, gravitational sedimentation dominates the transport of large particles,  $d_p > 1\mu\text{m}$ . For particles between the sizes of  $0.5 \mu\text{m} < d_p < 1\mu\text{m}$ , results yielded slower diffusion and sedimentation which maximizes the impact rate. Chaudhry et al. [50] analyzed the relationship between pressure, stress, and stretch ratio in the alveoli near the points where it could potentially burst. Using the length tension properties of the human alveolar wall, they

developed a strain energy function that was used to determine the relationship of the defined parameters. Results include graphs of transmural pressure versus stretch ratio and circumferential stress versus stretch ratio. Jessica de Ryk et al. [51] developed a model to study the stress distribution in normal and emphysematous lungs. Using finite-element analysis they evaluated the model at varying lung inflation levels by applying quasi-static loading of alveolar pressure. Results of this study showed that stress distributions in normal lungs appear to remain unchanged between 40% - 100% total lung capacity (TLC), even though the values of stress increased. In the case of the emphysematous alveolar model, pronounced differences in stress distribution are incurred as a result of elevated internal alveolar pressure. At 40% TLC the stress pattern is more evident as compared to 100% TLC.

Using a strain energy function model and uni-axial tension tests on living precision-cut rat lung slices, Rausch et al. [52] determined an essential elastic material law by discovering the material parameters describing lung parenchyma. By performing experiments on lung strips the elastic material law was deduced due to the application of preconditioning. This allowed for the development of a computational model for the lung slices using an in house multiscale and multiphysics research software platform. Development of this model allowed for an inverse analysis using different strain energy function models and coupling and decoupling those models resulting in an optimal fit to produce a nonlinear material description. This study focused to ascertain those material parameters for the elastic model which would be used for further continuum mechanics based predictive simulations.

Roan and Waters [53] performed an in depth review on the mechanical strain in lung alveoli by compiling data from various clinical and animal studies. The mechanics of the alveolus in terms of its basic structure, biology, and chemistry are discussed as well as comparisons of alveolar deformation from previous studies. To determine the mechanical determinant of the alveolus, Roan and Waters discussed that two length scales must be considered. These scales include the organ and alveolus level where loads at these length scales are considered important factors. An in depth discussion on the biology of the alveolus outlined information regarding the size and structural makeup of the walls including endothelial cells, epithelial cells, the basement membrane and interstitial space. The mechanical determinants of the strain field in particular comprise the composition of the alveolar basement membrane and the interfacial forces at the air-liquid interface. Details regarding the expansion of the alveolus with regard to the strain field and a review of several studies that focus on magnitude and distribution of strain within the alveolus are summarized. Finally, a finite element model of a spherical structure with an encapsulation was analyzed using the finite element software ABAQUS. The internal sphere represents the lung and the outer structures represents the collective response of the rib cage and tissue level boundary conditions. Contour plots of the strains in the y-direction were given with a maximum strain of 0.06. Furthermore, although the majority of the strain levels are positive indicating tension, the strain levels near the coverslip of the model were negative, which indicated compressive strains in the alveoli beneath the coverslip.

Another study by Rausch et al. [54] analyzed the local strain in real three dimensional alveolar geometries extracted from Synchrotron-based X-ray tomographic microscopy.

They ran a FE analysis on these the alveolar geometries by preparing isolated rat lungs. Each lung specimen was scanned and simultaneously modeled into a three-dimensional volume representation and discretizing the three-dimensional volume with a volume mesh with appropriate boundary conditions. The model was finally solved using an in-house research software platform BACI. Findings from the study showed that local strains are much higher than the global extension of the tissue cubes, where local strains were up to four times as high as global strains. Furthermore, strain hotspots were found near areas where thin structures existed. These thin regions became overstretched increasing the likelihood of excess damage.

Finally, to fully comprehend the dynamic behavior of the lung, one would need to incorporate the transient behavior in solid mechanics as well as fluid dynamics. As a result, fluid-structure interaction (FSI) capabilities provided an element that allows for coupling between the fluid and solid behavior models utilized in lung modeling. FSI simulations incorporate load transfer between the fluid and solid applications being utilized. Key components to these type of analyses are proper contact between the solid and fluid surface (i.e. fluid-solid interface on each model), remeshing frequency, strength of coupling between the solid and fluid solvers, and the possibility of artificial stiffening due to remeshing near boundaries [55,56]. At each time step, there is a coupling step between the fluid and solid solver. For example, the solid analysis would transfer the displacement while the fluid analysis would transfer the force at each time step. Details on this technique as it relates to this research work is found in the following chapter. Nevertheless, with applications focused on the lung, W.Wall et al. has done a wide array of research in this area utilizing FSI

techniques. Their efforts are focused on investigating the complex local stress and strain at the alveolar level and improving the material modeling in the tracheobronchial region that would allow for inclusion of fibrous cartilage [57,58,59,60].

#### **1.4 Thesis Objective**

The objectives of this thesis include:

- i. Investigate the damaging effects of forced air flow on a 3-D idealized lung alveolar model.
- ii. Incorporate aged and diseased modeling into the analysis in order to investigate these effects on the stress/strain environment.
- iii. Create a multi-scale modeling connection between the alveolar organ level models to the alveolar septal tissue model.
- iv. Perform a comprehensive study that includes the effects of aging and disease.

Although the model used throughout this study may be one of simplicity it does give an initial approximation of the distribution of stress/strain environment resulting from mechanical ventilation. Chapter 2 of this thesis analyzes three cases, particularly a normal healthy lung, normal lung with structural changes to mimic disease, and lastly a normal lung with mechanical property changes that resemble aging. As previously stated not only does injurious ventilation exacerbate previous lung injury it also introduces damage to healthy portions of the lung. This is where the importance of studying the mechanical forces induced by mechanical ventilation on healthy lungs come into play. Diseases such as emphysema which is known to destroy the lungs overtime are key causes as to why ventilators are



necessary. Nevertheless, there exists a need to understand how the disease state responds to injurious ventilation. The last case which is one that involves an analysis on aged lungs is extremely vital as a vast majority of critically ill patients up to 81% [61] in an intensive care unit (ICU) are above 65 years. Moreover, ICUs are the mainstays within hospitals for which treatments of mechanical ventilation are heavily administered to patients. According to previous research by Cullen et al., Leaf et al., McClean et al., and Tran et al. [61 – 64] the aged and chronically ill patients have become the primary consumer of intensive care. Therefore, a more detailed computational study would give insight into how the majority of mechanical ventilation utilizers respond to this type of treatment. A specific study [65] assessed the influence of age on the outcome of patients receiving prolonged mechanical ventilation in tandem with other factors such as severity of illness, reason for mechanical ventilation, duration of mechanical ventilation, and the length of ICU stay were taken into consideration. The findings yielded an outcome in which the influence of age in mechanically ventilated patients in ICU could not be ascertained. Notwithstanding, this thesis delves into this area for a computational approach.

Chapter 3 encompasses an analysis of an alveolar tissue model, a step towards a more microscopic approach. Specifically, this analysis investigates how the deformations at the organ level model translate directly to the tissue. Hence, observing damage on a more micro-scale. The tissue is analyzed by taking into consideration the solid structural aspects of the tissue (i.e. endothelial cell layer, basement membrane, and epithelial cell layer).

Chapter 4 specifically investigates a specialized case that integrates the developed model to mimic a real life scenario for which an aged patient undergoes mechanical

ventilation as treatment. This case will give the best assumptions and explanations as to the distribution and magnitude of mechanical forces induced on the alveolar region of the lungs. These results can be of great assistance to physicians in terms of sustaining the lives of patients and avoiding multiple organ system failure (MOSF).

Lastly, chapter 5 concludes the thesis by giving a synopsis of the various cases throughout the study and ties it all together in order to address the overall objectives.

## **CHAPTER 2**

### **Lung Alveolar Analysis**

#### **2.1 Methods**

A three-dimensional alveolar model representative of generations 22-24, with typical alveolar ducts and sacs in human lungs measured by Weibel [1], defined by supportive dimensions was created using the SolidWorks commercial CAD software. The geometry was modeled after that used by Dailey et al [7]. Table 2.1 gives the associated dimensions for the model. Specifically, the three dimensional model included the alveolar duct in the analysis of the lung parenchyma to accurately describe the overall mechanical behavior of the lung as recommended by Denny and Schroter [48]. Hence, for this particular analysis generations 22 up to 24 were used in order to include the alveolar ducts, particularly a main branch at 22 with 2 daughter branches at 23. Spherical geometry was used to define an alveoli sac. Figure 2.1 illustrates the idealized geometry as well as its comparison to the physiological model of the lung. Although previous research [70] describes the alveolar region of the lungs as being a tightly packed sleeve of cup like chambers that open to one duct in which adjacent walls are shared, this model is much more idealized. There still remains very few studies on FSI techniques associated with lung modeling, hence, the goal

is to gain an understanding of the interaction between fluid (air) and solid (alveolar septa) domains in order to qualitatively and quantitatively analyze the degree of mechanical forces imposed as a result. Moreover, for simplification purposes, in this particular model the effects of surface tension are ignored and hence the tethering forces that result are negligible.

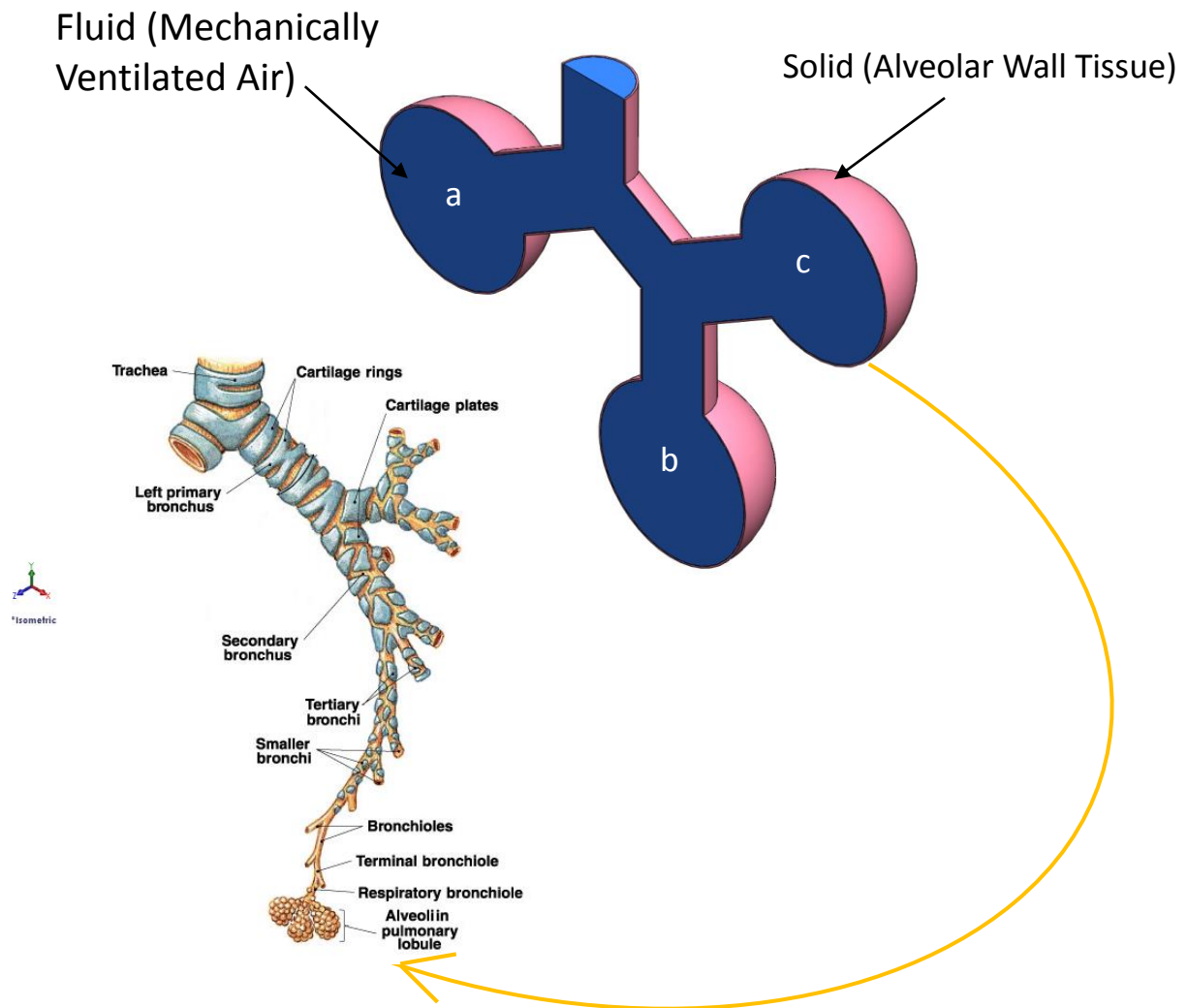


Figure 2.1. Geometric representations of the airway generations based on ICRP [69] tracheobronchial geometry and the idealized three-dimensional model of the alveolar geometry used for fluid-solid interaction analysis with each alveolar sac labeled.

The computational model involves both fluid and solid domains of the alveolar geometry. Table 2.1 shows the geometric parameters used to model the lung alveolar geometry. The alveolar geometry was considered as rigid (no deformation) in fluid analysis through computational fluid dynamics (CFD) from which the airway pressures and velocities were obtained. However, from coupled fluid-solid analysis through fluid-structure interaction, the strains on the alveolar geometry were obtained by considering the alveolar tissue as physiologically compliant (able to deform). The transient interactions between airflow and sac tissue during mechanical ventilation were investigated by solving two coupled sets of governing equations with specific boundary conditions. The governing equations for airflow and airways are described below.

Table 2.1 Description of geometric parameters for the idealized alveolar model.

<b>Dimensional Parameters for Alveolar Model</b>	
Inlet Duct Diameter	200 $\mu\text{m}$ [7]
Entrance Length	100 $\mu\text{m}$ [7]
Lobule Diameter	470 $\mu\text{m}$ [94]
Thickness	5 $\mu\text{m}$ [41,50]

### **2.1.1 Airflow Equations**

The governing equations for transient airflow are the Navier-Stokes equations on a moving mesh with the assumption of incompressible flow. Additionally, flow was assumed to be unsteady and laminar. These equations govern the principles of mass and momentum

conservation using Einstein's repeated index convention are illustrated below (Equations 2.1 and 2.2).

Conservation of mass:

$$\frac{\rho_g}{\sqrt{g}} \frac{\partial}{\partial t} (\sqrt{g}) + \rho_g \frac{\partial}{\partial x_j} \left( u_j - \frac{\partial \tilde{x}_j}{\partial t} \right) = 0 \quad (2.1)$$

Conservation of momentum:

$$\frac{\rho_g}{\sqrt{g}} \frac{\partial}{\partial t} (\sqrt{g} u_i) + \rho_g \frac{\partial}{\partial x_j} \left[ \left( u_j - \frac{\partial \tilde{x}_j}{\partial t} \right) u_i \right] = - \frac{\partial p}{\partial x_j} + \mu \frac{\partial^2 u_i}{\partial x_j^2} \quad (2.2)$$

In these equations  $\tilde{x}_j$  represents the moving mesh location,  $\sqrt{g}$  is the metric tensor determinate of the transformation, i.e. the local computational control-volume size,  $\rho_g$  is the fluid density,  $p$  is the fluid pressure,  $\mu$  is the fluid viscosity, and  $u$  is the fluid velocity.

### 2.1.2 Alveolar Wall Equations

The governing equations for the movement of the alveolar sac walls during inhalation and exhalation are the time-dependent structural equations shown below (Equations 2.3 and 2.4).

Equation of Motion:

$$\frac{\partial \sigma_{ij}}{\partial x_j} + F_i = \rho \frac{\partial^2 u_i}{\partial t^2} \quad (2.3)$$

Constitutive Relations:

$$\sigma_{ij} = C_{ijkl}\varepsilon_{kl} \quad (2.4)$$

In the equations above  $\sigma$  is the stress in each direction,  $F$  is the body force,  $\rho$  is the density,  $u$  is the displacement,  $C$  is the elasticity tensor, and  $\varepsilon$  is the strain in each direction.

### 2.1.3 Computational Simulations

The alveolar geometry was generated using SolidWorks® software and then imported into ANSYS Workbench, where FSI was conducted using ANSYS Mechanical (Version 14.5.7) and ANSYS CFX (Version 14.5.7). ANSYS Mechanical is a general finite element (FE) software program for structural modeling, and ANSYS CFX is a general purpose computational fluid dynamics (CFD) software program for modeling fluid flows. The individual models were coupled using a fluid-structure interaction (FSI) algorithm [57, 58,59]. Figure 2.2 depicts the FSI algorithm used in order to capture the physics of the model. The analysis assumed the solid portion was compliant, i.e. able to move. The fluid model equations were solved first to obtain fluid pressures, which were applied to the solid model. Displacements were solved for in the solid model equations, which were applied to the fluid model. The fluid model equations are resolved using the structural displacements at the boundaries. The process iterates until a converged solution is found for each time step.

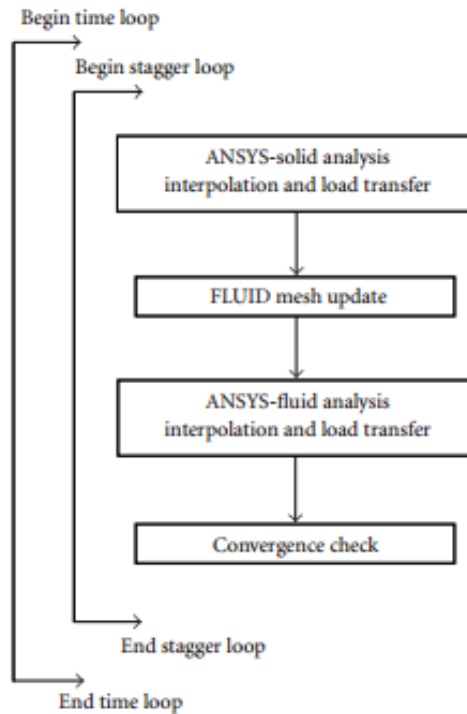


Figure 2.2. Fluid-structure interaction algorithm used to solve the model.

#### 2.1.4 Finite Element Meshes and Boundary Conditions

The fluid domain of the alveolar model comprised of 120,883 tetrahedral elements while the solid domain comprised of 120776 tetrahedral elements. These models were obtained after performing a mesh independence study. A graph demonstrating mesh independence can be seen in figure 2.3. Table 2.2 shows the details on number of elements for the three various analysis. Additional testing of mesh quality was done to ensure accuracy of results in terms of aspect ratios and skewness for the meshed models. Particularly, the skewness of a mesh represents the difference in between the shape of the cell and the shape of an equilateral cell. All elements of the solid model were below the value of 1 with more



than 99% of elements below 0.75 meaning they ranged from fair to excellent. Next, the aspect ratio of the elements is considered, which represents a measure of the stretch of a particular cell. In terms of the fluid model, mesh quality is measured in terms of orthogonality, expansion, and aspect ratio. Focus will be placed mainly on mesh aspect ratios. Such ratios for the fluid model revealed values of 5 which were all within good standing. Additionally, more than 99% of elements in the solid model has aspect ratios less than 4 with the maximum being 6.7. The mesh size should be chosen such that the results are independent of mesh size. Hence, after conducting a mesh study, mesh size was chosen to be 120,000 elements for both solid and fluid geometries. Figure 2.3 shows the mesh convergence plot and figure 2.4 illustrates meshing for the normal health lung model.

Table 2.2. Mesh sizes for the normal, diseased and aged lung alveolar models.

Model	Number of Solid Elements	Number of Fluid Elements
Normal	120776	120883
Diseased	120572	120780
Aged	120776	120883

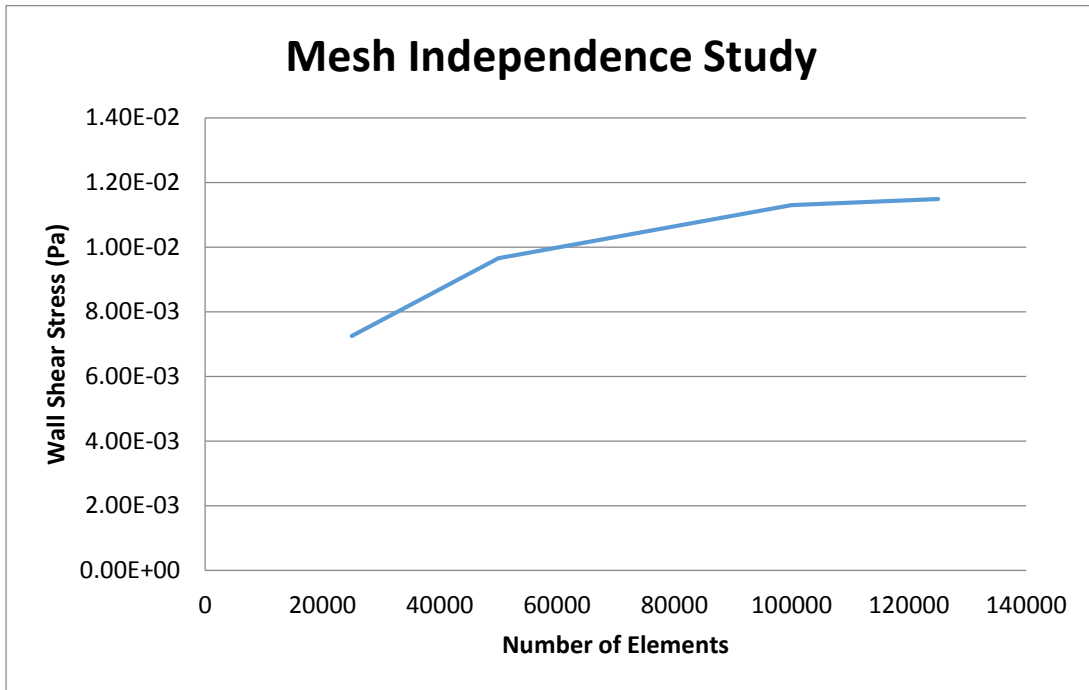


Figure 2.3 Chart of mesh independence study for FSI analysis

+

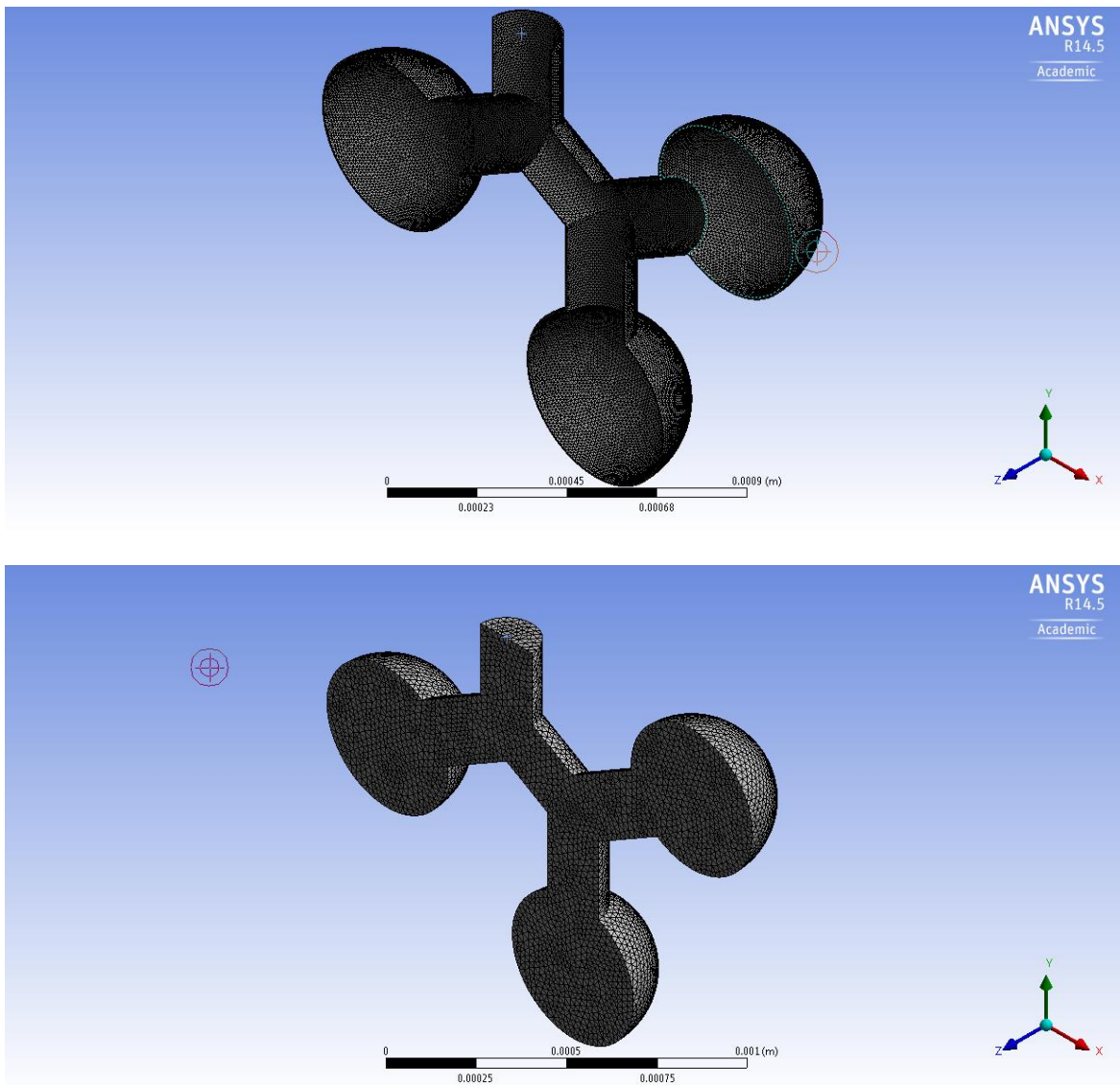


Figure 2.4. 3-D mesh for the normal lung solid (top) and fluid (bottom) model.

A no slip boundary condition was applied at the fluid-solid interface. At the inlet of both the fluid and solid model a zero displacement was applied. Additionally, a fluid solid interface was applied to both the solid and fluid models for load transfer to occur. The analysis ran as transient with a defined time step of 0.025 s which provided the best and

quickest convergence for results. Two separate input waveforms were used that included a normal breathing waveform and a ventilator waveform shown in figure 2.5. For the normal breathing waveform each breathing cycle was 4 seconds with 1.3s as inhalation and 2.7s as exhalation (1:2 ratio). For the ventilator waveform each breath cycle was 2 seconds with 0.4s as inhalation and 1.6s as exhalation (1:3 ratio). The formulas used to calculate the normal breathing and ventilator waveforms are found in Equation 2.5 and 2.6, respectively. The residuals were set to a value of 1E-4 as this was sufficient to give the most accurate results possible.

$$826.73 \sin(2.3621x) \text{ for } 0 \leq t \leq 1.33 \quad (2.5a)$$

$$411.82 \sin(1.1766(x + 1.34)) \text{ for } 1.33 \leq t \leq 4 \quad (2.5b)$$

$$Q_0 = 0.001 \frac{L}{s} \text{ for } 0 \leq t \leq 0.4 \quad (2.6a)$$

$$Q_0 = 0.001(-Exp(-\frac{(t-0.4)}{0.7})) \quad (2.6b)$$

$$Q_n = \frac{Q_0}{2^n} \quad (2.6c)$$

$$V_n = \frac{Q_n}{Area} \quad (2.6d)$$

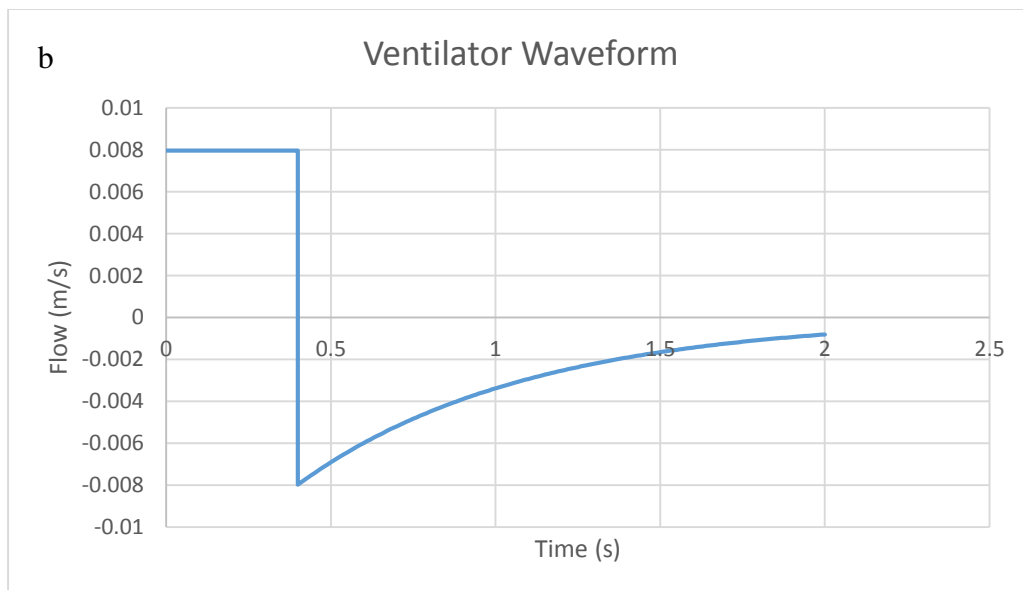
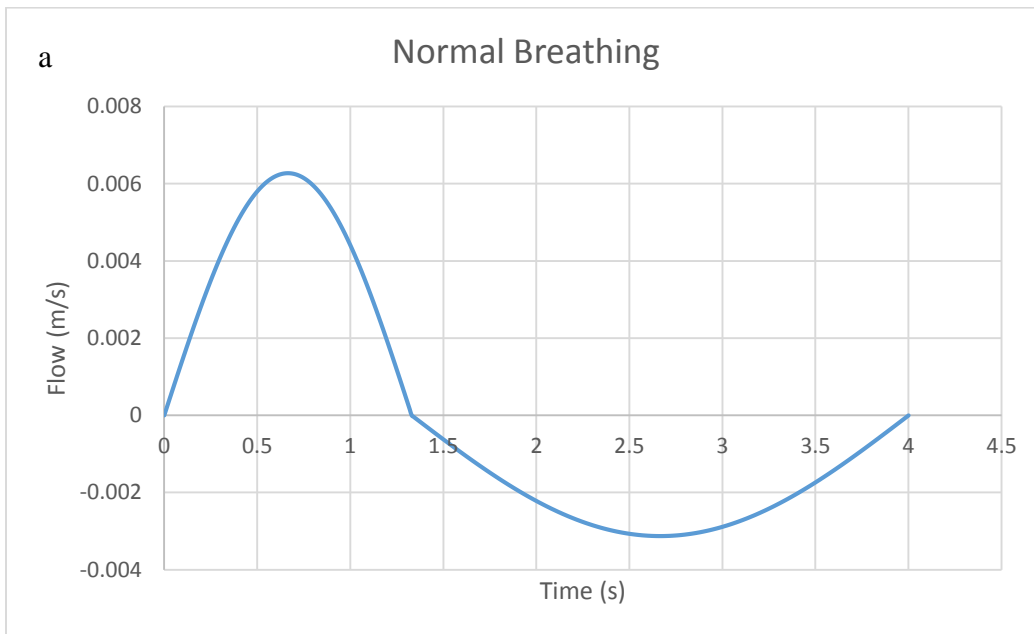


Figure 2.5 a. Normal breathing input waveform. b. Ventilator input waveform

### 2.1.5 Material Parameters

For the alveolar geometry model, the wall was assumed to be homogeneous, incompressible and behaved as a non-linear hyperelastic material assuming a Neo-Hookean model [49, 50, 52, 57, 60]. From this model the following parameter was applied (Equation 2.7):

$$W = \frac{\mu_1}{2} (\bar{I}_1 - 3) + \frac{K_1}{2} (J - 1)^2 \quad (2.7)$$

where  $C_I = \mu_1/2 = 1\text{kPa}$  and  $K_I = 13.5\text{kPa}$  [57]. Alveolar walls had a density of  $196\text{ kg/m}^3$  [49]. The air was assumed to be an incompressible fluid at  $37^\circ\text{C}$ .

### 2.1.6 Mechanical Ventilation Parameters

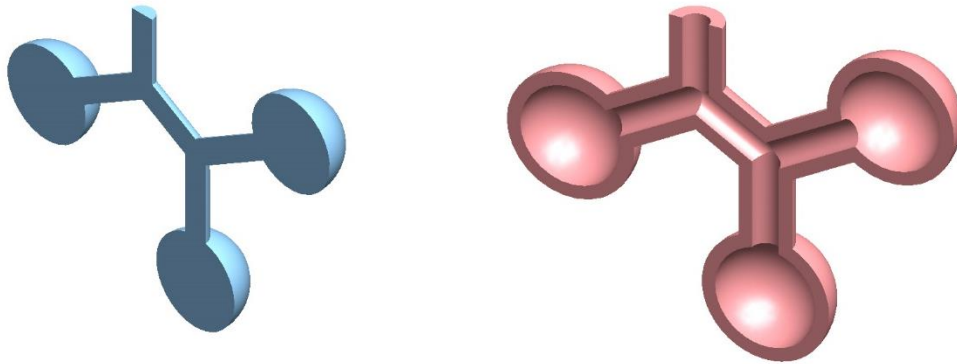
An inlet velocity profile (either normal breathing or ventilation waveform) was applied to the opening of the alveolar duct at generation 22 as shown in figure 2.5. Various studies have compared the effects of inspiratory waveform during ventilation such as comparing a sine wave versus a square wave [38, 39]. In this particular model, the sine wave represented the normal breathing waveform which was utilized for comparison. The velocity at the alveolar region is not specifically known and many studies have used various inlet waveforms, pressure inlet conditions, and other user defined functions to determine flow within the alveolar geometry. Assuming an idealized dichotomous lung the flow at the alveolar ducts would be based on the tracheal flow rate where the flow varies with each generation number, which can be derived from  $Q(n) = Q_{\text{tra}}/2^n$  [40,47]. Thus allowing the velocity over a breathing cycle to be determined for the alveolar duct at generation 22 using

a 60 L/min tracheal flow rate and converting that flow rate to a velocity. This was repeated for studies involving continuous breathing cycles.

### **2.1.7 Normal Lung with Structural Changes**

Particular importance to understand how ventilation affects the lungs with structural changes that obstruct airflow needs to be investigated. As previously stated, ventilation exacerbates preexisting lung disease and damages healthy parts of the lung. However, the specifics in terms of mechanical behavior is sought after. This analysis mimics those changes associated with disease. In the diseased state there are two distinct cases which include buildup of mucus and other particles that obstruct the airway hence decreasing the inner radius and structural changes which occur in a more advanced level of the disease and include change in elastic modulus of lung tissue [71,72]. Wall thickness was increased by 50% coupled with a 50% decrease in the radius in order to account for disease in the model. Figure 2.6 illustrates the lung alveolar model with structural changes due to disease as well as the accompanying meshed fluid and solid model.

a.



b.

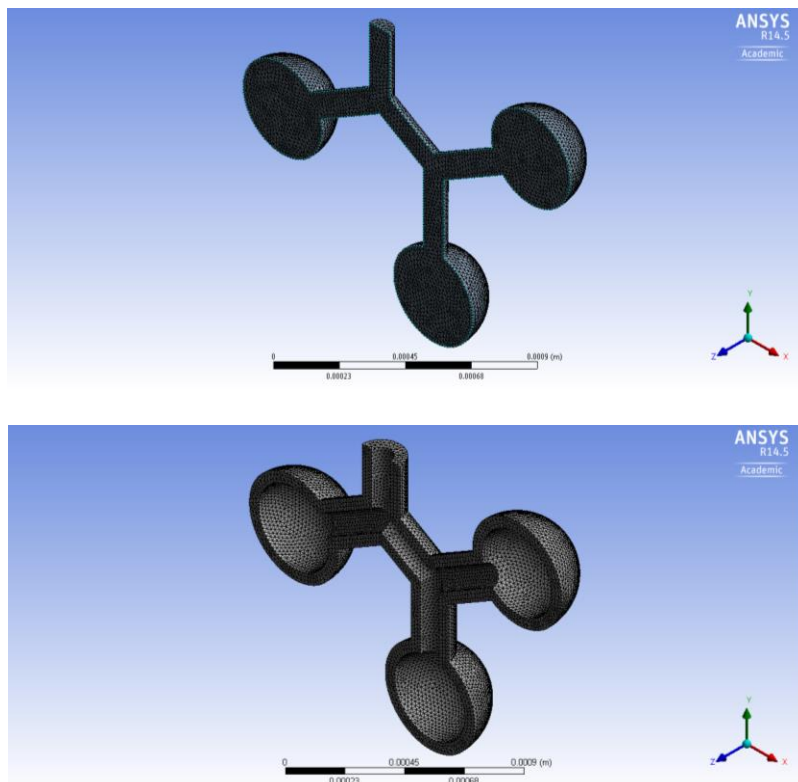


Figure 2.6 a) NLSC with both fluid (left) and solid (right) shown. b) 3-Dimensional meshed fluid (top) and solid (bottom) models.



### 2.1.8 Normal Lung with Mechanical Property Changes

It is important to consider and include aging when investigating mechanical ventilation due to the fact that more than 50% of patients on mechanical ventilation are over the age of 65 [73]. Parameters to model aging include changes in the material properties of the lung tissue. Referencing the study done in by Lai-Fook et al [74] parameters in terms of bulk modulus, shear modulus, Poisson ratio, and elastic modulus were all computed for a person of age 70 (Equations 2.8-2.11).

$$K = 8.9 + 0.25Age \quad (2.8)$$

$$\mu = 2.6 + 0.011Age \quad (2.9)$$

$$\sigma = 0.40 + 5.2 \times 10^{-4} Age \quad (2.10)$$

$$E = 3K(1 - 2\nu) \quad (2.11)$$

where K is the bulk modulus,  $\mu$  is the shear modulus,  $\sigma$  is Poisson ratio and E is the elastic modulus or Young's modulus. Additionally the above equations all correspond to a transpulmonary pressure of 4 cmH<sub>2</sub>O which is at functional residual capacity. Table 2.3 gives the values for the various material properties at age 70.

Table 2.3 Material properties for the NLMPC model at age 70.

Material parameter	Value
K (Pa)	2588.96
$\mu$ (Pa)	330.48
$\sigma$	0.44
E (Pa)	987.95

## **2.2 Results**

Three sets of results were obtained pertaining to (i) normal lung alveolar analysis with the ventilator and normal breathing input waveforms (ii) normal lung alveolar analysis with structural changes modeling disease (TLC) and (iii) normal lung alveolar analysis with mechanical properties modeling an aspect of aging. The results of airway mechanics parameters, specifically the wall shear stresses as well as stresses/strains were analyzed to show the effects of mechanical ventilation on various lung conditions. Moreover, for each analysis results are analyzed after 2 breathing cycles at 2.2s (midway through inspiration) and 2.825 (40% into the breathing cycle). The same was done for the normal breathing waveform, however, results were analyzed at 4.725s and 5.625. These values were chosen due to i) it was important to see how fluid as well as solid behavior were changing between inspiration and expiration and ii) midway through inspiration would represent a lung at 45% total lung capacity (TLC) and at 40% into the breathing cycle accounts for 70% TLC.

### **2.2.1 Fluid Pressures and Velocities**

Results for the analysis are given in terms of fluid pressures and velocities for which the contours of these can be found in figures 2.7 and 2.8 for the normal healthy lung case with ventilator and normal breathing input boundary conditions. Fluid velocities were 17.8% higher in the ventilator waveform as compared to the normal breathing waveform. Flow during expiration is less in each case as is expected seeing that flow is exiting and working against gravity. Fluid pressures were 26.6% higher in the ventilator waveform as compared

to the normal breathing waveform. Additionally, in the ventilator waveform case there remained a larger distribution of higher pressures across the model. Even in the case of expiration a larger distribution and magnitude of higher pressures were found in the ventilator waveform case. Figure 2.9 and 2.10 display plots of pressure vs time throughout the analysis. In figure 2.9 the pressure transient can be compared to the theoretical outputs of pressure from the ventilator that's shown in the smaller image. Both pressure outputs are similar in shape but vary due to the slight differences between the flow waveform used in this analysis and that used in the figure.

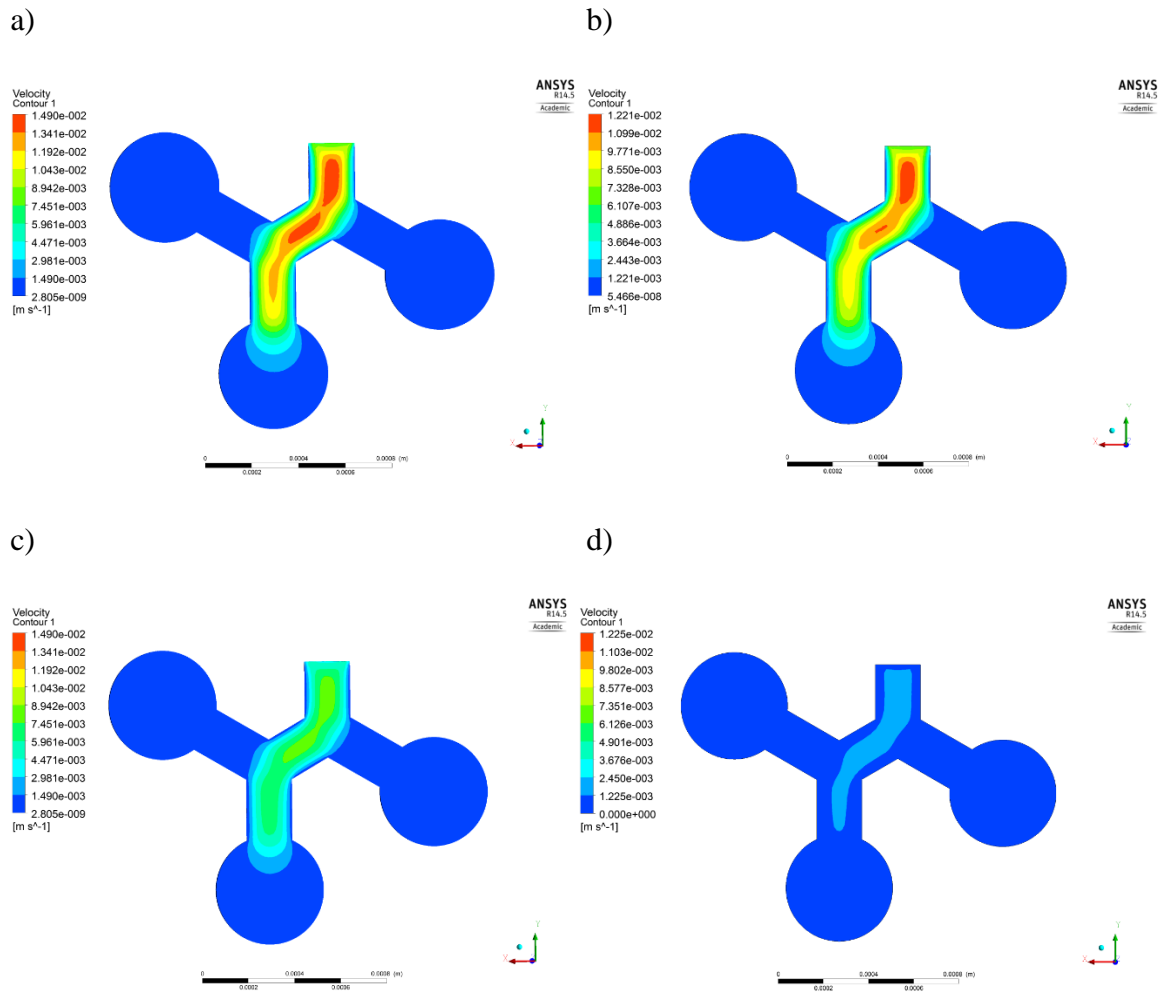


Figure 2.7 Contours of velocity magnitudes for the a) ventilator waveform at 2.2s, b) normal breathing waveform at 4.725s, c) ventilator waveform at 2.285s, and d) normal breathing waveform at 5.725s.

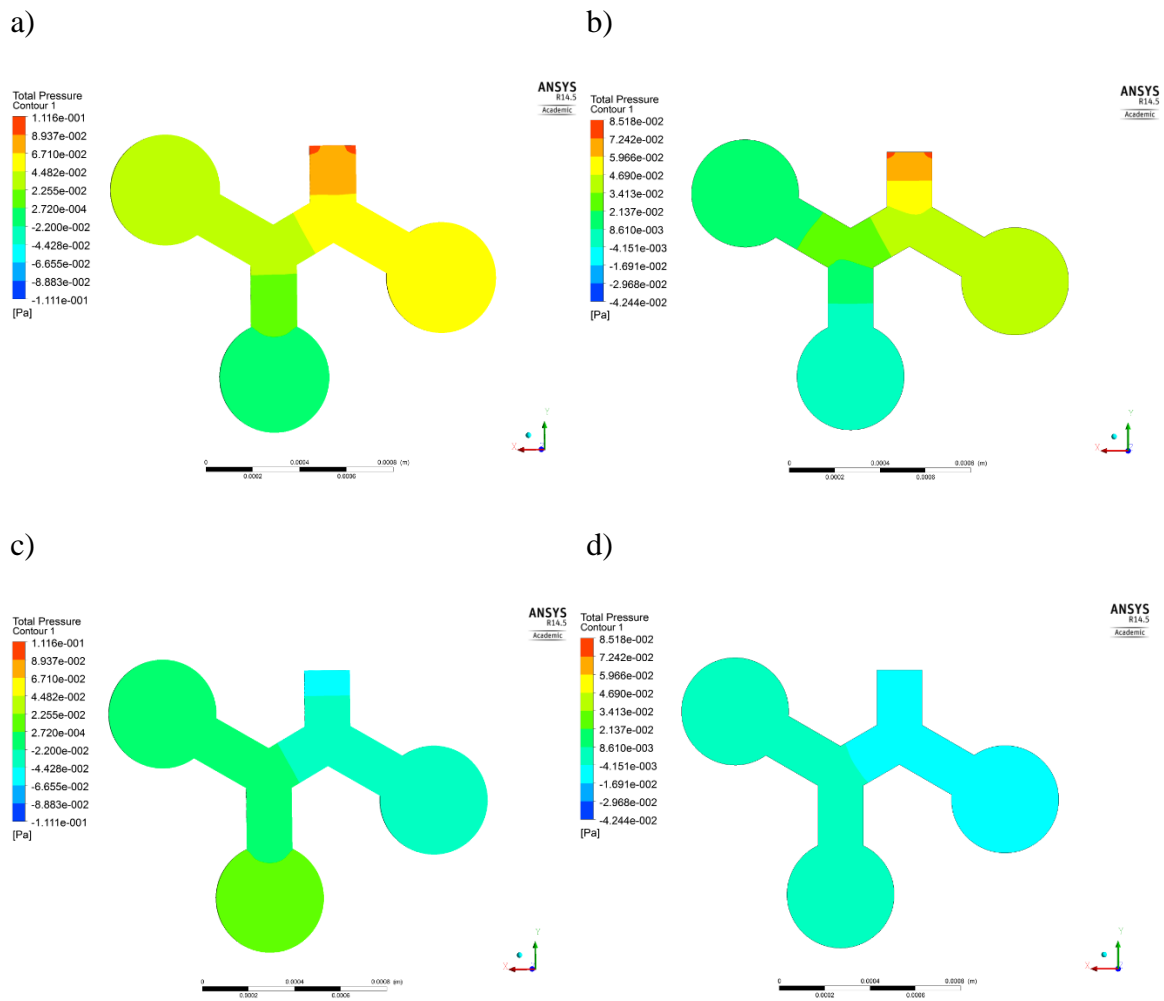


Figure 2.8 Contours of pressure magnitude for the a) ventilator waveform at 2.2s, b) normal breathing waveform at 4.725s, c) ventilator waveform at 2.285s, and d) normal breathing waveform at 5.625s.

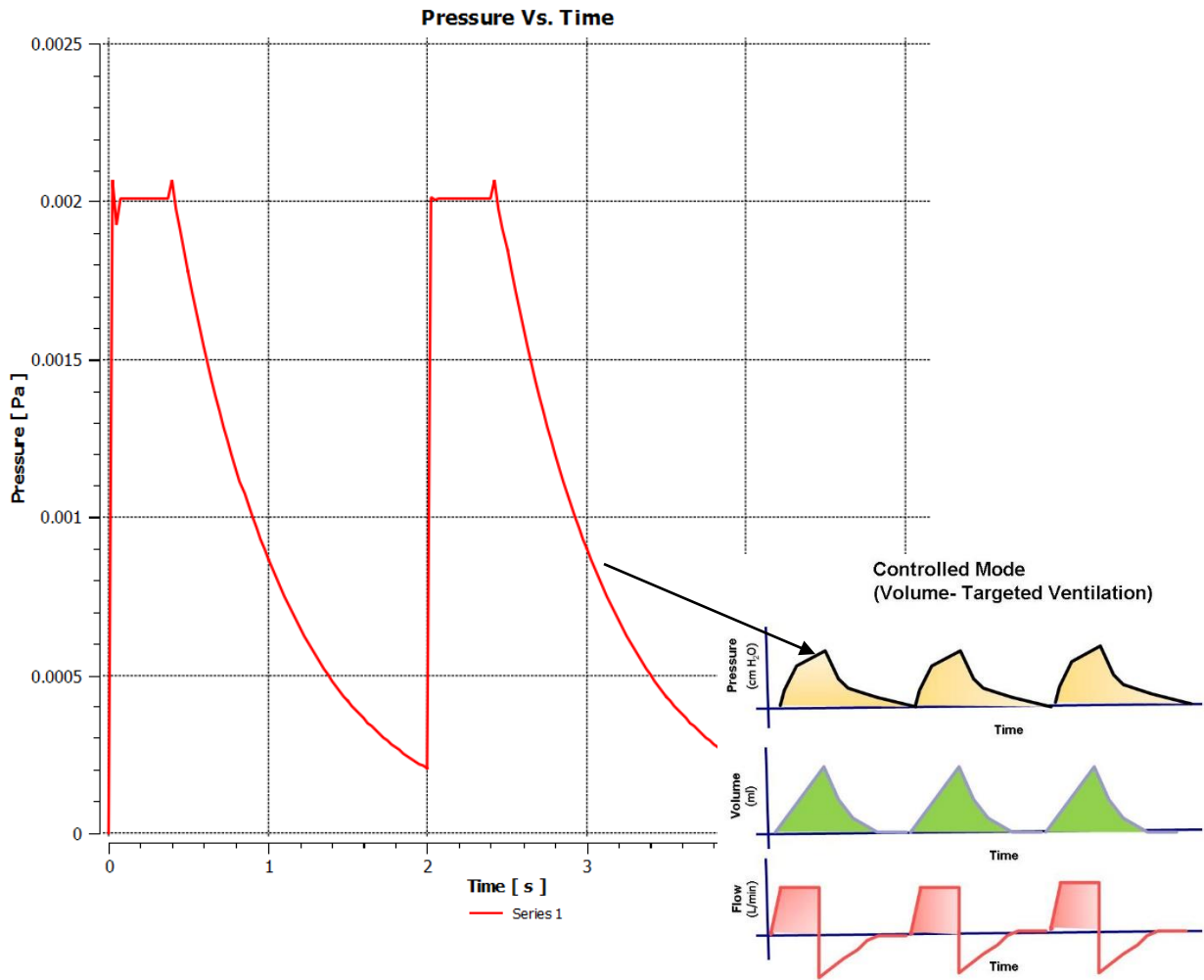


Figure 2.9 Pressure vs. Time transient for the ventilator waveform. Figure on right source [88].

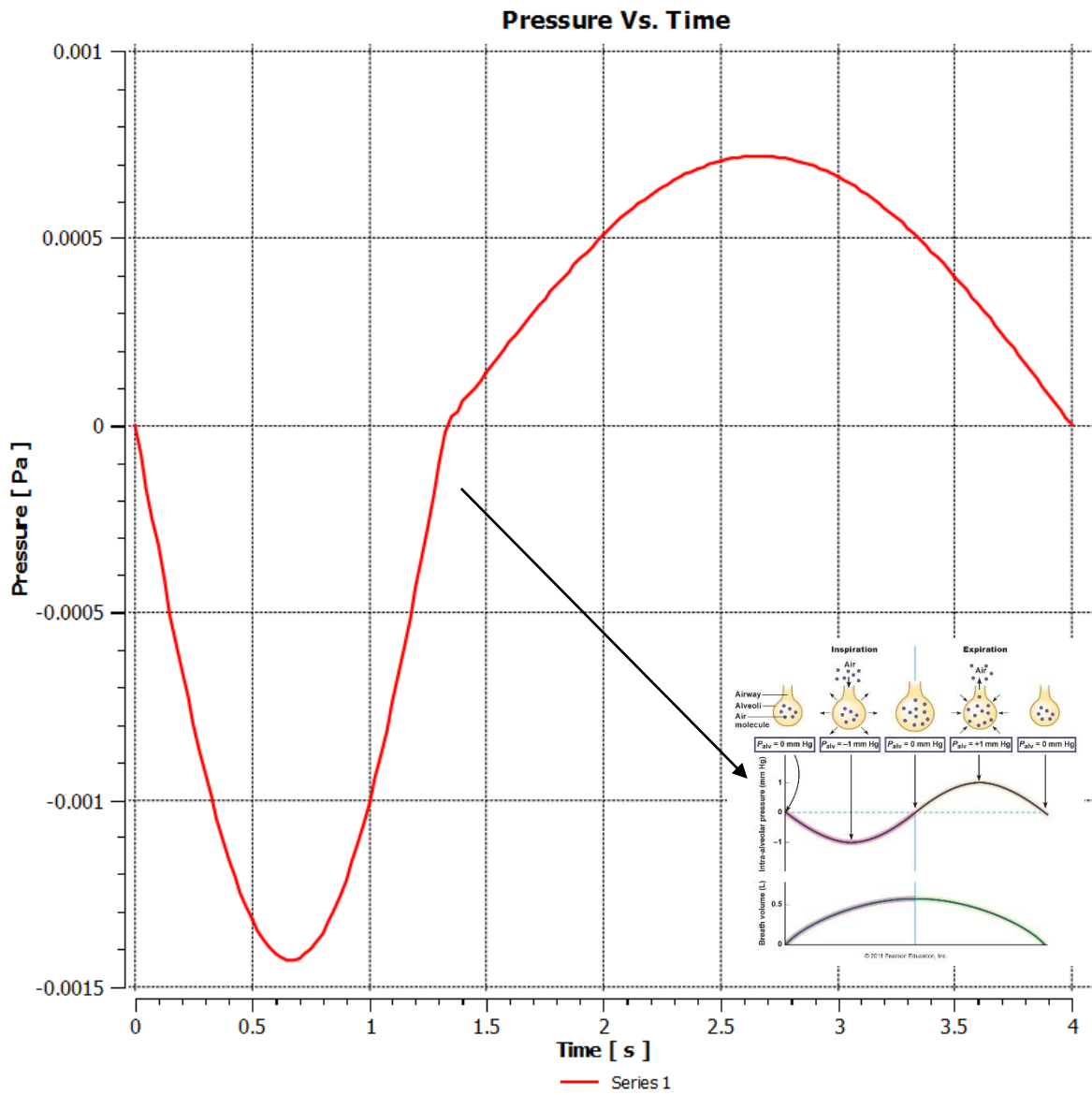
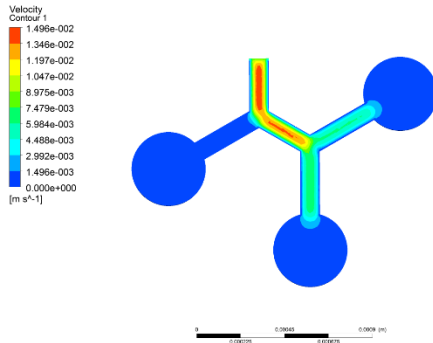


Figure 2.10 Pressure vs. Time transient for the normal breathing waveform. Source for figure [89]

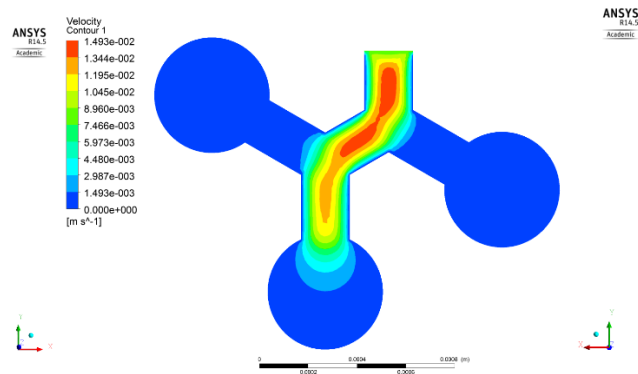
Figure 2.11 and 2.12 respectively, display the fluid velocities and pressures for the normal lung with structural change (NLSC) and normal lung with mechanical property

changes (NLMPC). In this case fluid velocities in the NLSC were not significantly higher, 0.2%, than in the NLMPC. However, fluid pressure in the NLSC was 67% higher than in the NLMPC. For the NLSC there are structural changes with no change in mechanical properties. The radius of the alveolar ducts are decreased. Therefore as flow enters, seeing that there are no major increases in flow, it is expected with a decrease in radius that an increase in pressure ensues.

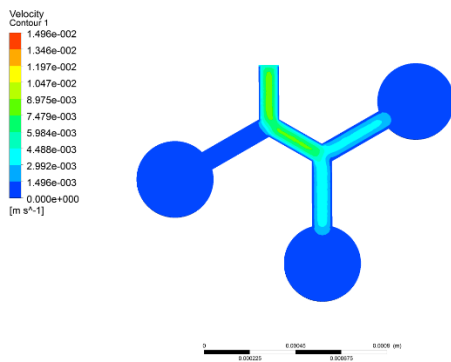
a)



b)



c)



d)

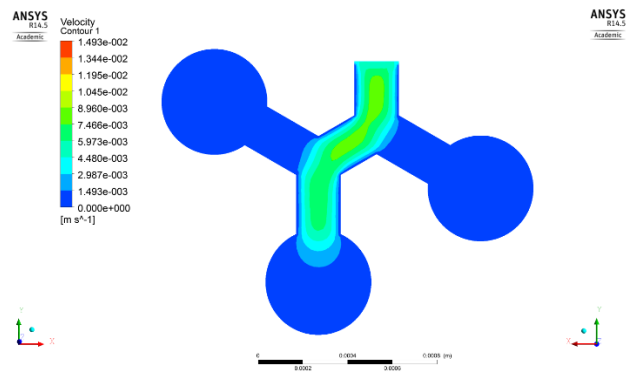


Figure 2.11 Contours of velocity magnitude for the a) diseased lung model at 2.2s, b) aged lung model at 2.2s, c) diseased lung model at 2.285s and d) aged lung at 2.285s with ventilator waveform.



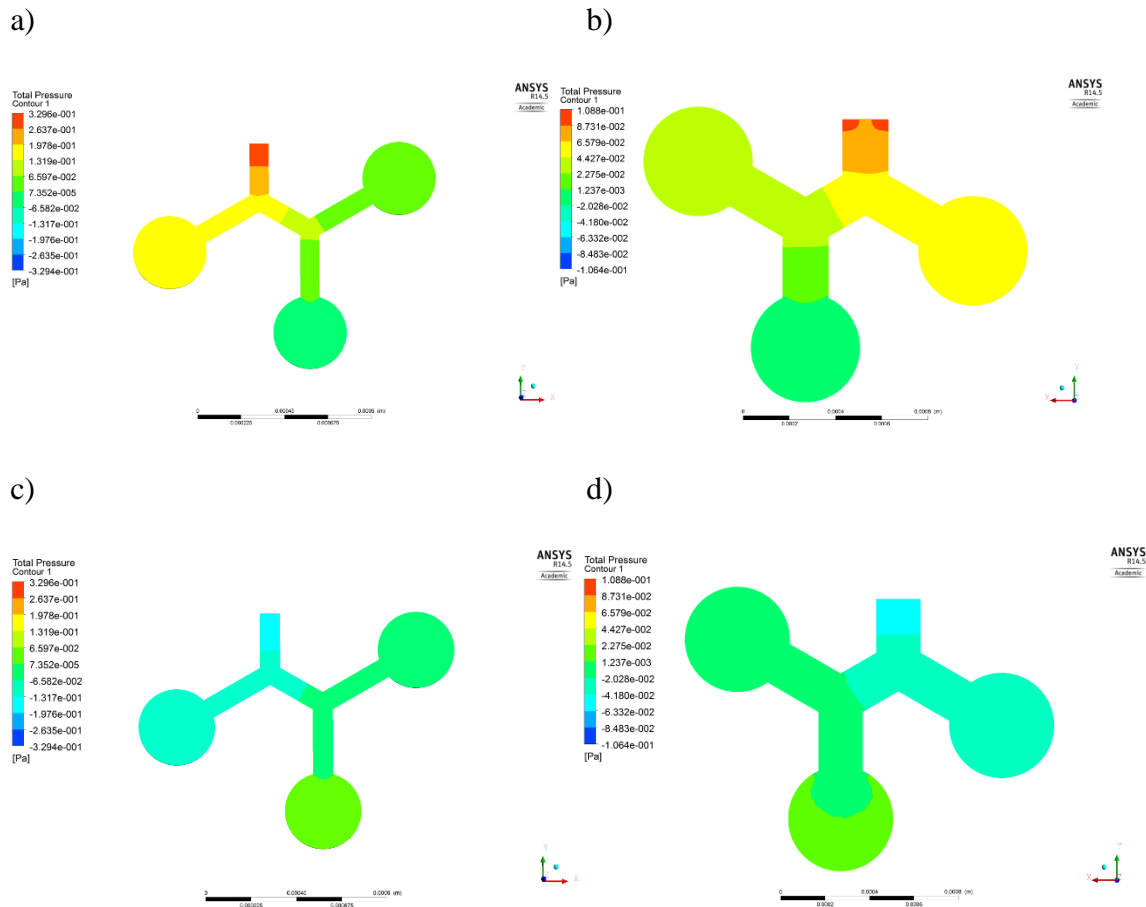


Figure 2.12 Contours of pressure magnitude for the a) diseased lung model at 2.2s, b) aged lung model at 2.2s, c) diseased lung model at 2.285s and d) aged lung at 2.285s with ventilator waveform.

## 2.2.2 Structural Displacements and Stresses

The solid analysis results were given in terms of total displacement, the von Mises stress and principal stresses. Figure 2.13 through figure 2.17 depict the total displacement, von Mises stress and principal stresses (first, second, and third), for the normal breathing and ventilator waveform. Particularly for the ventilator waveform it shows that the lung

alveolar model is being displaced 25.2% more than in the case of the normal breathing waveform. As a result, the stresses seen in figures 2.14-2.17 are higher by approximately 25% in the ventilator case than in the normal breathing case. Distributions of stresses are more predominantly seen in the alveoli sacs that contain greater distributions of displacement. This also can be verified mathematically with the fact that where Eq 2.3 is dependent on the displacement  $x_j$  and as a result the stresses obtained are therefore dependent on the displacements. Figure 2.18 displays bar charts comparing the ventilator versus normal breathing waveform in terms of inspiration and expiration. Parameters compared are the total displacement, von Mises stress and first principal stress. It then shows that during inspiration for the ventilator waveform case displacements and therefore stresses are larger in magnitude.

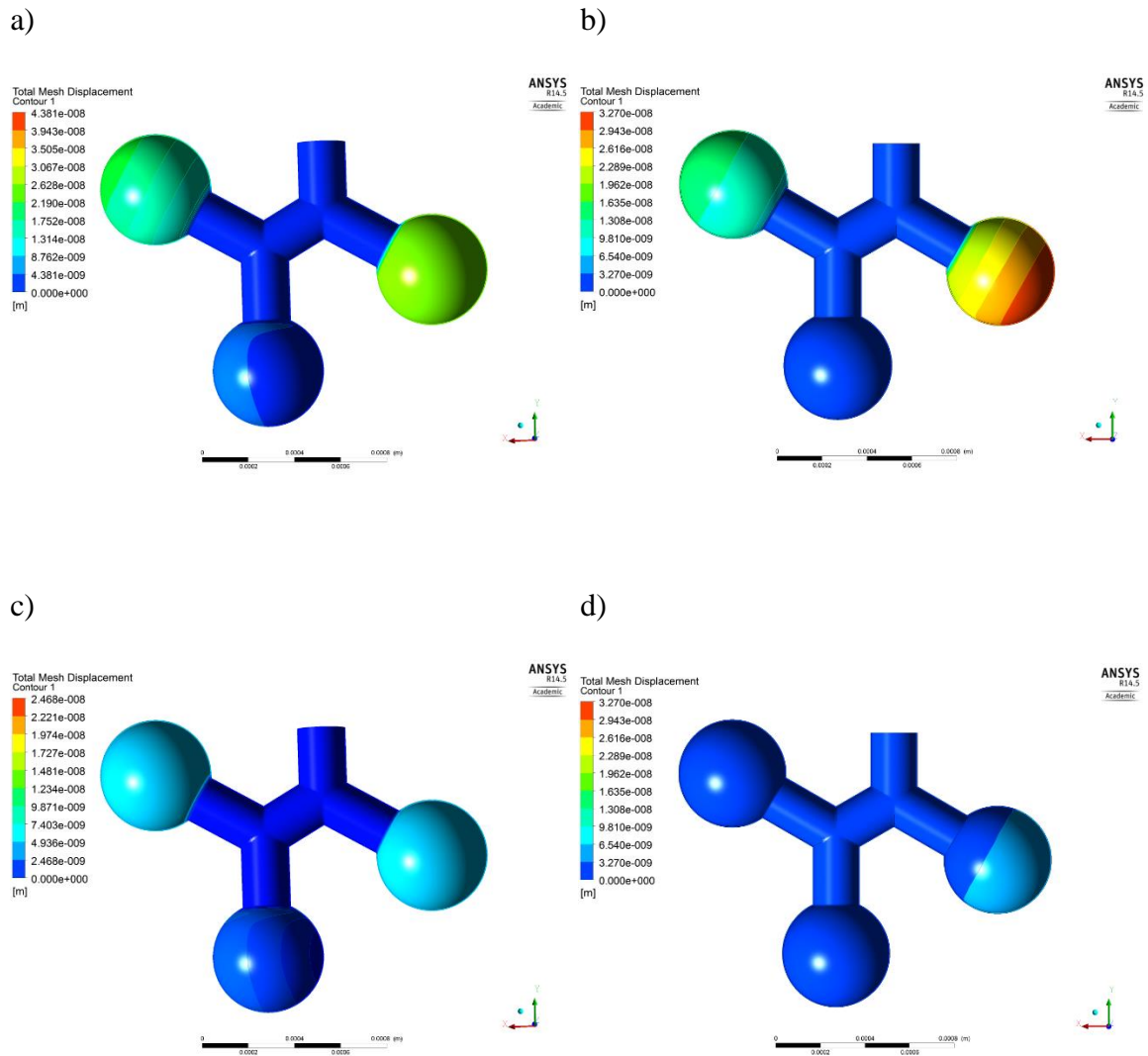


Figure 2.13 Contours of total mesh displacement for the a) ventilator waveform at 2.2s, b) normal breathing waveform at 4.725s, c) ventilator waveform at 2.285s, and d) normal breathing waveform at 5.625s.

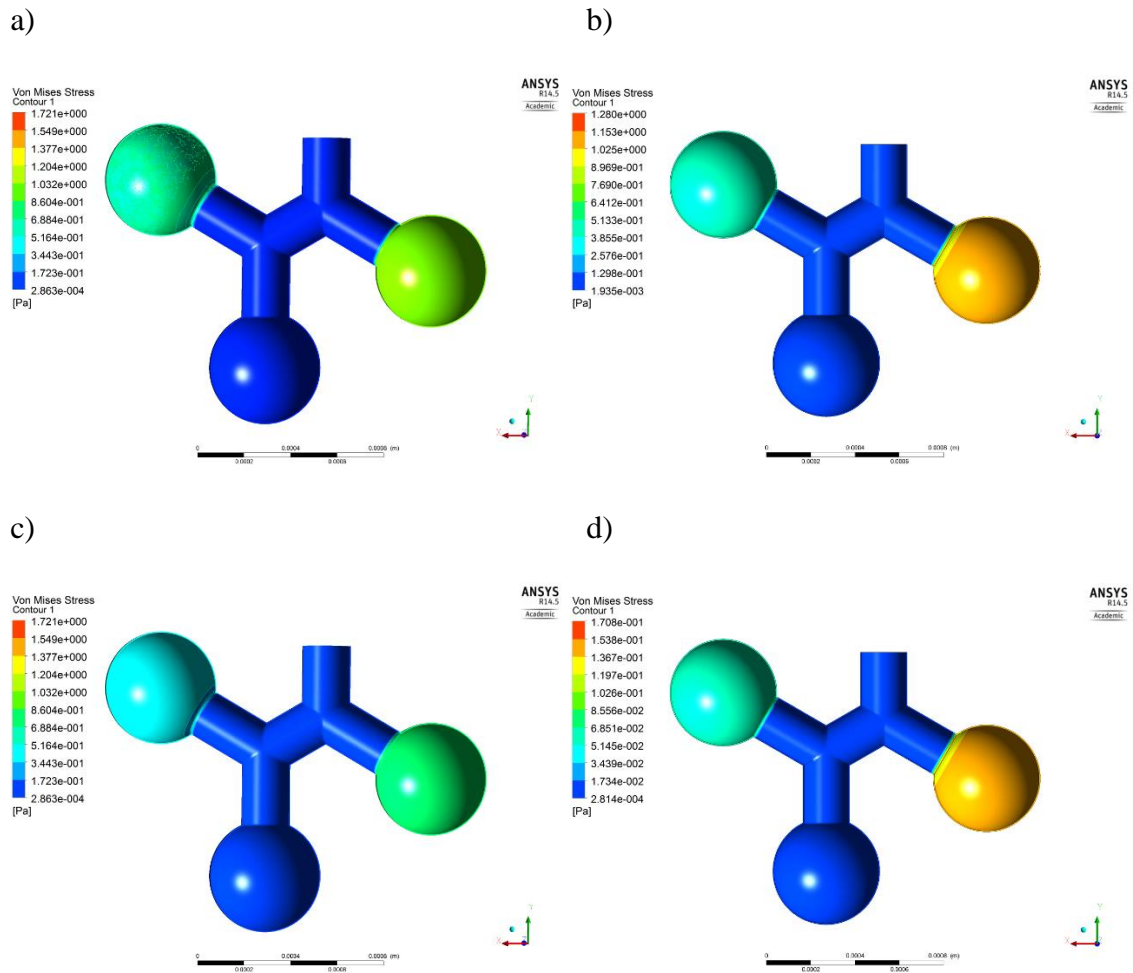


Figure 2.14 Contours of von Mises stress for the a) ventilator waveform at 2.2s, b) normal breathing waveform at 4.725s, c) ventilator waveform at 2.285s, and d) normal breathing waveform at 5.625s.

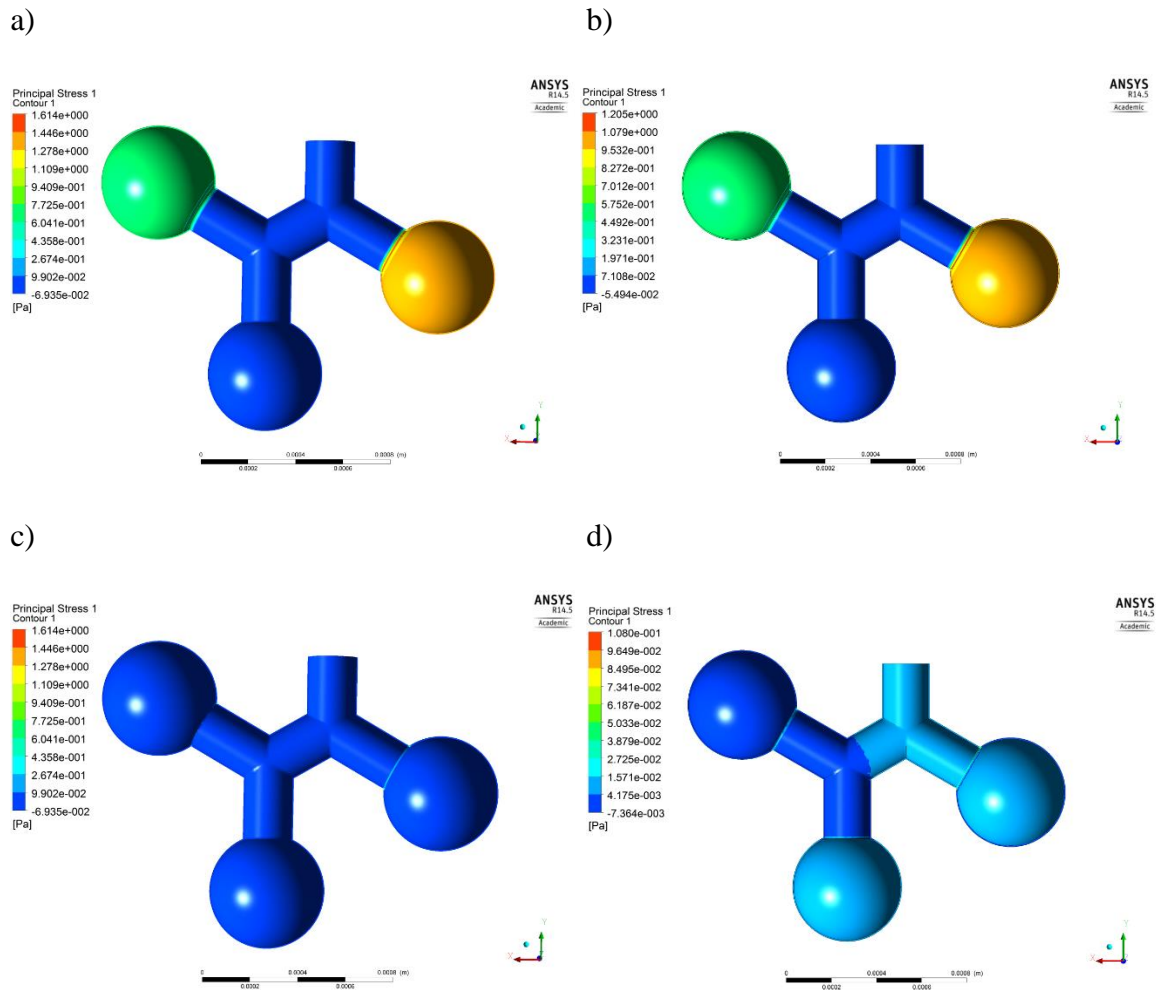


Figure 2.15 Contours of first principal stress for the a) ventilator waveform at 2.2s, b) normal breathing waveform at 4.725s, c) ventilator waveform at 2.285s, and d) normal breathing waveform at 5.625s.

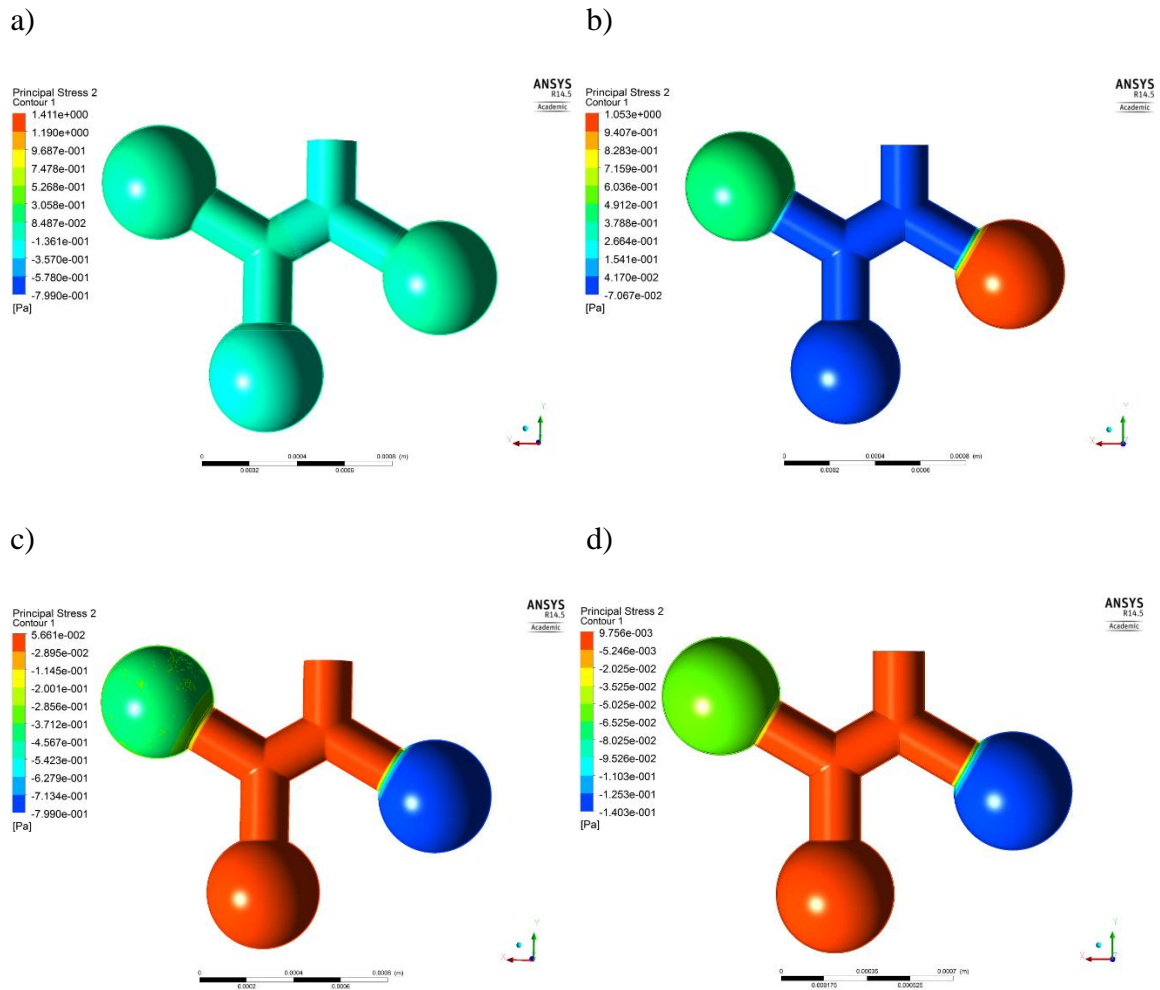


Figure 2.16 Contours of second principal stress magnitude for the a) ventilator waveform at 2.2s, b) normal breathing waveform at 4.725s, c) ventilator waveform at 2.285s, and d) normal breathing waveform at 5.625s.

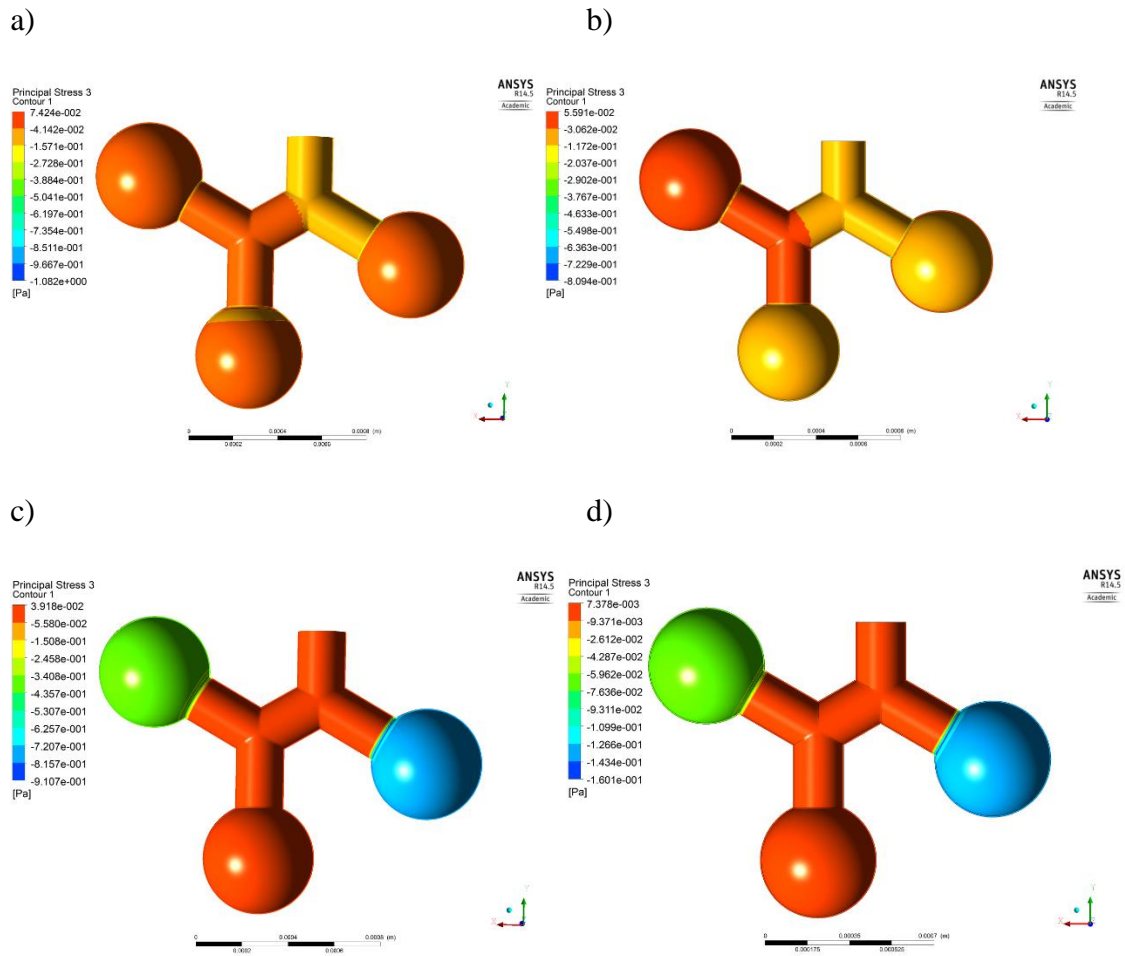


Figure 2.17 Contours of third principal stress magnitude for the a) ventilator waveform at 2.2s, b) normal breathing waveform at 4.725s, c) ventilator waveform at 2.285s and d) normal breathing waveform at 5.625s.

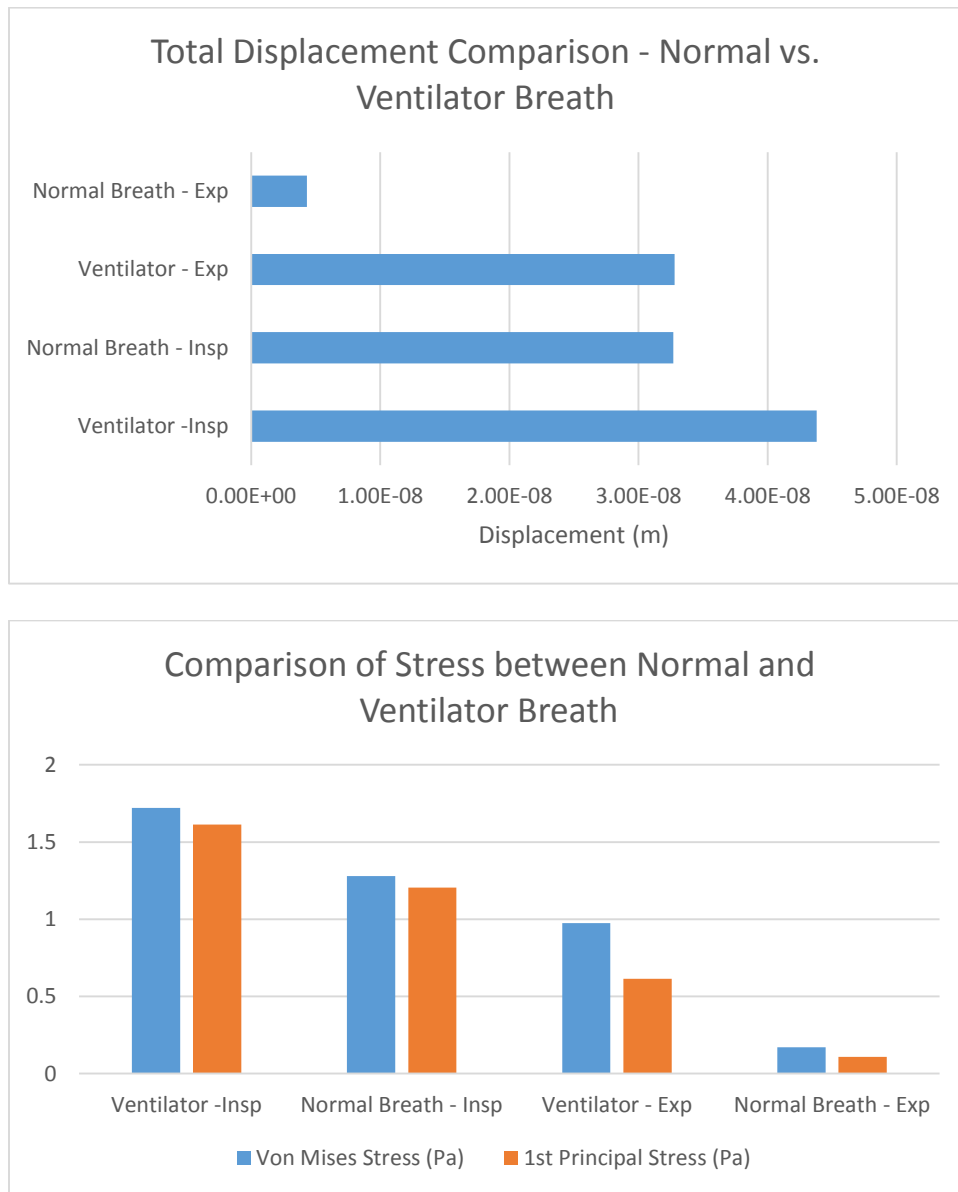


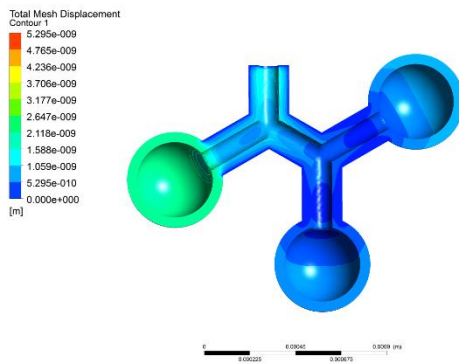
Figure 2.18 Comparison plots of normal versus ventilator breath for total mesh displacement (top) and significant stresses (bottom)

The total displacement for the NLSC and NLMPC are found in figure 2.19. Displacements are shown to be 98% higher in the case of the NLMPC compared to the

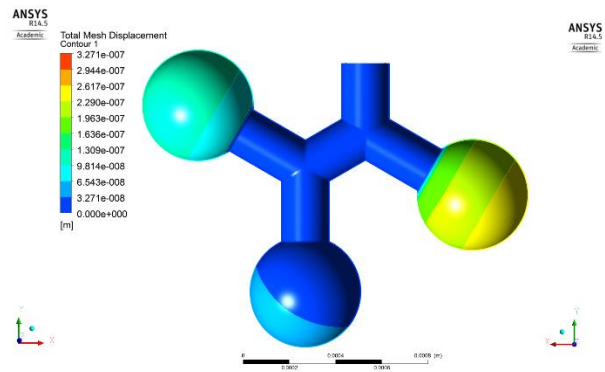


NLSC. This is found to be plausible due to that fact that within the NLMPC, elasticity decreases thus making it less rigid and more flexible. As a result with increased flexibility the lungs are therefore more compliant and able to expand more as the lungs fill with air. Equation 2.3 is dependent on displacements in order to calculate stress. Figures 2.20 - 2.23 depict the various stresses for the NLSC and NLMPC cases. For example, the von Mises stresses are 80.2% higher and the first principal stress is 81.6% higher in the NLMPC than in the NLSC. Figure 2.24 displays a bar chart of comparisons between displacements and von Mises stress for the diseased and aged lung models.

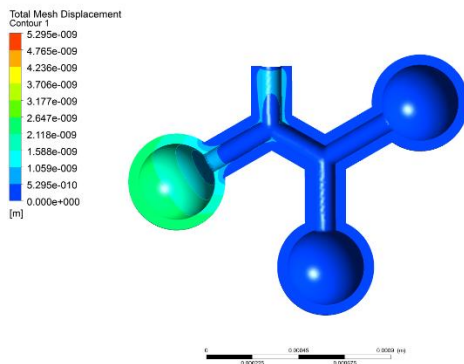
a)



b)



c)



d)

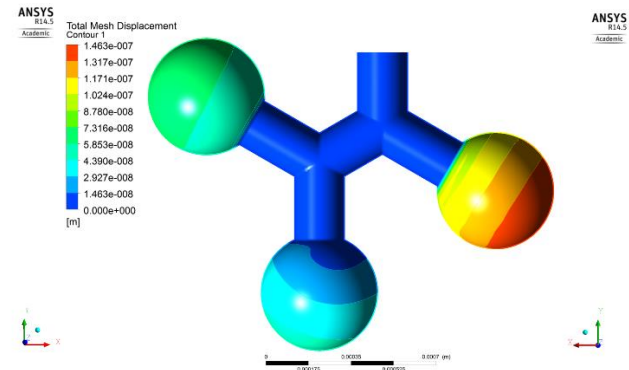


Figure 2.19. Contours of total mesh displacement magnitude for the a) NLSC model at 2.2s, b) NLMPC model at 2.2s, c) NLSC model at 2.285s and d) NLMPC model at 2.285s with ventilator waveform.

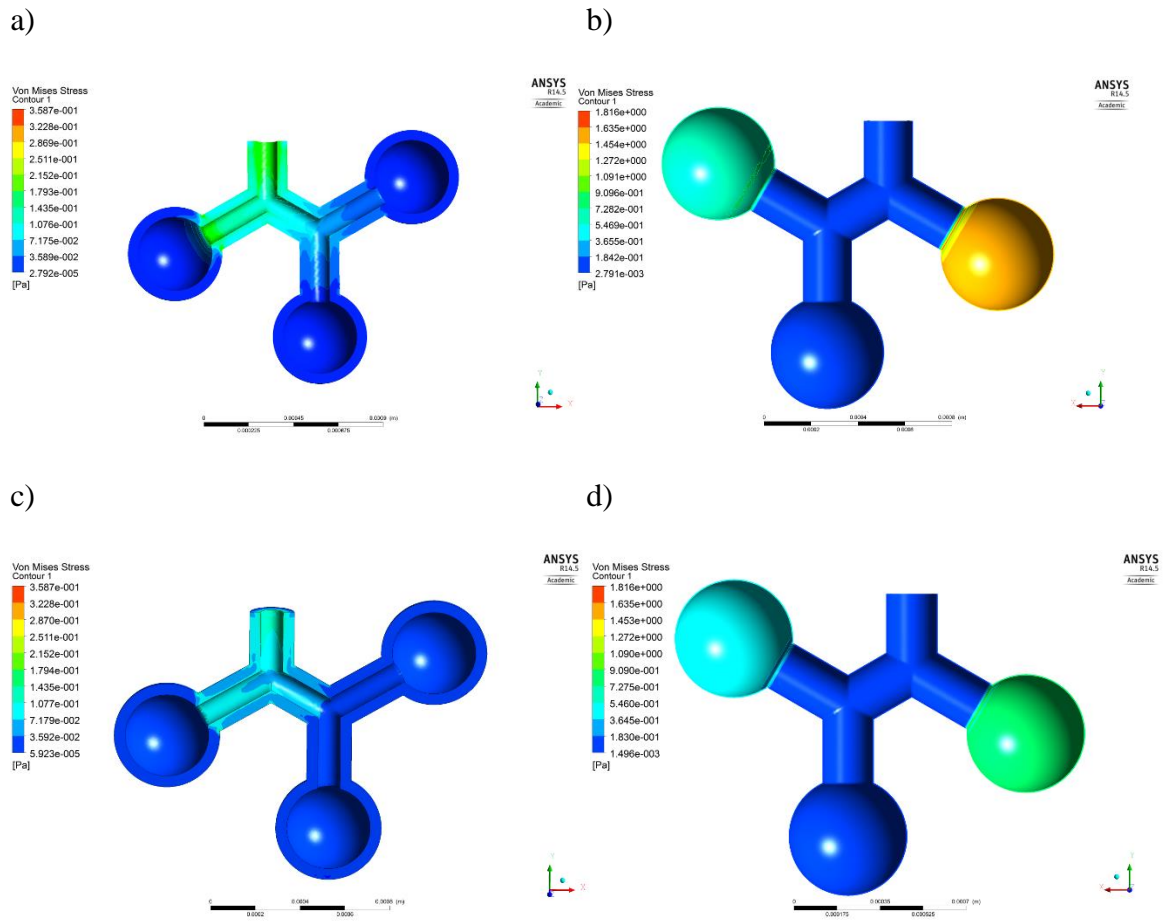


Figure 2.20 Contours of von Mises stress magnitude for the a) NLSC model at 2.2s, b) NLMPC model at 2.2s, c) NLSC model at 2.285s and d) NLMPC model at 2.285s with ventilator waveform.

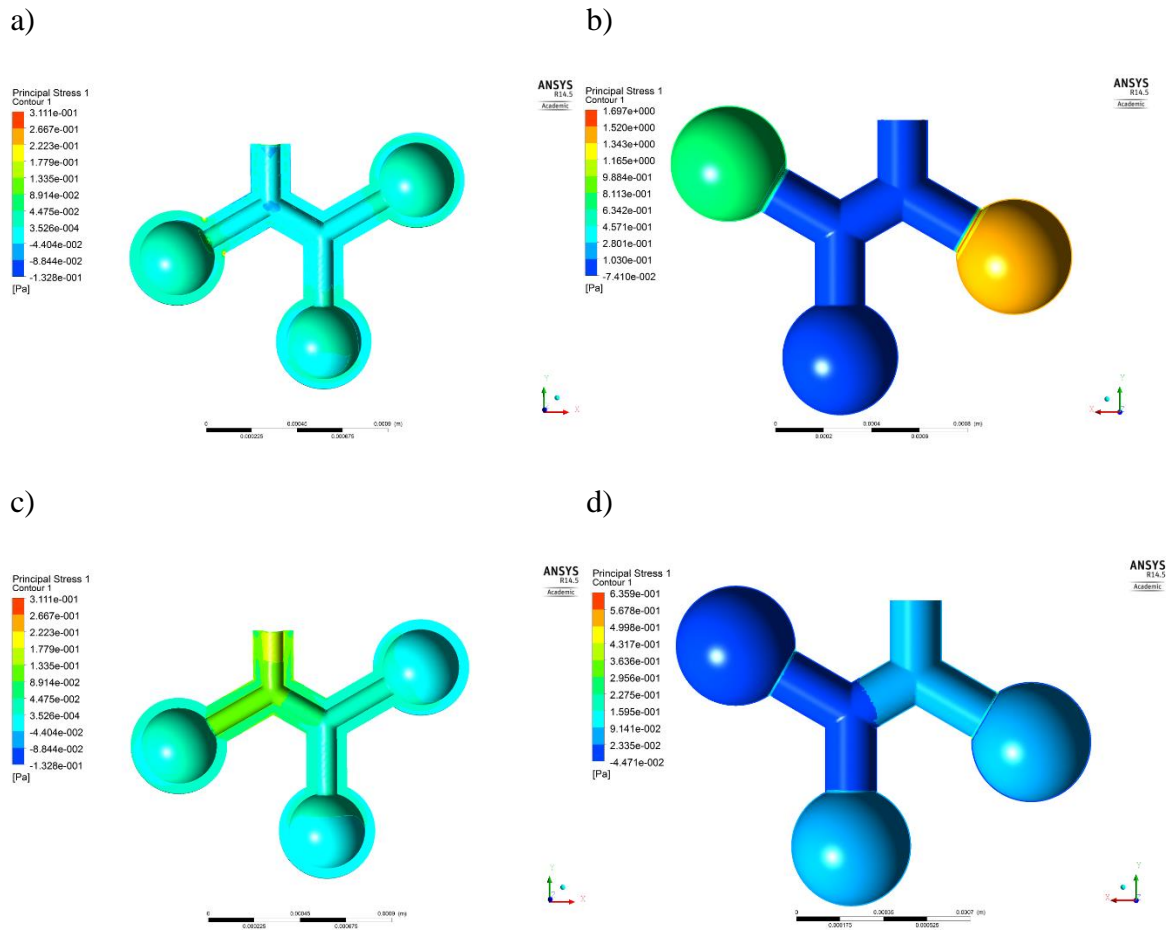
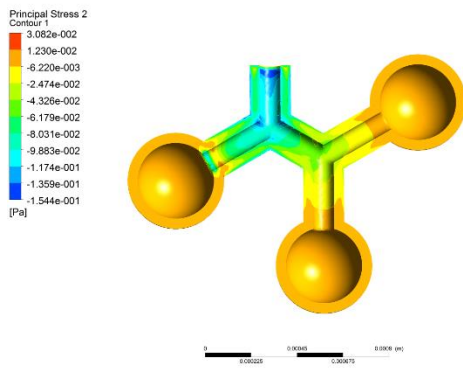
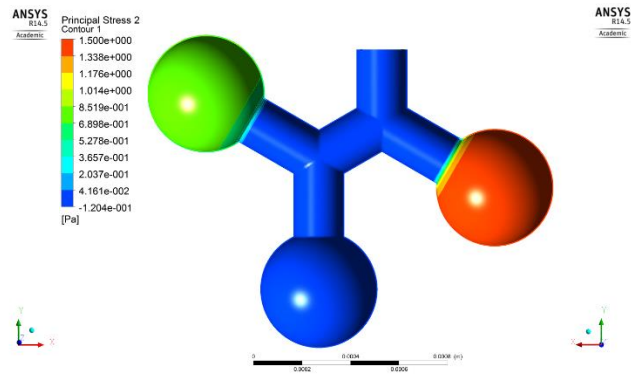


Figure 2.21 Contours of first principal stress for the a) NLSC model at 2.2s, b) NLMPC model at 2.2s, c) NLSC model at 2.285s and d) NLMPC model at 2.285s with ventilator waveform.

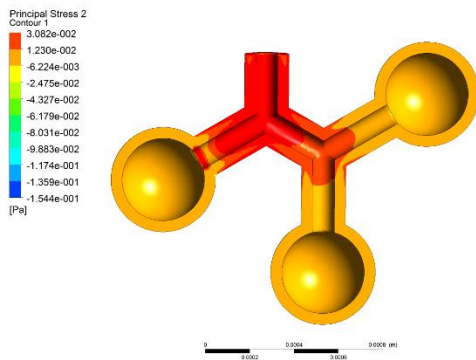
a)



b)



c)



d)

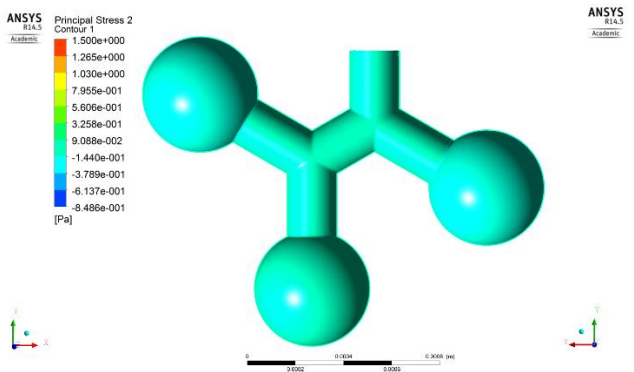
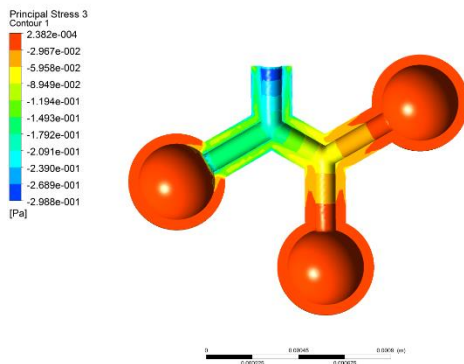
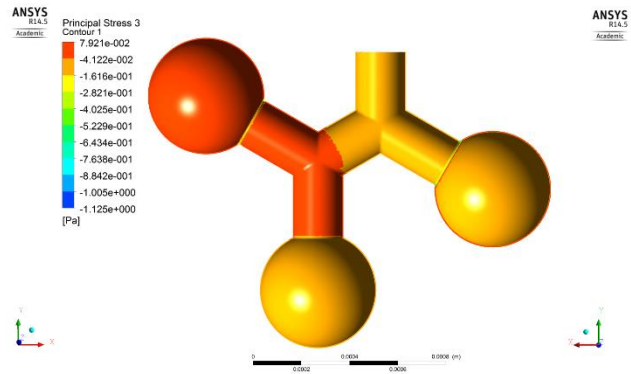


Figure 2.22 Contours of second principal stress for the a) NLSC model at 2.2s, b) NLMPC model at 2.2s, c) NLSC model at 2.285s and d) NLMPC model at 2.285s with ventilator waveform.

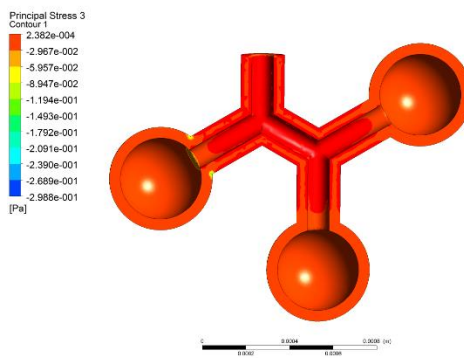
a)



b)



c)



d)

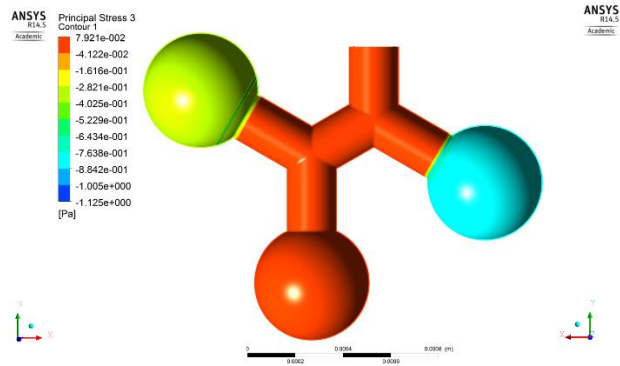


Figure 2.23 Contours of third principal stress for the a) NLSC model at 2.2s, b) NLMPC model at 2.2s, c) NLSC model at 2.285s and d) NLMPC model at 2.285s with ventilator waveform.

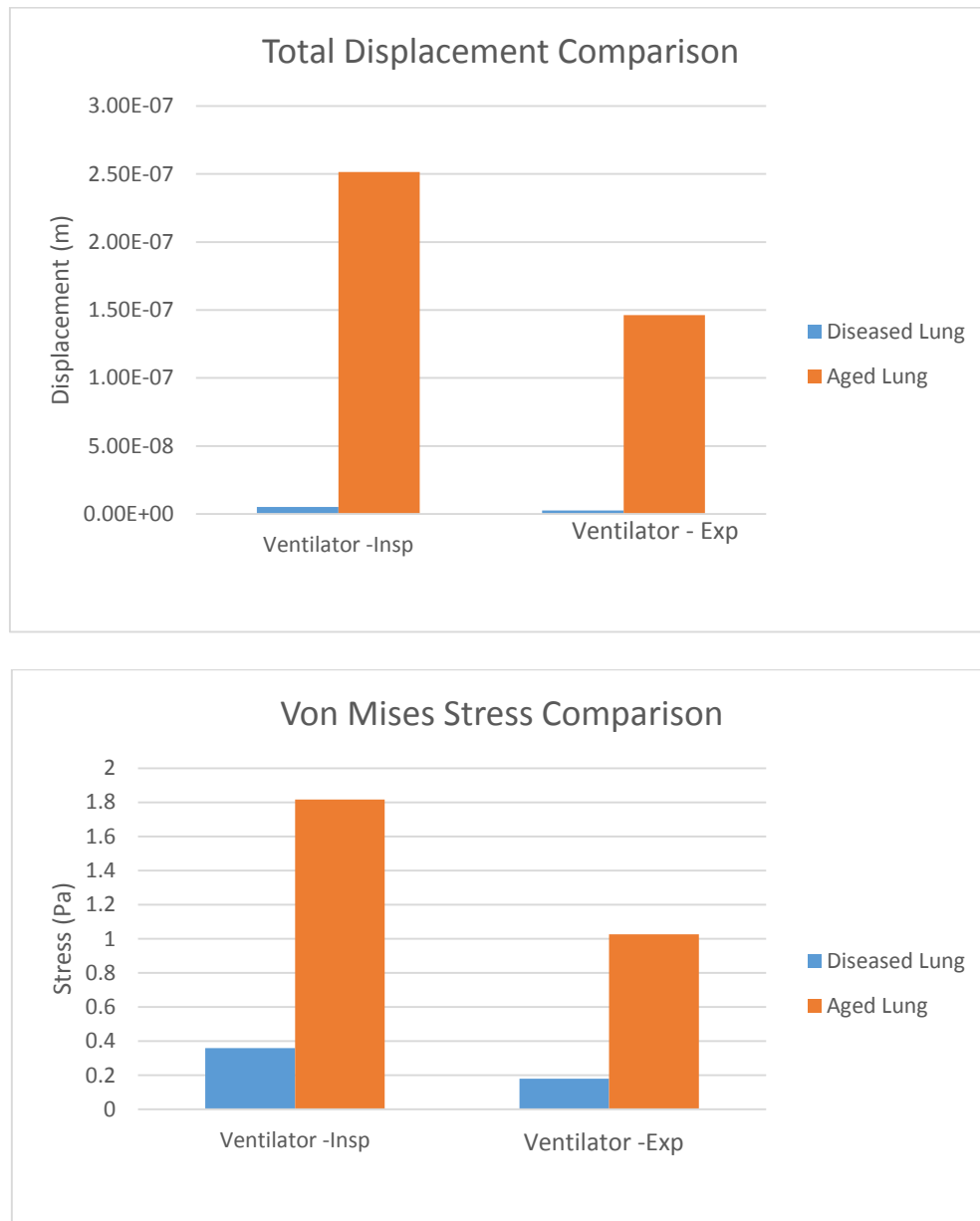


Figure 2.24 Comparison plots of total displacement (top) and von Mises stress (bottom) between NLSC and NLMPC models.

### 2.3 Discussion

The ventilator waveform was applied as an inlet boundary condition to a normal healthy lung model and compared to a normal breathing waveform that was applied as an inlet boundary condition to the normal healthy lung. Results showed that for these cases the ventilator waveform exhibit higher fluid velocities and pressures. Pressures were 26.6% higher in the ventilator case compared to the normal breathing case. Obtained stresses were 25% higher in the ventilator case. Overall, positive peak pressures and stresses show that the alveolar model is undergoing tension throughout the breath cycle both in inspiration and expiration. Malvé et al. [90] performed a study on the human trachea for which a fluid structure interaction was done. They compared the cases of normal breathing to ventilation and showed that the fluid pressures in the trachea were much higher in the ventilator waveform than compared to the normal breathing waveform. Additionally, the displacements during inspiration for ventilation were approximately 71% higher than in normal breathing during inspiration. Furthermore, stresses in their model showed that in the ventilator case stresses were more than 50% higher. Hence, the trends shown in this study are in agreement that ventilation would cause higher displacements and stresses in the lung model, as well as higher fluid pressures.

In the NLSC and NLMPC models results showed that flow intensities for both models were similar while pressures experienced in the NLSC model during inspiration were significantly higher by 67% compared to the NLMPC. At present in the literature no studies have shown incorporation of aging factors into a finite element analysis of a lung alveolar model. As a result lungs become more compliant with decreased elasticity. In the case of the



elderly more compliant lungs allows for an increase of the airspace. In a study by Frank et al [91] on mechanical behavior of the lungs in the elderly, 28 subjects were tested of age 50 years and older. It was noted that the magnitude of changes with ages are generally small, nonetheless those changes were present for which lung compliance was relatively higher in older subjects. In another study by Ionescu et al. [80] the mechanical properties of the respiratory system were studied, particularly in reference to a pathologic case for which there are changes in the physical structure and mechanical properties. Results showed that in the case of disease higher pressures must be applied to obtain the same air flow. This study showed that when modeling disease, if velocity remains is the same pressure must increase to compensate for change in area. As a result this study exhibits the same trend compared to the previously stated study and is therefore in good agreement.

Mechanical stresses and displacements were found to be higher in the NLMPC model than in the NLSC model. Changing the mechanical properties drastically changes the mechanical behavior (i.e. stress/strain). Results showed that stresses were 80% higher in the aged lung when compared to the diseased lung. There are currently no other studies that take into account components of disease and age within one lung alveolar model.

In conclusion, fluid velocities and pressures as well as displacement and stresses were presented for the case of normal healthy lungs, normal lungs with structural changes similar to a diseased lung and normal lungs with mechanical property changes a component of aging. Results determined that in normal healthy lungs under normal breathing and ventilator breathing, fluid forces (i.e. pressures) and mechanical stresses are higher in mechanical ventilation. The NLSC model exhibited higher pressures due to changes in inner

radius. On the other hand, a more compliant lung (NLMPC) exhibited higher displacements and mechanical stresses. Therefore, this study gives a better understanding on how ventilation impacts functional lung units as well as how components of age and disease are incorporated into ventilation impact. Future work can be done by extending the analysis time to account for longer breath cycles for which higher flows can matriculate to the individual alveoli sacs. This will aid in the understanding of the long term impact of mechanical ventilation.

## **CHAPTER 3**

### **Alveolar Tissue Analysis**

#### **3.1 Introduction**

The lungs are naturally comprised of walls that are structurally suited to carry out the everyday function of gas exchange as one inhales and exhales. This study focuses on the walls of individual alveoli that are commonly referred to as alveolar septa which are comprised of thin permeable membranes, on the order of 1 – 5  $\mu\text{m}$  [41]. The structure of the alveolar septa has been of significant importance to researchers in understanding the mechanics of gas exchange. Further investigation within the structure of the alveolar septa has been researched for many decades with studies in the late 1950's by Karez [6] who determined the wall is comprised of a continuous endothelial cell layer, basement membrane, and epithelial cell layer. Several studies emerged later, particularly by Weibel [16, 17, 18, 19] that focused on the morphology of lung parenchyma which included alveoli and the walls that separate them. Other studies focused on the interalveolar septum specifically the basement membrane [75]. Aside from the above-mentioned layers, an additional layer was defined as the alveolar liquid lining layer. This layer is responsible for stabilizing alveoli

from collapse during inflation in conjunction with the surfactant produced and secreted by alveolar epithelial II cells. Therefore, the four layers comprising the alveolar wall consist of the endothelial cell layer, basement membrane, epithelial cell layer, and the alveolar lining liquid layer that forms the air liquid interface. From these studies it is pertinent that there lacks a theoretical, investigative model that would allow one to understand how local deformation in the walls is translated from the organ to the tissue level contained within the lung. Additionally, knowledge that pertains to such deformations at the alveolar region as a result of introducing mechanical ventilation has currently been highly demanded. Therefore, this study will focus on the modeling, observation and analysis of mechanically induced stresses and strains prompted by mechanical ventilation on the alveolar septal tissue.

### **3.2 Methods**

The geometric model used for this study is illustrated in figure 3.1 and was created via the SolidWORKS® 2013 commercial software. The alveolar septa was modeled as a heterogeneous tissue denoting each layer as previously defined. Each layer has varied thickness which is shown in table 3.1. The material properties for each layer are distinct and can be found in table 3.2. Every individual layer is modeled with hyperelastic behavior that exhibits a nonlinear material behavior. The Neo Hookean model was additionally utilized to describe the material characteristics of the septal tissue. Furthermore, to be consistent the mechanical properties utilized in the normal lung model with mechanical property change as a component of aging was also used in this study. Table 3.3 shows the material parameters utilized for defining the Neo Hookean model for this analysis. The tissue was meshed with

a hexahedral mesh containing 209600 elements and 159378 nodes. Figure 3.2 displays the meshed model with applied boundary conditions.

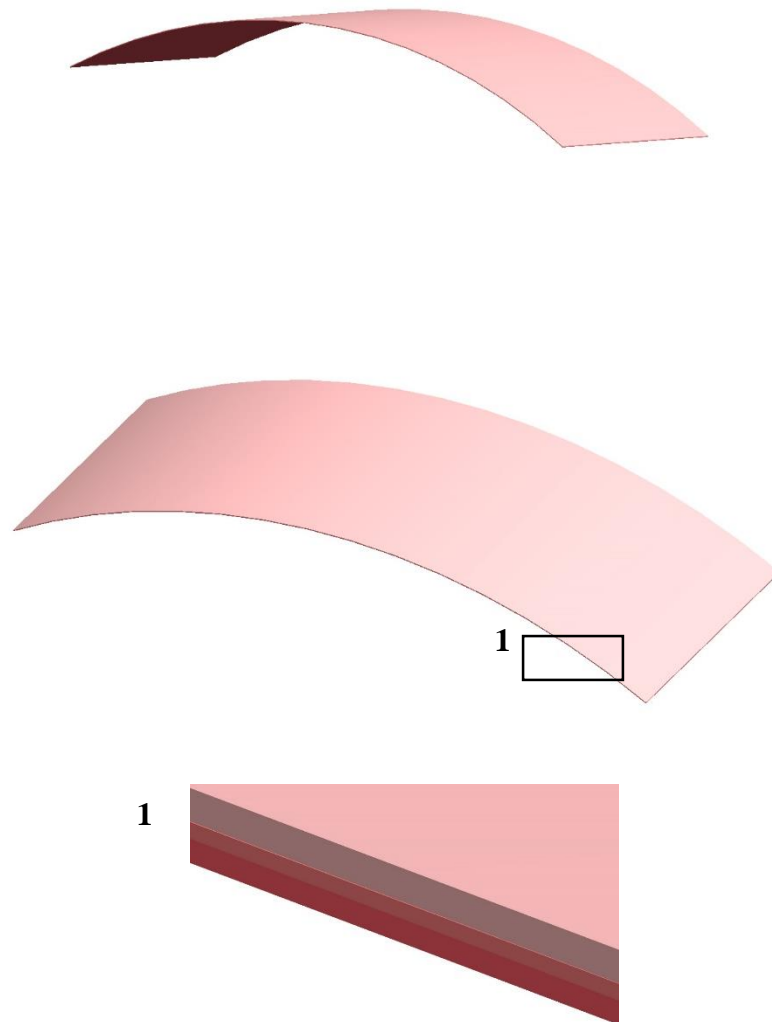


Figure 3.1 3-Dimensional model of the alveolar tissue geometry in various views.

Table 3.1 Dimensions for thickness of alveolar septal layers

Layer	Dimensions ( $\mu\text{m}$ )
Endothelial Cell Layer	0.2 [76]
Basement Membrane	0.1 [77]
Epithelial Cell Layer	0.15 [78]
Alveolar Lining Liquid Layer	0.2 [79]
<b>Other Tissue Dimensions</b>	
Total length (m)	0.0025 [87]
Total width (m)	0.001 [87]

Table 3.2 Material property characteristics for each layer of the tissue model.

Layer	Elastic Modulus (Pa)	Poisson Ratio
Endothelial Cell Layer	3.5 E6 [80]	0.40 [81]
Basement Membrane	3.0 E6 [82]	0.47 [83]
Epithelial Cell Layer	0.45 E3 [84]	0.30 [85]

Table 3.3 Material property characteristics utilized for the tissue analysis.

Layer	Shear Modulus (Pa)	Bulk Modulus (Pa)
All	330.5	2588.96

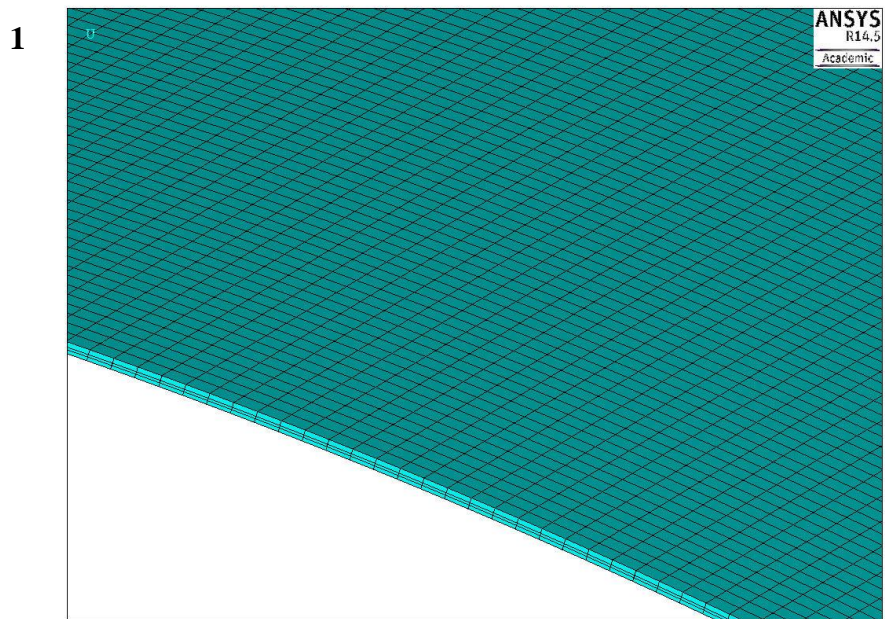
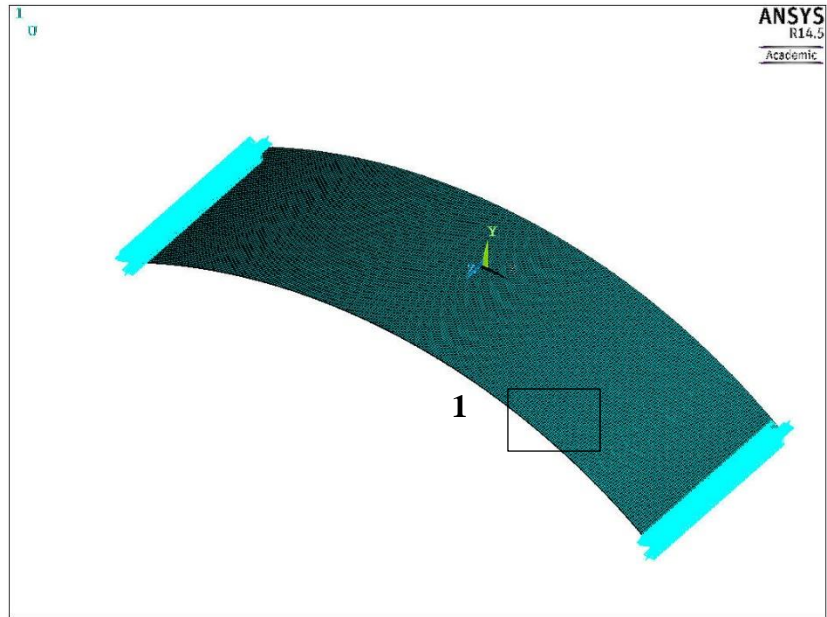


Figure 3.2. 3-Dimensional tissue model with hexahedral mesh and applied boundary conditions displayed.

In terms of boundary conditions, displacements were applied radially to the tissue model. Specifically, the displacements studies that were obtained from the normal lung model with mechanical property changes during inspiratory flow were utilized. These boundary conditions were then applied to observe how the tissue would deform over time. A transient analysis was specified for the model with a time step of 0.025s to be consistent with parameters utilized in previous model studies.

### **3.3 Results**

#### ***3.3.1 Total Displacements***

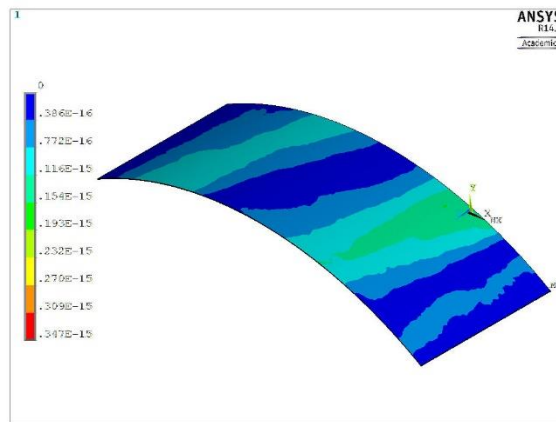
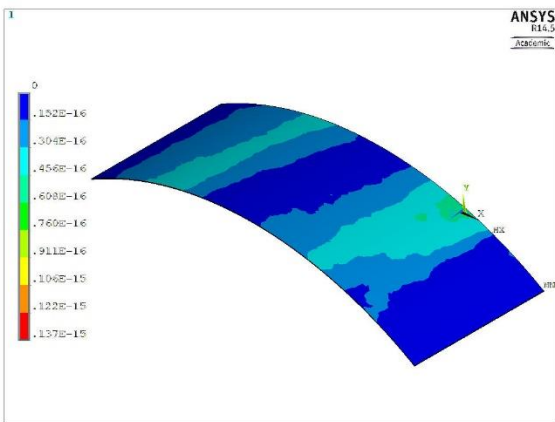
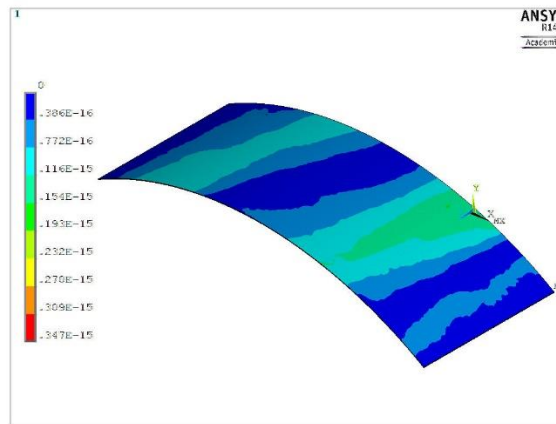
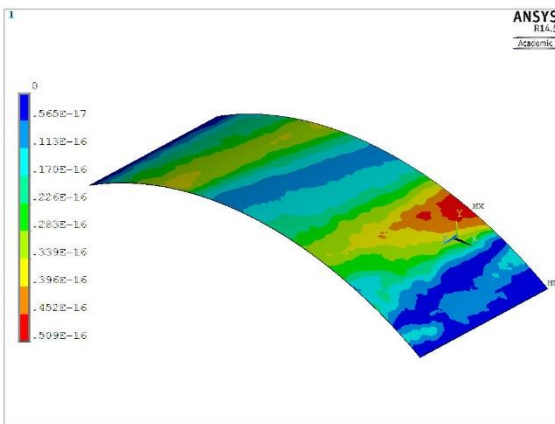
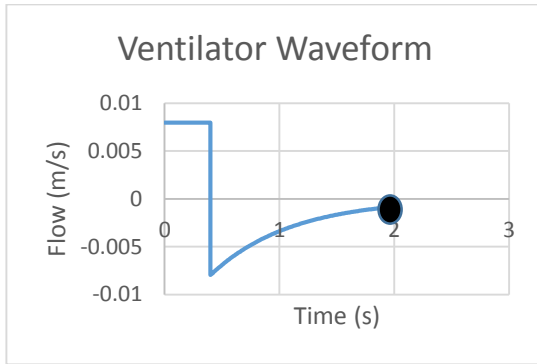
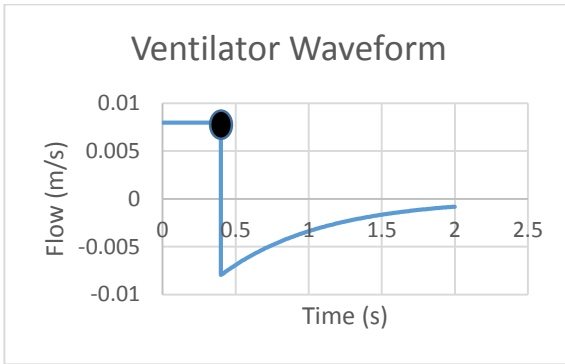
Figure 3.2 (a) and (b) illustrates the total mesh displacement with contours of deformation that exists for each tissue layer at peak inhalation and exhalation. Both figures show that the entire tissue is being displaced while exhibiting a higher range of displacement magnitudes and distribution during expiration in each layer. These results further proves that during exhalation the tissue is being displaced more over a breathing cycle.

#### ***3.3.2 Mechanical Stresses***

The mechanical stresses that were analyzed included the von Mises stress and the first, second, and third principal stresses. Figures 3.3-3.7 display the contours for each of these stresses during inhalation and exhalation corresponding to each tissue layer. These figures illustrate that in each case higher stress distributions exist during expiration. Results from this study determined that the tissues exhibited locations where high concentrations of



stress points occurred. These points along the tissue are where the majority of the displacement stresses are concentrated.



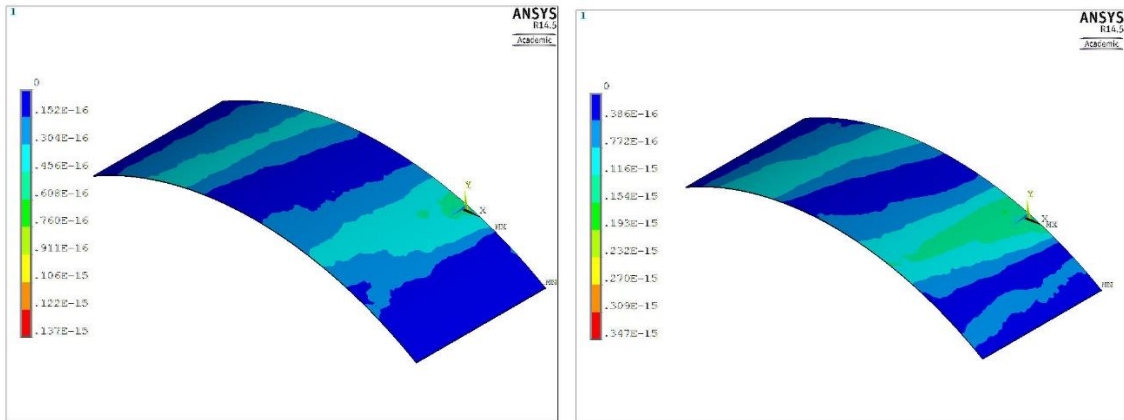


Figure 3.3 Contours of total displacement in each tissue layer endothelial cell layer (top), basement membrane (middle) and epithelial cell layer (bottom) at 0.4s (left) and 2s (right).

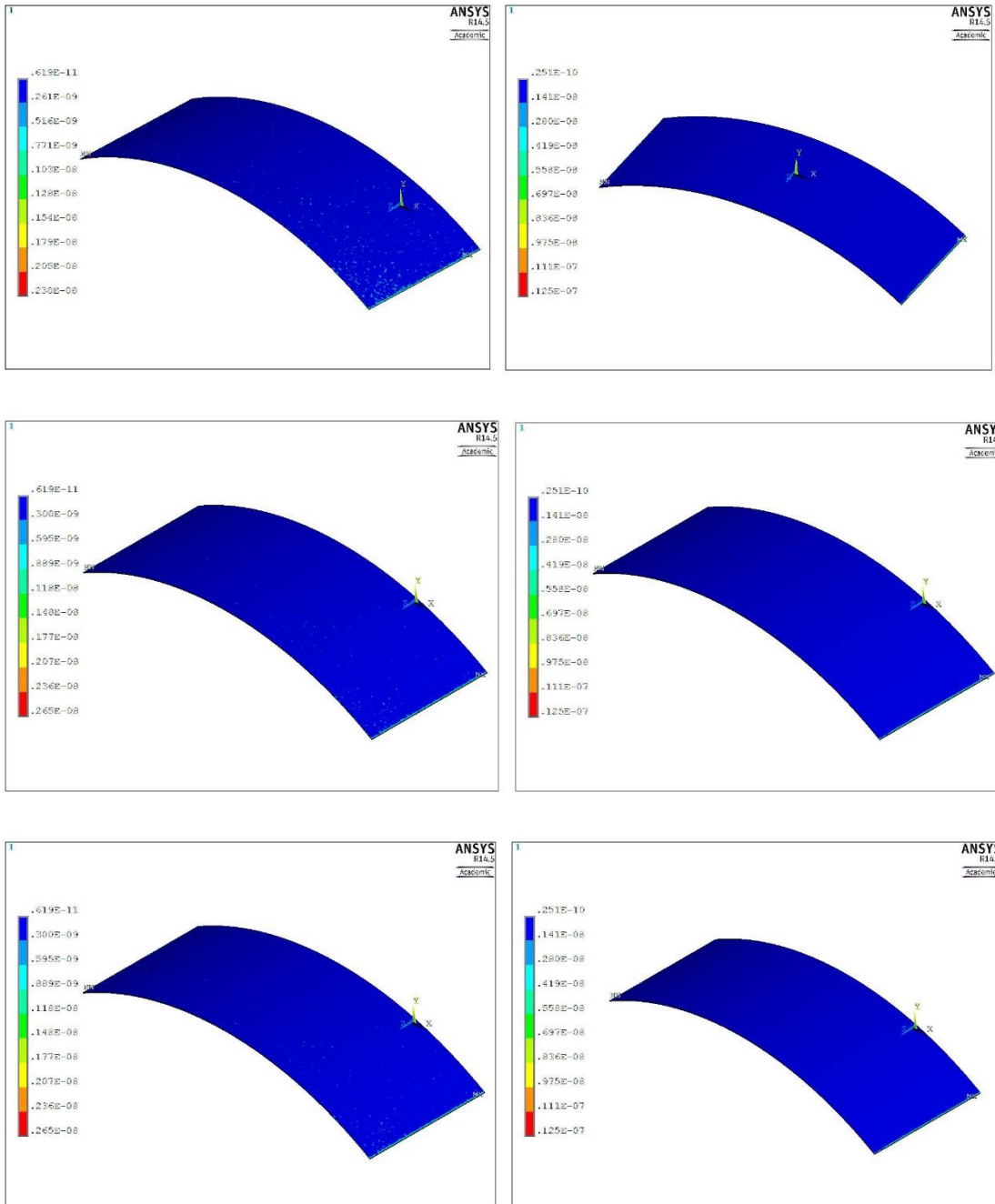


Figure 3.4 Contours of von Mises stress in each tissue layer endothelial cell layer (top), basement membrane (middle) and epithelial cell layer (bottom) at 0.4s (left) and 2s (right).

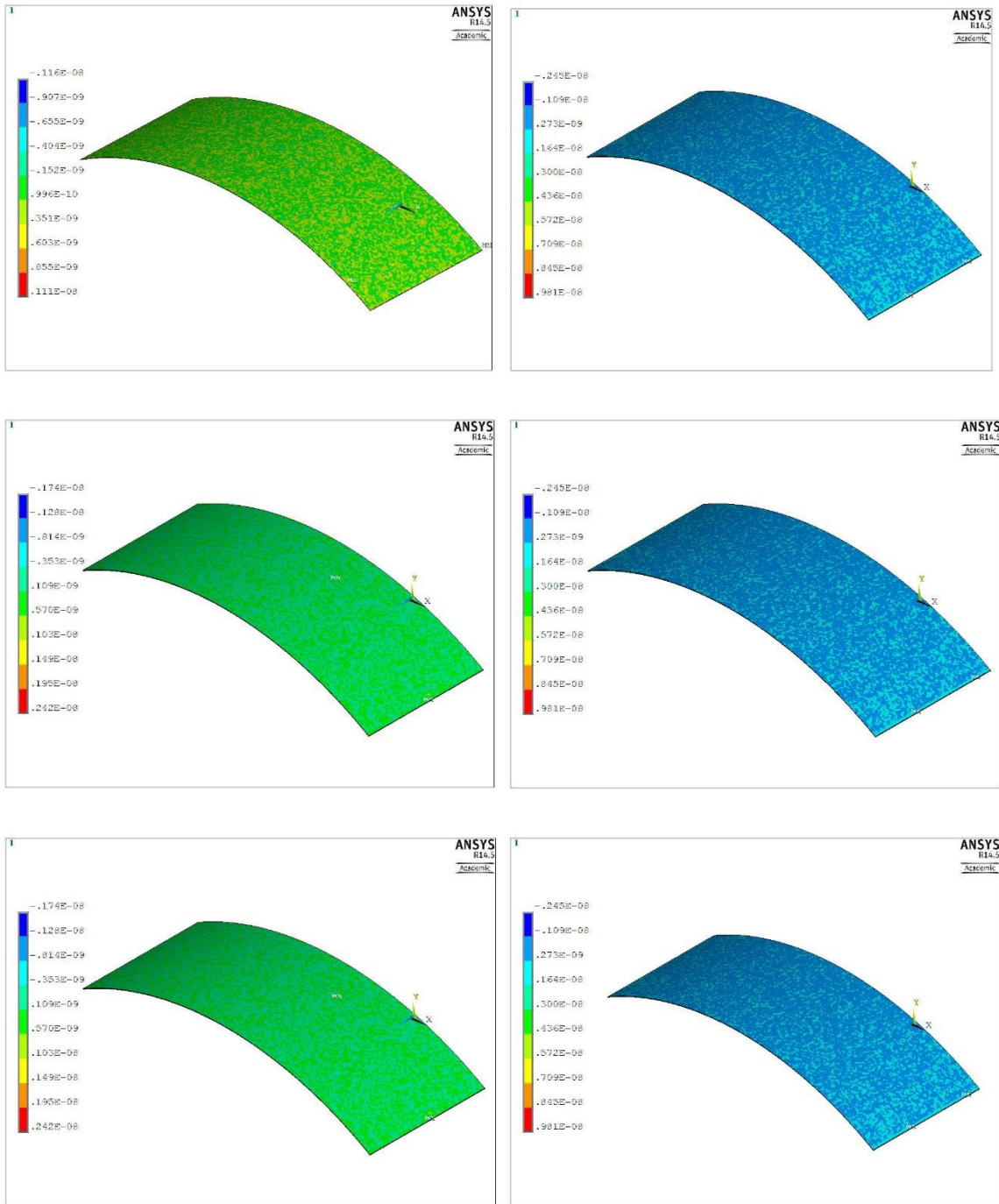


Figure 3.5 Contours of first principal stress in each tissue layer endothelial cell layer (top), basement membrane (middle) and epithelial cell layer (bottom) at 0.4s (top) and 2s (bottom).

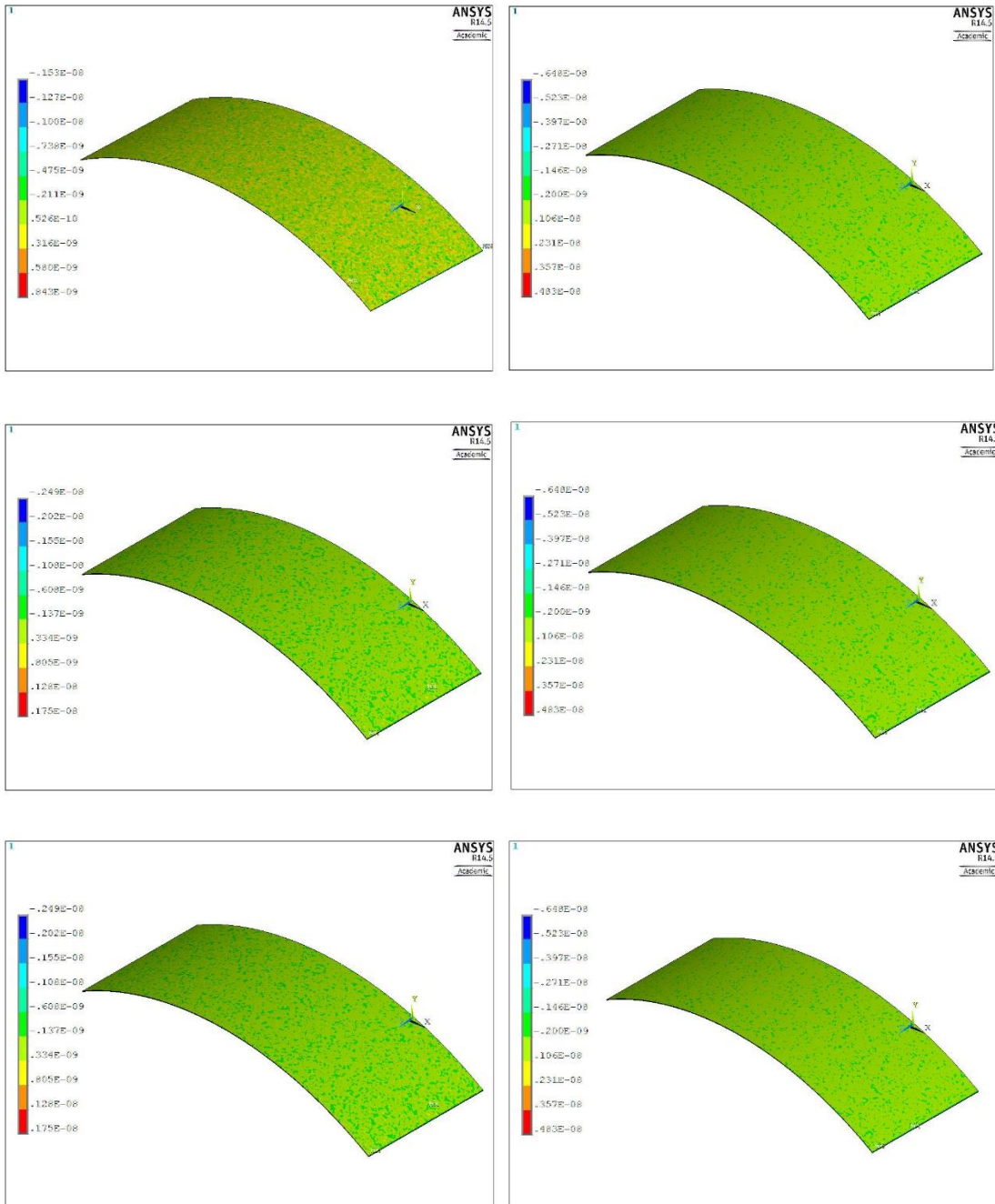


Figure 3.6 Contours of second principal stress in each tissue layer endothelial cell layer (top), basement membrane (middle) and epithelial cell layer (bottom) at 0.4s (top) and 2s (bottom).

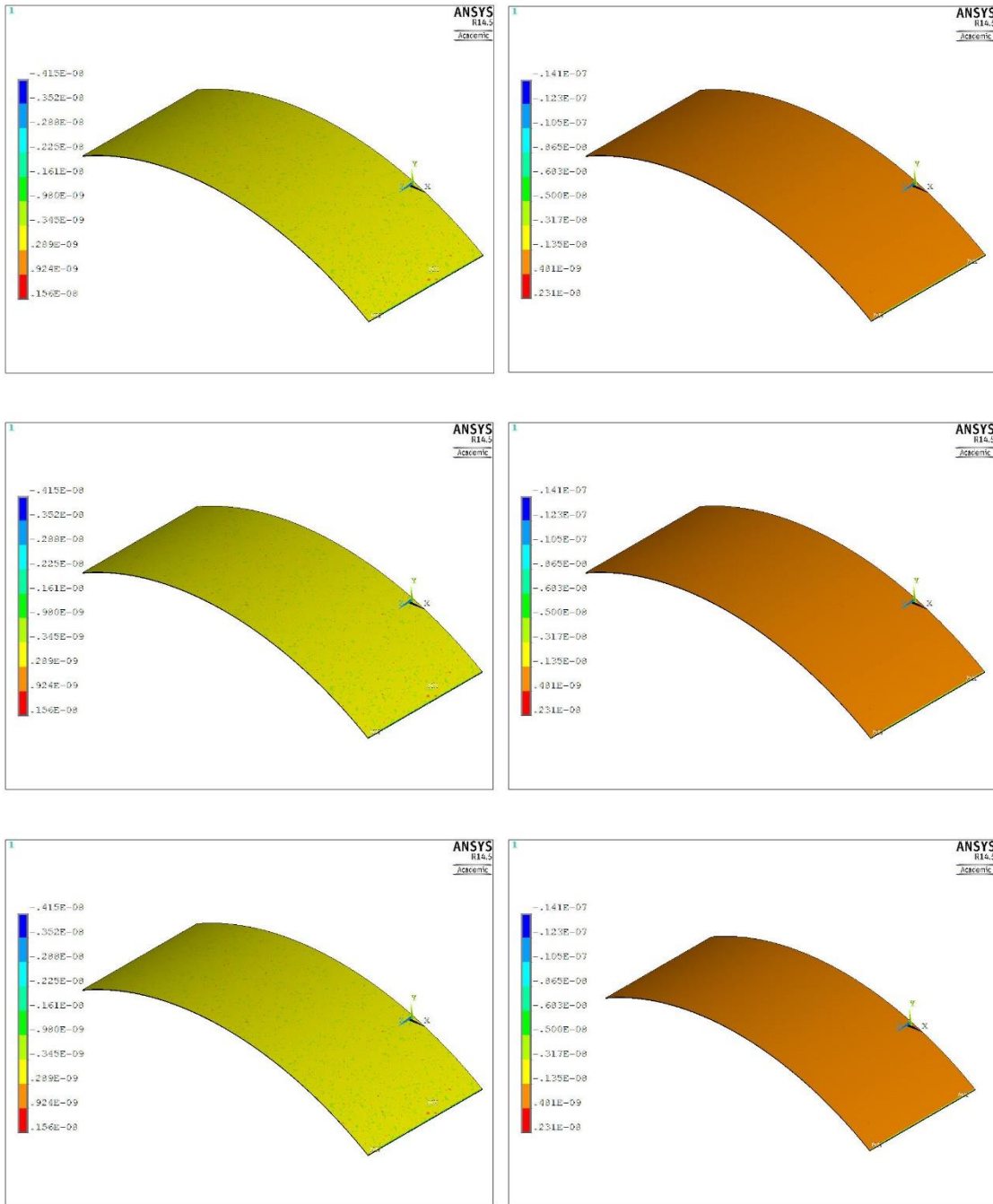


Figure 3.7. Contours of third principal stress in each tissue layer endothelial cell layer (top), basement membrane (middle) and epithelial cell layer (bottom) at 0.4s (top) and 2s (bottom).

Comparing the various layers of the tissue model it was determined that epithelial cell layer contains the highest amount of stress distribution. This indicates that this tissue layer experiences higher mechanical forces and undergoes deformation more rapidly as compared to the other tissue layers. Figure 3.8 depicts a comparison plot of the various stresses during inspiration and expiration. These plot results further prove that the stress magnitudes during exhalation are greater.

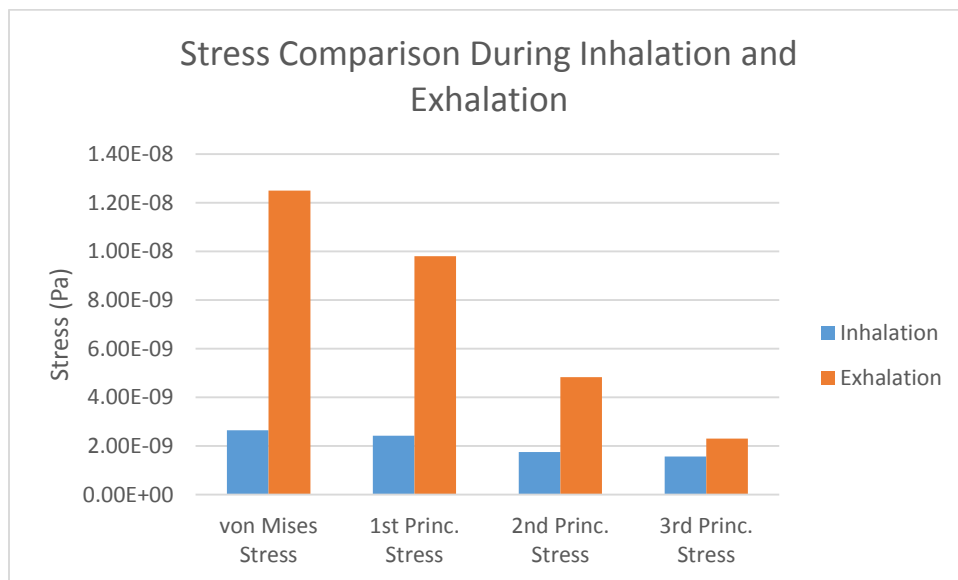


Figure 3.8 Comparison plot of various stresses during inspiration and expiration.

### 3.4 Discussion

This research focused on the development and analysis of an alveolar tissue to perform a structural analysis study that investigated deformations within a series of tissue layers. Introducing mechanical displacements created a multi-scale connection between the organ level models that allowed results to be obtained for the displacements and stresses. Results

showed that during expiration the tissue was displaced over a greater magnitude during the breath cycle. It must be noted that expiration accounted for the majority of higher stresses. A study by Gefen et al. [79] analyzed the stress distribution in a two-dimensional alveolar geometry comparing a normal case versus emphysema. This study is not suitable for comparison as the model is two-dimensional. Future work will need to be investigated to validate the theoretical results obtained through experimentation. Additionally, it may be beneficial to focus on the characterization of specific non-linear elastic properties for each layer to assess the nonlinear deformation behavior of the tissue. These research areas would expand this research study to align the model in terms of the physiological behavior.



## **CHAPTER 4**

### **Comprehensive Modeling**

#### **4.1 Introduction**

Earlier chapters discussed several analyses that were performed to observe the variations in mechanical forces as a result of each condition. In many circumstances these conditions are not mutually exclusive and in fact are concurrent. Of particular importance are the cases involving structural changes and mechanical property change which are the most severe and life threatening incidents regarding the utilization of mechanical ventilation. Approximately 52.2% of patients in critical care on ventilators are over the age of 65 and pulmonary disease is the second highest among patients with comorbidities [86]. Diseases such as asthma and COPD cause structural changes in the airways that are very pronounced. Specifically, asthma significantly reduces the radius of airways due to mucus and inflammation obstructing the airway. On the other hand, tissue destruction and increased resistance are found in the case of COPD where advanced stages of COPD, cause changes in the mechanical properties of lung tissue such as an increase in elastic modulus (i.e. increased stiffness) [80]. Therefore with instances of mechanical ventilation being more

tailored to older patients suffering from diseases such as COPD and asthma, this study provided a more in depth understanding on how these combined effects influence the mechanical behavior of the lung.

## **4.2 Methods**

Utilizing the normal lung with a structural change, that is a 50% increase in wall thickness and 50% decrease in radius and applying the aged material properties for a 70 year old patient, both adapted from chapter 2, a comprehensive model was created. This analysis incorporated the same conditions as those done in previous chapters which included a transient analysis with a time step of 0.025s and a ventilator waveform applied at the inlet of the fluid model. No slip boundary conditions were applied to the wall of the fluid and a zero displacement boundary condition was applied at the ducts of solid model.

## **4.3 Results**

As in previous chapters the results for this analysis will be analyzed at times 2.2s and 2.285s for the same reasons mentioned in earlier chapters. Results are shown in the form of fluid velocities and pressures as well as total displacements and stresses. Additionally, results from this comprehensive lung model are then compared with the normal lung model utilizing the ventilator waveform.

### ***4.3.1 Pressures and Velocities***

The fluid velocities and pressures can be found in figure 4.1 and 4.2. A maximum velocity of 1.496 cm/s was obtained with a maximum pressure of 0.33 Pa. In both cases maximum values are found near the inlet of the model. The velocity magnitudes also show that the velocity distribution is relatively higher (0.4% difference) within the comprehensive model than the normal lung model. On the other hand, the pressure in the comprehensive model is 66.2% higher than the normal lung model.

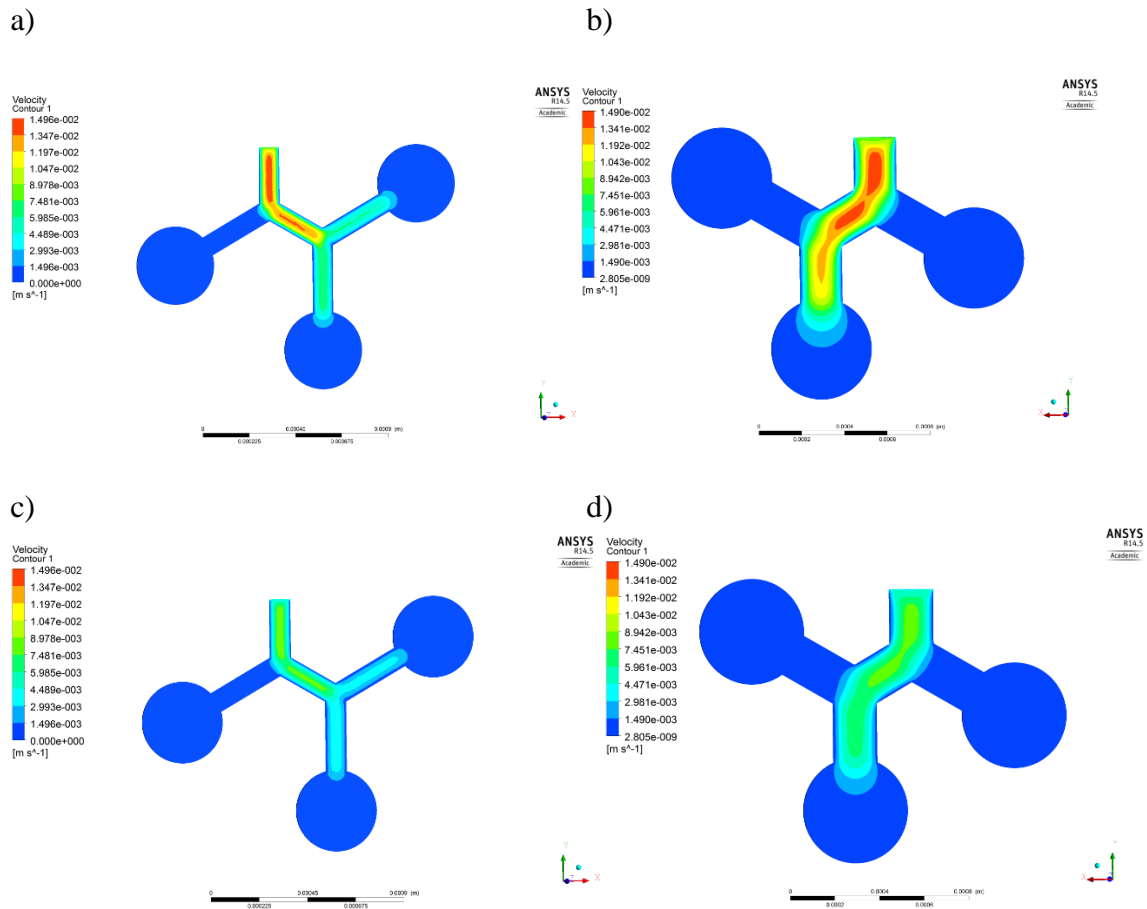
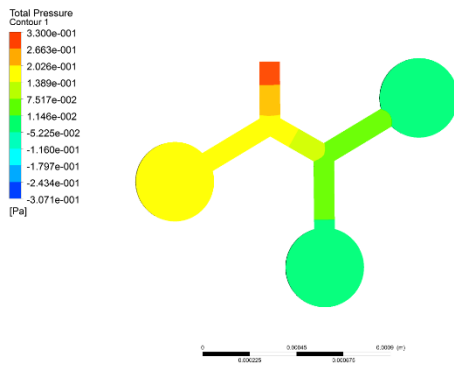
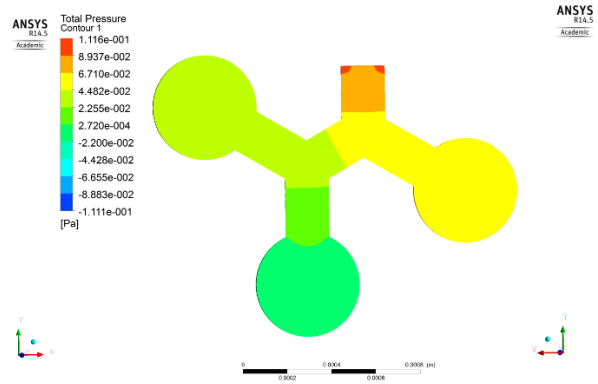


Figure 4.1 Contours of velocity magnitude for the a) comprehensive lung model at 2.2s, b) normal lung model at 2.2s, c) comprehensive lung model at 2.285s, and d) normal lung model at 2.285s with ventilator waveform.

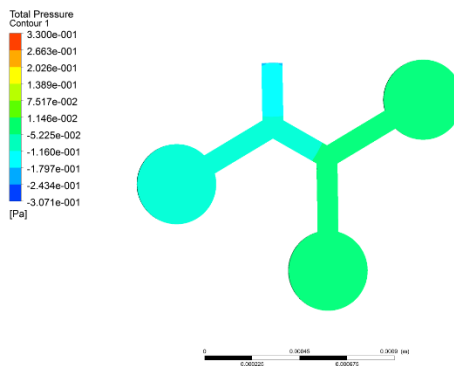
a)



b)



c)



d)

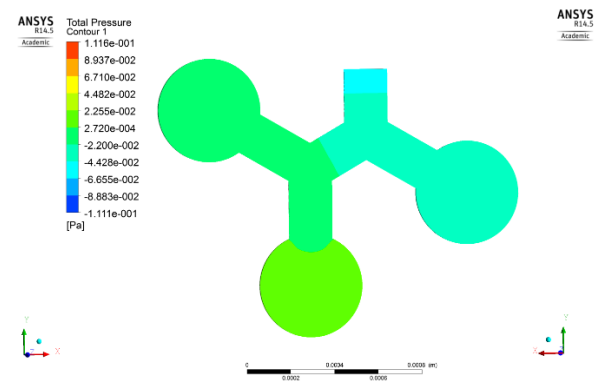


Figure 4.2 Contours of pressure magnitude for the a) comprehensive lung model at 2.2s, b) normal lung model at 2.2s, c) comprehensive lung model at 2.285s, and d) normal lung model at 2.285s with ventilator waveform.

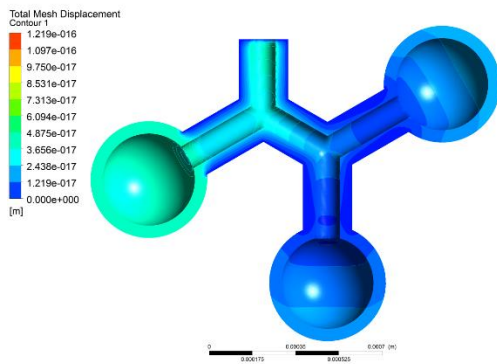
### ***4.3.2 Structural Displacements and Stresses***

Results from the solid analysis model were analyzed in terms of total displacements, von Mises stress, and the first, second and third principal stresses. Figure 4.3 displays the contour plots of displacement during inhalation and exhalation for both the comprehensive and normal lung models. Displacement in this analysis were very minor on the order of  $10^{-16}$  for the comprehensive lung model. On the other hand, in the normal lung model case the displacements are on the order of  $10^{-8}$ . Thus, the normal lung model is displaced more readily during mechanical ventilation than the diseased model. A maximum von Mises stress of 0.483 Pa was obtained in the comprehensive model and is shown in figure 4.4. When comparing the von Mises stress in the comprehensive model to the normal lung model it shows that the normal lung model experienced 71.9% higher stress. Figure 4.5, 4.6 and 4.7 shows the first, second and third principal stresses obtained in the model during inhalation and exhalation. Contour plots show larger distributions of those stresses occurring during exhalation in the comprehensive model but during inhalation for the normal lung model. Furthermore, the normal lung model shows stresses that are 76.7%, 93.4% and 89.7% higher for the first, second and third principal stresses, respectively, compared to the comprehensive model.

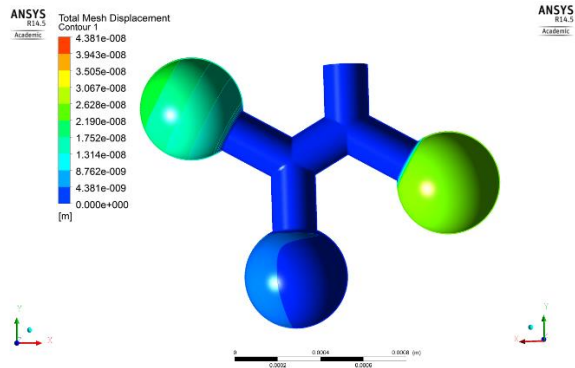
Finally, figure 4.8 illustrates the comparisons between the normal lung with structural changes (NLSC), normal lung with mechanical property changes (NLMPC), comprehensive and normal lung models. The plots show that the higher stresses are obtained in the NLMPC model. Specifically, taking into consideration the von Mises stress, the NLMPC model has an 80.2% higher magnitude compared to the NLSC lung and a 73.2%

higher magnitude than the comprehensive model. However, when the normal lung model is compared to the other models, there is only a 5% difference in von Mises stresses in the NLMPC model for both inhalation and exhalation. On the other hand, the von Mises stress during inhalation for the normal lung model is 79.2% higher and 71.9% higher than the NLSC and comprehensive models, respectively. The first principal stress magnitude during inhalation in the NLMPC is also higher than those obtained in the NLSC, comprehensive and normal lung models. Specifically, the first principal stress in the NLMPC is 81.7%, 77.8% and 4.89% higher than the NLSC, comprehensive and normal lung models, respectively.

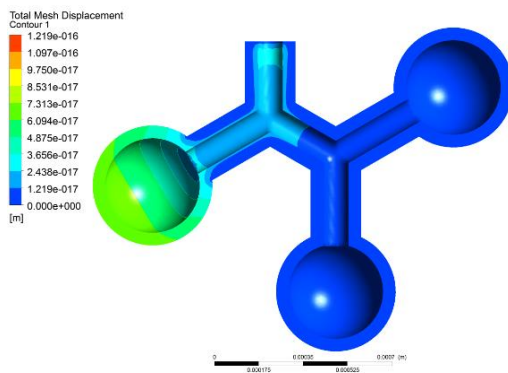
a)



b)



c)



d)

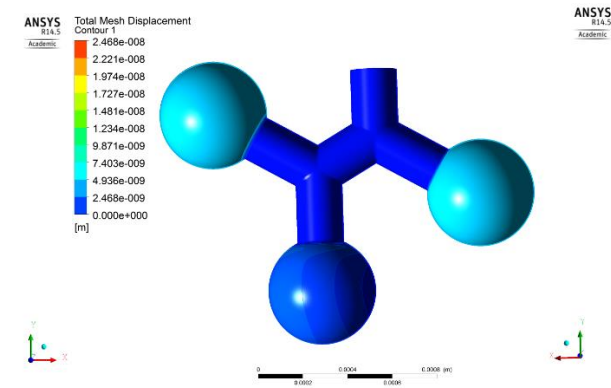
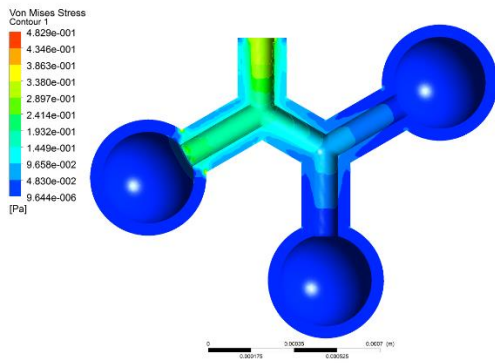


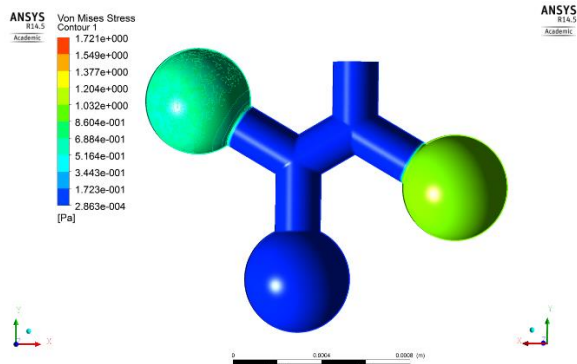
Figure 4.3 Contours of total mesh displacement magnitude for the a) comprehensive lung model at 2.2s, b) normal lung model at 2.2s, c) comprehensive lung model at 2.285s, and d) normal lung model at 2.285s with ventilator waveform.



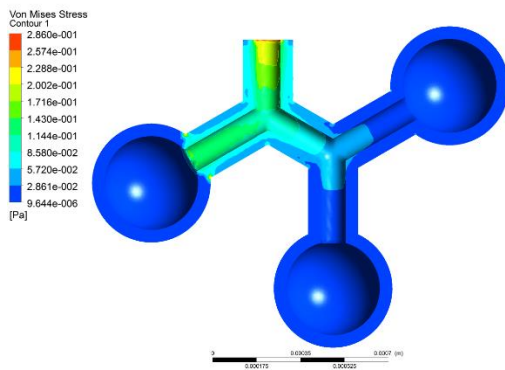
a)



b)



c)



d)

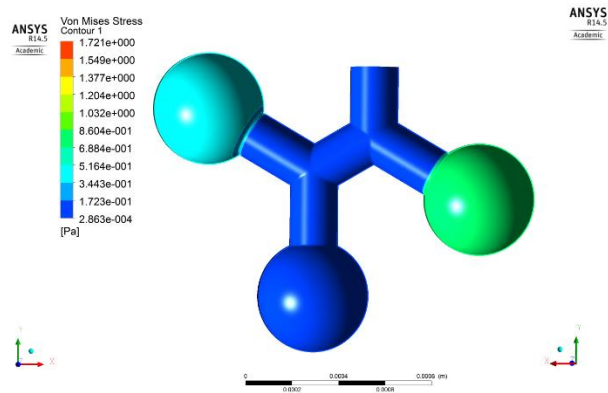


Figure 4.4 Contours of von Mises stress magnitude for the a) comprehensive lung model at 2.2s, b) normal lung model at 2.2s, c) comprehensive lung model at 2.285s, and d) normal lung model at 2.285s with ventilator waveform.

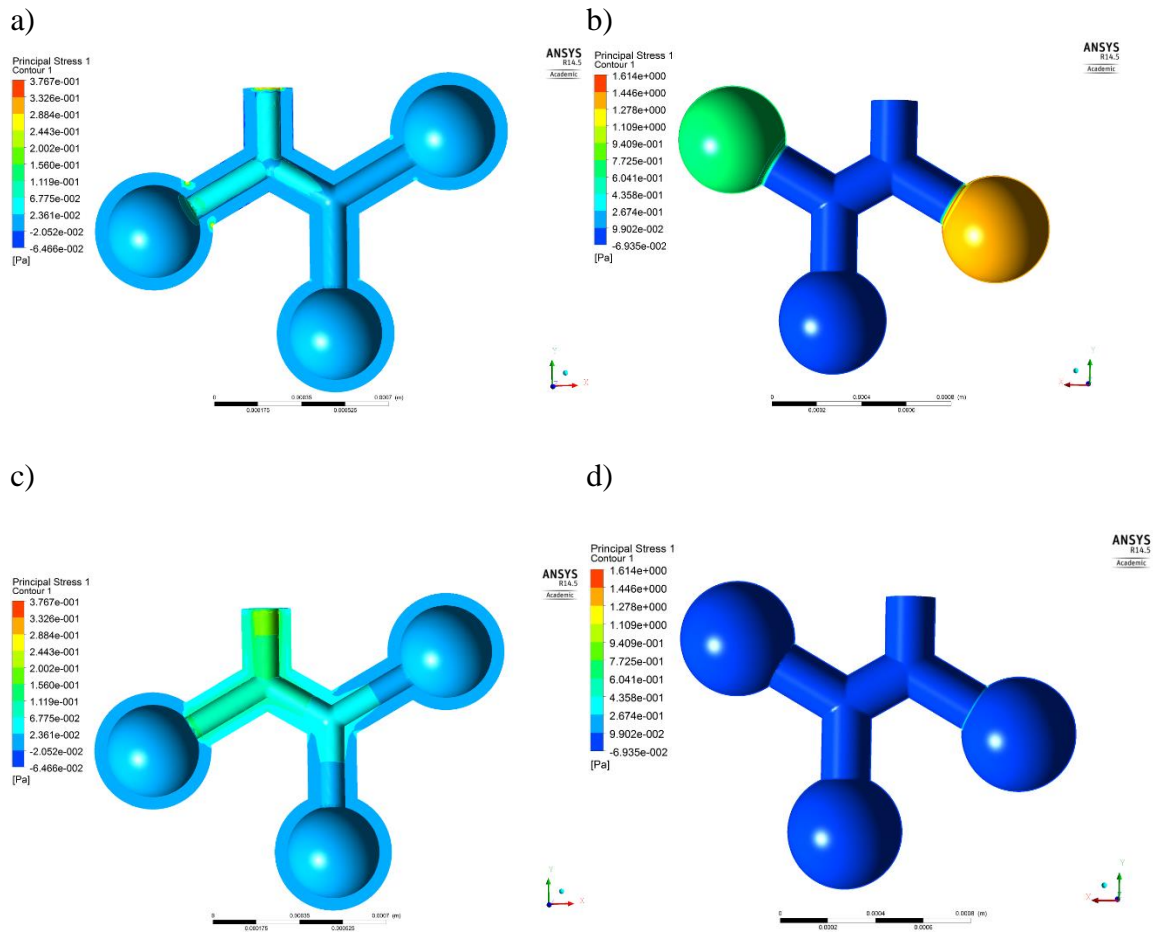


Figure 4.5 Contours of first principal stress magnitude for the a) comprehensive lung model at 2.2s, b) normal lung model at 2.2s, c) comprehensive lung model at 2.285s, and d) normal lung model at 2.285s with ventilator waveform.

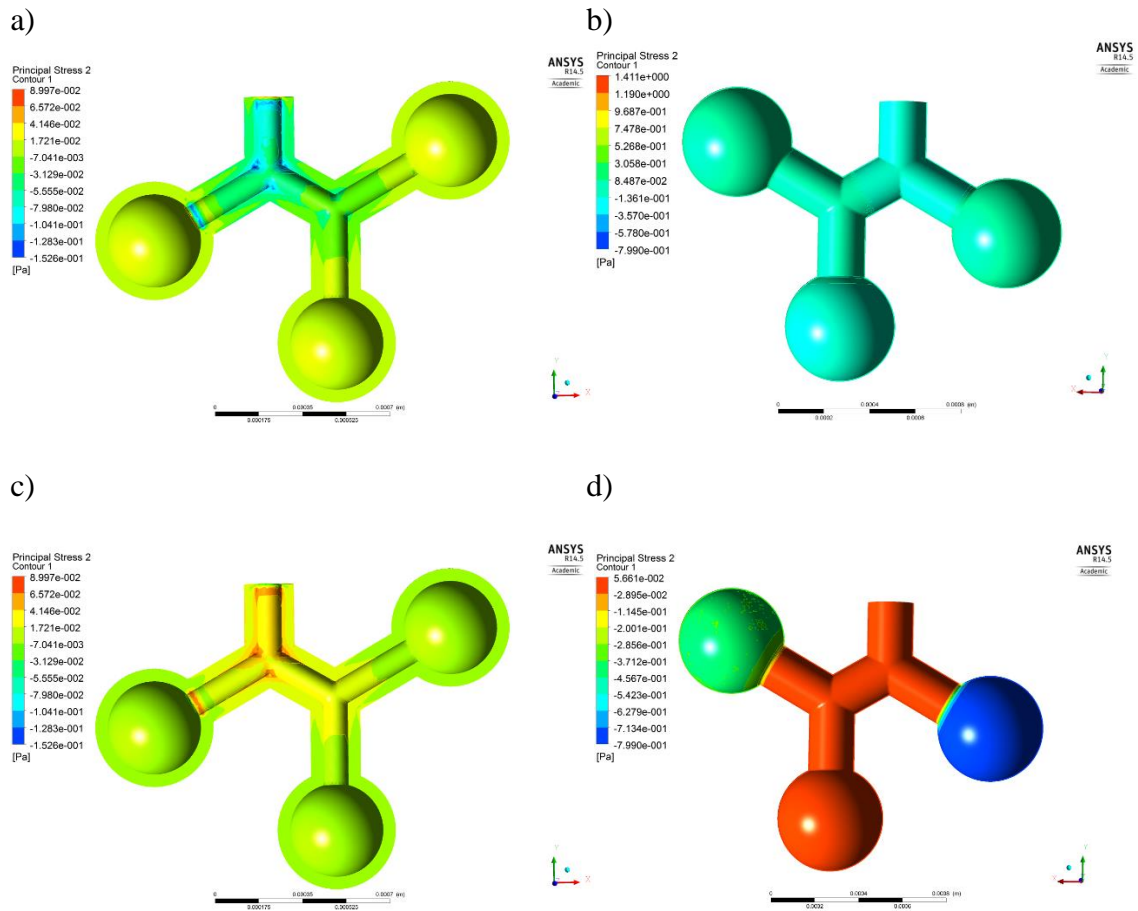


Figure 4.6 Contours of second principal stress magnitude for the a) comprehensive lung model at 2.2s, b) normal lung model at 2.2s, c) comprehensive lung model at 2.285s, and d) normal lung model at 2.285s with ventilator waveform.

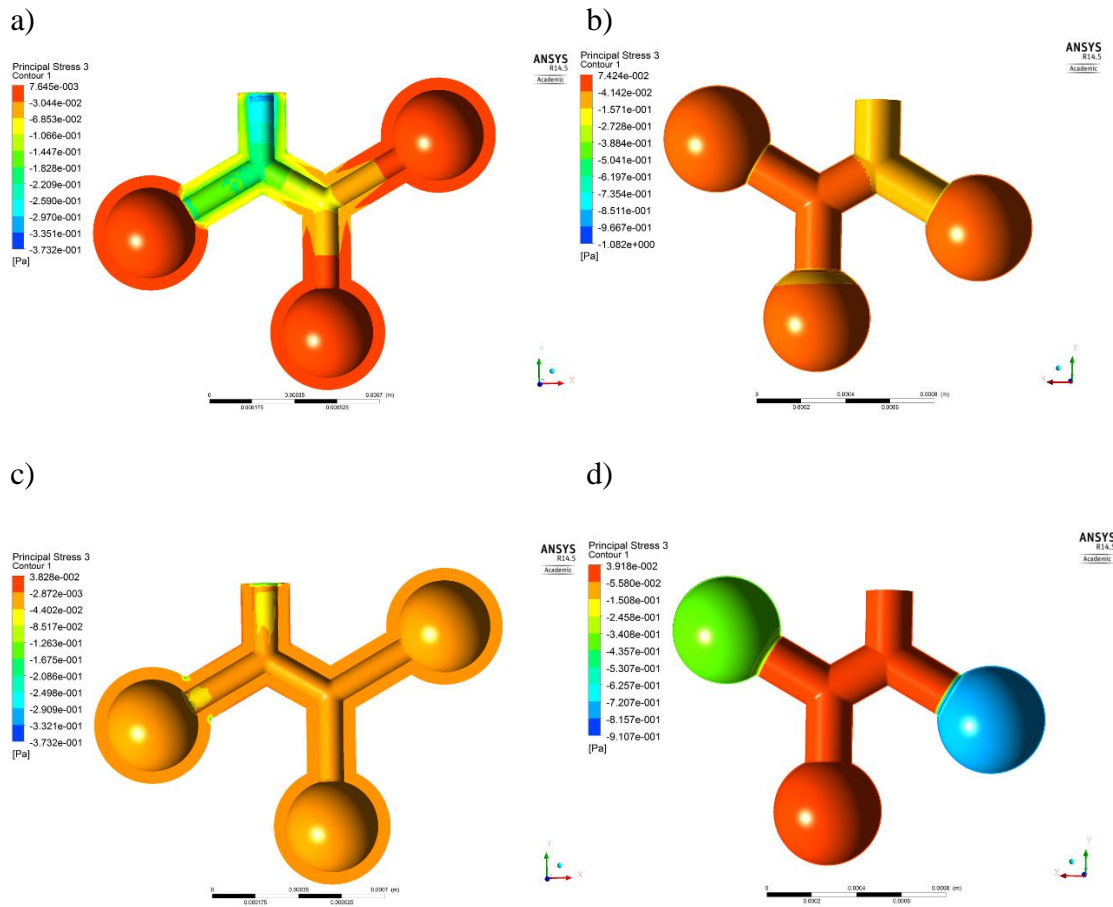


Figure 4.7 Contours of third principal stress magnitude for the a) comprehensive lung model at 2.2s, b) normal lung model at 2.2s, c) comprehensive lung model at 2.285s, and d) normal lung model at 2.285s with ventilator waveform.

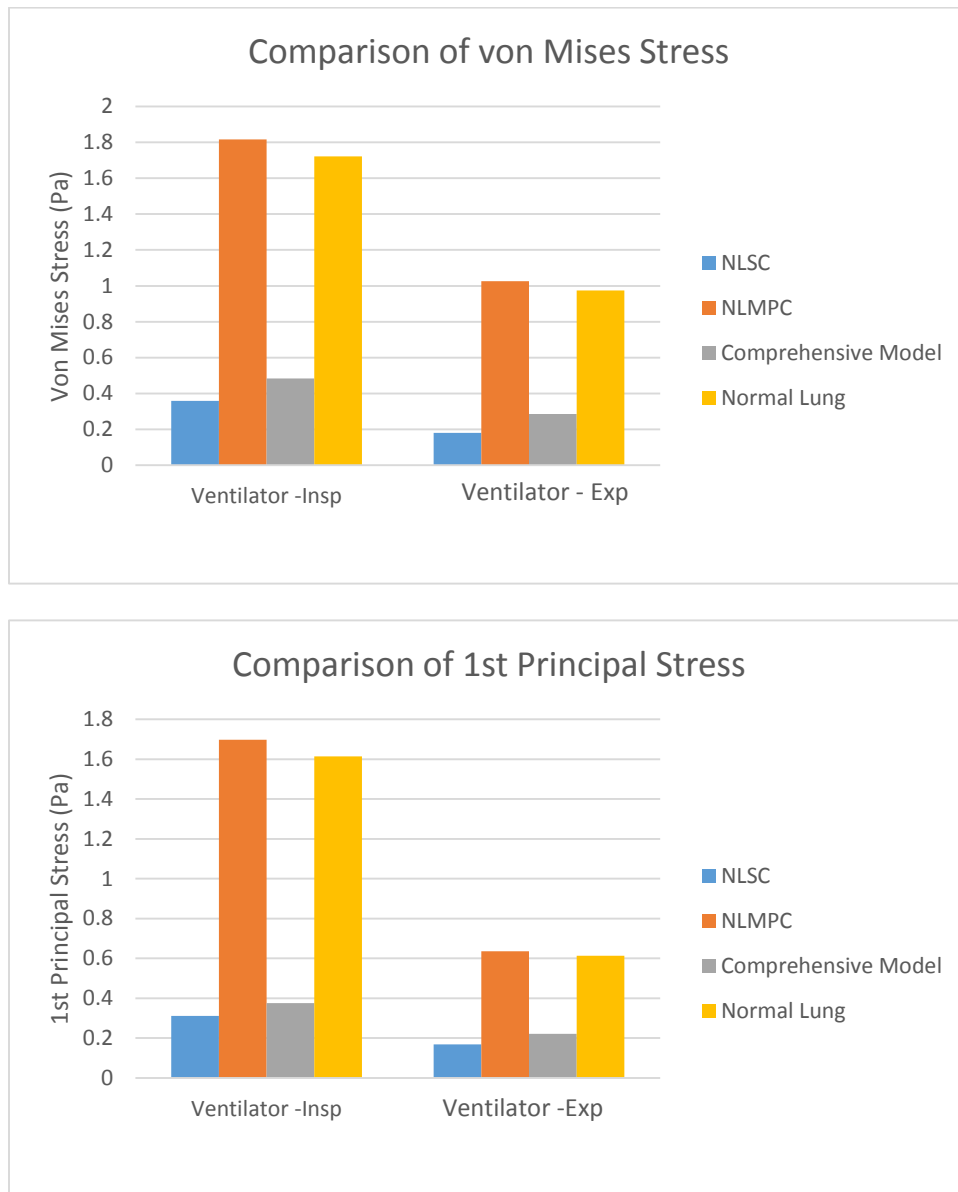


Figure 4.8 Comparison plots of the von Mises stress (top) and first principal stress (bottom) for the NLSC, NLMPC, comprehensive, and normal lung models with ventilator waveform.

#### 4.4 Discussion

In this analysis changes to the inner radius as well as elastic modulus were performed in order to account for disease and age respectively. The inner radius was decreased by 50% while the elastic modulus was varied based on equations relative to age, see Equations. 2.6 – 2.9. Many of the patients undergoing ventilation are over the age of 65 and suffer more commonly from some type of lung disease. Due to this observation a model was created that takes into account both aspects of age and disease yielding reasonable approximations of the mechanical behavior as a result of mechanical ventilation. Results showed that a maximum flow of 1.65 cm/sec was found near the inlet. Moreover, the velocity magnitude in the comprehensive model compared to the normal lung model was quite small, 0.4%, hence the flow magnitude was relatively constant between both models. The total pressure maximum was found to be 0.33Pa, nevertheless when compared to the normal lung this pressure was 66.2% higher. A maximum von Mises stress of 0.829 Pa was shown to occur during inspiration. When comparing this model to the individual NLMPC, NLSC and normal lung cases, figure 4.4-4.7 illustrates that the stresses in the normal lung model greatly exceed those in the comprehensive model in terms of magnitude and distribution. Figure 4.8 shows that the von Mises stress and first principal stress in the NLMPC and normal lung models are more than 70% higher than those obtained in the comprehensive model. Specifically, stresses in the NLMPC model are 73.4% higher than in the comprehensive model and stresses in the normal lung model are 71.9% higher than the comprehensive model. Alternatively, the stresses in the comprehensive model are greater than those in the NLSC model by 25.7%. Furthermore, figure 4.9 shows that the alveolar pressures in the NLSC and

the comprehensive model show little to no variation. Therefore, it can be deduced that in a lung model with components of aging included along with the structural changes fluid pressures and velocities are greatly impacted by the physical changes to the lung as opposed to changes in mechanical properties. Conversely, mechanical strain/stresses are impacted more by mechanical property changes than physical changes to the structure. However, the thickening of the walls which makes lung tissue stiffer and at the same time a decrease in elastic modulus making the walls more compliant are both working against each other.

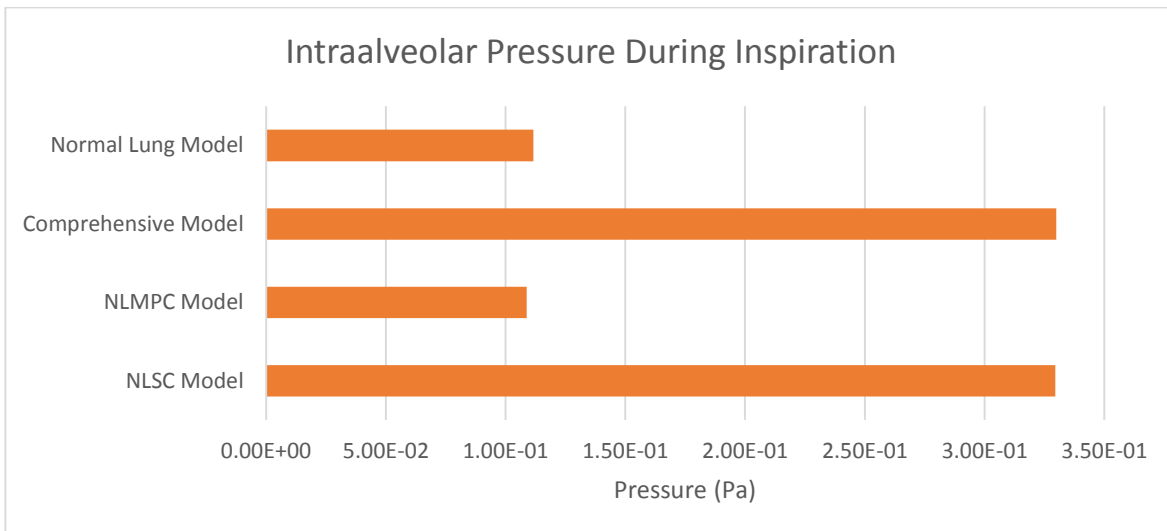


Figure 4.9 Comparison plot of intraalveolar pressure during inspiration for the normal, comprehensive, NLMPC and NLSC models.

In conclusion, a comprehensive analysis was performed to include components of age and disease. Results yielded fluid pressures that were just as high as in the NLSC model. Furthermore, stresses were higher in the comprehensive model than in the NLSC model.

Notwithstanding, the NLMPC model stresses still exceeded the comprehensive and NLSC model. Future work should include comparisons of various ages as well as decreases in inner radius to provide a better understanding of diverse levels of age and disease.



## **CHAPTER 5**

### **Conclusions and Future Work**

The objectives outlined within the thesis were investigated, studied, and concluded. In summary the (i) investigation of the damaging effects of forced air flow on a 3 dimensional idealized lung alveolar model, (ii) incorporation of structural and mechanical property changes to model disease and aging into the analysis to investigate these effects on the stress/strain environment, (iii) generation of a multi-scale modeling connection between the alveolar organ level models to the alveolar septal tissue model, and (iv) the performance of a comprehensive study that includes the effects of aging and disease were all accomplished in the preceding chapters.

#### **5.1. Lung Alveolar Analysis**

In the lung alveolar analysis several studies were carried out. These included an analysis of a normal healthy lung for which different ventilation conditions were implied (normal breathing and mechanical ventilation), normal lung with structural changes (NLSC) and normal lung with mechanical property changes (NLMPC). Results showed that the

ventilator waveform produces higher pressures of more than 26% and stresses that were 25% higher than in the normal breathing waveform. These results were in good agreement with the trends found in other similar studies. Analysis of the NLSC and NLMPC models revealed that the pressures in the NLSC model were 67% higher than in the NLMPC model. On the other hand, displacements as well as stresses in the NLMPC model were 98% and 80% higher, respectively. The NLSC model due to increase of wall thickness and reduction in radius induced stiffening of the tissue thus making the lungs less compliant. Conversely, in the NLMPC where elasticity decreases, lungs become more compliant while simultaneously increasing the expansion rate during inspiration. As a result, larger displacements and stresses are found within the NLMPC model. These findings emphasize the variation in fluid dynamics as well as solid mechanics when analyzing ventilation in disease and aging conditions. Furthermore, results show how mechanical ventilation may induce injurious stresses to healthy lungs as well as overinflate diseased lungs and create large deformations and stresses in aged lungs. Future work is needed to include extended run times for the simulations as well as the use of various ages and various decreases in inner radius.

## **5.2. Alveolar Tissue Analysis**

A structural analysis was performed on a heterogeneous model of alveolar tissue. Displacements from the NLMPC model during inspiration were applied as boundary conditions to the tissue model. Results showed that tissue displacements were higher during expiration as well as stresses. However, results did show that for various stresses the epithelial cell layer showed a larger distribution of higher stresses. It is concluded from

this study that the epithelial cell layer is the part of the tissue that bears the most stress and strain due to mechanical forces. Therefore, as the alveolar wall is loaded the epithelial cell layer exhibits the most damage and any cell signaling inflammation may be directed from this area of the tissue. Further experimental work needs to be done to validate the results discussed in this study. Experimental work will give indication as to whether or not cells within the epithelial cell layer experience greater stretch leading to greater mechanical forces.

### **5.3 Comprehensive Model Analysis**

It was important to understand how both conditions of disease and age impact the lungs simultaneously or collectively. As the first chapter gave insight into how each individual aspect impacted the lungs in tandem with mechanical ventilation, analyzing how both phenomena operate within the lung is equally or even more pertinent. The models for NLSC and NLMPC were simply combined into one model and an analysis was carried out under two breathing cycles using the ventilator waveform. Results yielded fluid velocities that were maximum near the inlet with a magnitude of 1.496 cm/sec. Pressures were found to be a maximum near the inlet with a maximum velocity of 0.33 Pa. During inspiratory flow, stresses are seen to be highest during this phase while expiratory flow encounters 40% less stress.

Furthermore, with comparisons between NLSC, NLMPC, normal, and comprehensive models findings show that the NLMPC stresses exceeded NLSC, normal and comprehensive studies by 80.25%, 5.0% and 73.4%, respectively. On the other hand,

alveolar pressures in the NLSC and comprehensive model vary only by 0.001%, hence, there is no significant difference. This leads to the conclusion that the inclusion of disease has a greater impact on the fluid dynamics whereas the inclusion of age has a greater impact on the tissue mechanics. Future work needs to be done to find comparable sources for the results yielded from this analysis coupled with multiple combinations of aging and disease parameters in the analysis model.

#### **5.4 Final Remarks**

Mechanical ventilation has been a staple for over a century with first use dating back to 1929 [92] with negative pressure ventilators that are no longer used in modern medicine. Today's ventilation standard includes positive pressure ventilation with modes such as PEEP being the most commonly used. There are several forms of positive pressure ventilation where volume cycled ventilation is the most common and investigated within this study. Much research was studied to grasp a better understanding of mechanical ventilation and its impacts on lung mechanical behavior. As a result of such high mortality rates in patients with ARDS and in elderly patients the need for reassessment will continue to be vital for its continued use. Mechanical ventilation accounts for a 34.5% in hospital mortality rate which equates to more deaths annually than breast and prostate cancer combined [86]. Furthermore, ventilation costs approximately \$27 billion dollars per year accounting for 12% of hospital costs [86]. Although ventilation particularly with PEEP has been an effective modality, the true costs of ventilation is found within the physiological derangements it causes [93]. Ventilator induced lung injury and its subcomponents (volutrauma, barotrauma, atlectrauma

and biotrauma) have all induced far more damage than originally presented. Mechanisms such as redistribution of alveolar ventilation, altered capillary perfusion, functional changes in surfactant etc. result in increased difficulty to ventilate lungs. Complications recently recognized in ventilation have been attributed to barotrauma and inflammation, moreover, prolonged ventilation is associated with lung injury, infection, and even MOSF [93]. Therefore the real costs of ventilation has always been higher than originally realized.

With ventilation having such high costs, all the more germane is research that seeks to shed light on the evaluation of physiological complications associated with mechanical ventilation. In chapter 1 the literature review covered a wide array of studies on the lungs in terms of computational fluid dynamics and solid mechanics. Of more importance are the studies that incorporate both of the aforementioned phenomena. The literature presents only very few studies that combine fluid dynamics and solid mechanics, particularly in FEA with fluid-structure interaction. Not to mention even less studies at the alveolar region with mechanical ventilation as an input to the model. This study comprises of under-explored areas of lung research including FSI analysis. However, future applications of this research may include a more physiologically correct model instead of an idealized model, applications of normal breathing waveforms to each analysis for comparison purposes and finally a whole lung model to incorporate mechanical forces from the organ level to the cellular level. Considering the grave impact that ventilation has on the lungs continued research must be done to further assess mechanical forces imposed on the lungs in order to quantitatively and qualitatively reveal lung injury induced via ventilation.

## **Literature Cited**

Literature Cited

- [1] Weibel, E.R. 1963. *Morphometry of the Human Lung*. Berlin, Springer Verlag.
- [2] Mader, S.S. 1995. *Human Biology*. Dubuque, IA: Wm. C. Brown Publishers
- [3] ICRP. 1994. *Human Respiratory Tract Model for Radiological Protection*. New York, Elsevier Science Ltd.
- [4] Ochas, M., Nyengaard, J.R., Jung, A., Knudsen L., Voigt, M., Wahlers, T., Richter, J., and Gundersen, H.J.G. 2004. "The Number of Alveoli in the Human Lung" *Am J of Respir and Crit Care Med* 169(1): 120-124.
- [5] Hyde, D.M., Tyler, N.K., Putney, L.F., Singh, P., and Gundersen, H.J.G. 2004. "Total Number and Mean Size of Alveoli in Mammalian Lung Estimated Using Fractionator Sampling and Unbiased Estimates of the Euler Characteristic of Alveolar Openings" *The Anatomical Record Part A* 274A: 216-226.
- [6] Haefeli-Bleuer, B., & Weibel, E. R. 1988. Morphometry of the human pulmonary acinus. *The Anatomical Record*, 220, 401–414.
- [7] Dailey, H.L., and Ghadiali, S.N., 2007, "Fluid-structure analysis of microparticle transport in deformable pulmonary alveoli". *J. Aerosol Science*. 38, 269-288.
- [8] U.S. Department of Health & Human Services. National Institute of Health 2012 Factbook Disease Statistics
- [9] James, M.M and Beilman, G.J. 2012 "Mechanical Ventilation" *Surgical Clinics of North America* 92 (6): 1463-1474
- [10] Slutsky, A.S., and Tremblay, L.N. 1998 "Multiple System Organ Failure Is Mechanical Ventilation a Contributing Factor?" *Am J Respir Crit Care Med* 157: 1721–1725.
- [11] American Thoracic Society 1999, "International Consensus Conferences in Intensive Care Medicine: Ventilator-associated Lung Injury in ARDS" *Am J Respir Crit Care Med* 160: 2118-2124.
- [12] Hurst, J.M., Branson, R.D., Davis, K., Barrette, R.R., and Adams, K.S. 1989. "Comparison of conventional mechanical ventilation and high frequency ventilation" *Annals of Surgery* 211(4): 486-491.
- [13] The HIFI Study Group. 1989. "High-frequency oscillatory ventilation compared with conventional mechanical ventilation in the treatment of respiratory failure in preterm infants" *N Engl J Med* 320: 88-93.

- [14] Slutsky, A.S. 1999. "Lung Injury caused by mechanical ventilation" *Chest* 116(1): 9-15
- [15] M. Klaas et al. (Eds), 2011. "Mechanostimulation and mechanics analysis of lung cells, lung tissue and the entire lung organ" *Fundamental Medical and Engineering Invest.* 116: pp 129 -154.
- [16] Weibel, E.R. 1973 "Morphological basis of the alveolar-capillary gas exchange" *Physiol Rev* 53: 419-495
- [17] Weibel, E.R. 1986 "Functional morphology of the lung parenchyma. In: *Handbook of Physiology. The Respiratory System. Mechanics of Breathing.* Bethesda, MD: Am. Physiol. Soc. 3(3): 89-111.
- [18] Weibel, E.R. 1989 "Lung Morphometry and models in respiratory physiology" In: *Respiratory Physiology: An Analytical Approach.* New York: Dekker 1 -55.
- [19] Weibel, E.R. 1996 "The Structural Basis of Lung Function" In: *Respiratory Physiology: People and Ideas* New York; Oxford Univ. Press, 3-46.
- [20] Horsfield, K., and Cumming, G. 1967. "Angles of branching and diameters of branches in the human bronchial tree" *The bulletin of mathematical biophysics* 29(2): 245-259.
- [21] Horsfield, K., and Cumming, G. 1968. "Morphology of the bronchial tree in man" *J. Appl. Physiol.* 24(3): 373-383.
- [22] Horsfield, K., Dart, G., et al. 1971. "Models of the human bronchial tree" *J. Appl. Physiol.* 31(2): 207-217.
- [23] Horsfield, K. 1990. "Diameters, generations, and order of branches in the bronchial tree" *J. Appl. Physiol.* 68(2): 457-261.
- [24] Hyatt, R.E., MD. and Fry, D.L., MD. 1960. "Pulmonary mechanics: A unified analysis of the relationship between pressure, volume and gasflow in the lungs of normal and diseased human subjects" *The American Journal of Medicine* 29(4): 672-689.
- [25] Hyatt, R.E., MD. and Wilcox, R.E. 1963. "The pressure-flow relationships of the intrathoracic airway in man" *Journal of Clinical Investigation* 42(1): 29-39.
- [26] Schroter, R.C., and Sudlow, M.F. 1969. "Flow patterns in models of the human bronchial airways" *Respiration Physiology* 7(3): 341-355.
- [27] Jaeger, M.J. and Matthys, H. 1968. "The pattern of flow in the upper human airways" *Respiration Physiology* 6(1): 113-127.
- [28] Pedley, T. J., Schroter, R. C. Sudlow, M. F. 1970a. "Energy losses and pressure drop in models of human airways". *Respir. Physiol.* 9: 371-86



- [29] Pedley, T. J., Schroter, R. C, Sudlow, M. F. 1970b. "The prediction of pressure drop and variation of resistance within the human bronchial airways". *Respir. Physiol.* 9: 387-405
- [30] Pedley, T. J., Schroter, R. C, Sudlow, M. F. 1971. "Flow and pressure drop in systems of repeatedly branching tubes". *J. Fluid Mech.* 46: 365-83
- [31] Pedley, T. J., Sudlow, M. F., Milic-Emili, J. 1972. "A non-linear theory of the distribution of pulmonary ventilation". *Respir. Physiol.* 15 : 1-38
- [32] Olson, D.E., Dart, G.E., and Filley, G.F. 1970. "Pressure drop and fluid flow regime of air inspired into the human lung" *J. Appl Physiol.* 28(4): 482-494
- [33] Olson, D.E., Sudlow, M.F., Horsfield, K., and Filley, G.F. 1973. "Convective patterns of flow during inspiration" *Arch Intern Med.* 131(1): 51-57
- [34] Pedley, T. J., Schroter, R. C, Sudlow, M. F. 1977. Gas flow and mixing in the airways. See West 1976, Chap. 2
- [35] Balásházy, I., Heistracher, T., and Hofmann, W. 1996. "Air flow and particle deposition patterns in bronchial airway bifurcations: the effect of different CFD models and bifurcation geometries" *Journal of Aerosol Medicine* 9(3): 287-301.
- [36] Wilquem, F., and Degrez, G. 1997. "Numerical modeling of steady inspiratory airflow through a three-generation model of the human central airways" *J. Biomech Eng.* 119(1): 59-65.
- [37] Liu, Y., So, R.M.C., and Zhang, C.H. 2002. "Modeling the bifurcating flow in a human lung airway" *Journal of Biomechanics* 35(4): 465-473.
- [38] Liu, Y., So, R.M.C., and Chang, C.H. 2003. "Modeling the bifurcating flow in an asymmetric human lung airway" *Journal of Biomechanics* 36(7): 951-959.
- [39] Ertbruggen, C.V., Hirsch, C., and Paiva, M. 2005. "Anatomically based three-dimensional model of airways to simulate flow and particle transport using computational fluid dynamics" *J. Appl Physiol* 98(3): 970-980.
- [40] Harrington, L., and Prisk, K., and Darquenne, C. 2006. "Importance of the bifurcation zone and branch orientation in simulated aerosol deposition in the alveolar zone of the human lung" *Journal of Aerosol Science* 37(1): pp 37-62.

- [41] Fung, Y-CB, Tong, P., and Patitucci, P. 1978. "Stress and strain in the lung" *Journal of the Engineering Mechanics Division, Proceedings for the American Society of Civil Engineers*, 100, EMI: 201-223.
- [42] Matthews, F.L., and West, J.B. 1972. "Finite element displacement analysis of a lung". *Journal of Biomechanics* 5(6):591-600
- [43] Dale, J.P., Matthews, F.L., and Schroter, C. 1980. "Finite element analysis of lung alveolus" *J. Biomechanics* 13: 865-873.
- [44] Kowe, R., Schroter, R.C., Matthews, F.L., and Hitchings, D. 1986. "Analysis of elastic and surface tension effects in lung alveolus using finite element methods" *J. Biomechanics* 19(7): 541-549
- [45] Karakaplan, A.D., Biekiek, M.P., and Skalak, R. 1980. "A mathematical model of lung parenchyma" *Journal of Biomechanical Engineering* 102: 124-136.
- [46] Harding Jr., E.M. and Robinson, R.J. 2010. "Flow in a terminal alveolar sac model with expanding walls using computational fluid dynamics" *Inhalation Toxicology* 22(8): 669-678.
- [47] Li, Z., and Kleinstreuer, C. 2011. "Airflow analysis in the alveolar region using the lattice-Boltzmann method" *Med Biol Eng Comput* 49: 441-451.
- [48] Denny E, Schroter R. 1995 "The mechanical behavior of a mammalian lung alveolar duct model." *J Biomech Eng* 117: 254 –261.
- [49] Gefen, A., Elad, D., and Shiner, R.J. 1999. "Analysis of stress distribution in the alveolar septa of normal and simulated emphysematic lungs" *Journal of Biomechanics* 32: 891-897.
- [50] Chaudhry, H.R., Bukiet, B., and Kirshblum S. 2004 "Analysis of stress and pressure in the human alveolar wall before bursting" *Journal of Mechanics in Medicine and Biology*. 4(2): pp 153-159.
- [51] de Ryk, J., and Thiesse, J., and Namati, E., and McLennan, G., 2007. "Stress Distribution in a three dimensional geometric alveolar sac under normal and emphysematous conditions" *International Journal of COPD*. 2(1): 81-91.

- [52] Rausch, S.M.K., and Martin, C., and Borneamann, P.B., and Uhlig, S., and Wall, W.A. 2011, "Material Model of lung parenchyma based on living precision-cut lung slice testing" *Journal of the Mechanical Behavior of Biomedical Materials*. 4:583-592.
- [53] Roan, E. and Waters, C.M., 2011, "What do we know about mechanical strain in lung alveoli?" *Am J Physiol Lung Cell Mol Physiol* 301: 625-635.
- [54] Rausch, S.M.K., and Haberthur, D., and Stampanoni, M., and Schittny, J.C., and Wall, W.A. 2011, "Local Strain Distribution in Real Three-Dimensional Alveolar Geometries" *Annals of Biomedical Engineering*. 39(11):2835-2843.
- [55] Tezduyar, Tayfun E., and Sunil Sathe. 2007. "Modeling of Fluid–structure Interactions with the Space–time Finite Elements: Solution Techniques." *International Journal for Numerical Methods in Fluids* 54(6-8): 855-900.
- [56] Sathe, Sunil, and Tayfun E. Tezduyar. 2008. "Modeling of Fluid–structure Interactions with the Space–time Finite Elements: Contact Problems." *Computational Mechanics* 43(1): 51-60.
- [57] Wiechert, L., Rabczuk, T., Comerford, A., Metzke1, R., and Wall, W.A. 2008. "Towards stresses and strains in the respiratory system" *ESAIM: Proceedings* (23): pp 98-113.
- [58] Wall, W.A. and Ranczuk, T. 2008 "Fluid-structure interaction in lower airways of CT-based lung geometries" *Int. J. Numer. Meth. Fluids* (57): pp 653-675
- [59] Wall, Wolfgang A., and Rabczuk, T. 2008 "Fluid–structure Interaction in Lower Airways of CT-based Lung Geometries." *International Journal for Numerical Methods in Fluids* 57(5):653-75.
- [60] Wall, W.A., Weichert, L., Comerford, A., and Rausch, S. 2010 "Towards a comprehensive computational model for the respiratory system" *Int. J. Numer. Meth. Biomed. Engng*, 26: pp 807-827.
- [61] Cullen, D.J., Ferrara, L.C., and Briggs, B.A. 1984, "Results, charges and benefits of intensive care for critically ill patients: Update 1983." *Crit Care Med* 12: 982-987.
- [62] Leaf A. 1977, "Medicine and the aged" *N Engl J Med* 297: 887-890.
- [63] McLean, R.F., McIntosh, J.D., and Kung, G.Y., 1985, "Outcome of respiratory intensive care for the elderly" *Crit Care Med* 13: 625-629.

- [64] Tran, D.D., Johan Groeneveld, A.B., Der Meulen, J.V., Nauta, Jos J.P., Strack Van, S., Rob, J.M, and Thus, L.G. 1990, "Age, chronic disease, sepsis, organ system failure, and mortality in a medical intensive care unit" *Crit Care Med* 18(5): 474-479.
- [65] Pesau M.D., B., Falger M.D., S., Berger M.D., E., Weimann M.N., J, Schuster, E., Leitner, C., and Frass M.D., M. 1992, "Influence of age on outcome of mechanically ventilated patients in an intensive care unit" *Crit Care Med* 20(4): 489-492.
- [66] McPhee, S.J., and Ganong, W.F. *Pathophysiology of Disease: An Introduction to Clinical Medicine*, 5<sup>th</sup> Edition. <http://www.accessmedicine.com>
- [67] Gattinoni, L. MD, and Protti, A., MD. 2008 "Ventilation in the prone position: For some but not for all?" *CMAJ* 178(9): 1174-1176
- [68] <http://www.nhlbi.nih.gov/health/health-topics/topics/vent/while.html>
- [69] ICRP, *Human Respiratory Tract Model for Radiological Protection*, Elsevier, New York, NY, USA, 1994.
- [70] Weibel, E.R., Sapoval, B., and Filoche, M. 2005. "Design of peripheral airways for efficient gas exchange" *Respiratory Physiology and Neurobiology* 148: pp 3-21.
- [71] Dammann, J.F, McAslan, T.C, and Maffeo, C.J. 1978 "Optimal flow pattern for mechanical ventilation of the lungs. 2. The effect of a sine versus square wave flow pattern with and without an end-inspiratory pause on patients" *Crit Care Med*. 6(5): 293-310.
- [72] Yang, S.C., MD, and Yang, S.P., MD. 2002 "Effects of Inspiratory Flow Waveforms on Lung Mechanics, Gas Exchange, and Respiratory Metabolism in COPD Patients during Mechanical Ventilation" *Chest* 122(6): 2096-2104.
- [73] Chelluri, L, Ah Im, K., Belle, S., Schulz, R., Rotondi, A.J., Donahoe, M.P., Sirio, S.A., Mendelsohn, A.B., and Pinsky, M.R. 2004. "Long term mortality and quality of life after prolonged mechanical ventilation" *Crit Care Med* 32(1): 61-69.
- [74] Lai-Fook, S.J. and Hyatt, R.E. 2000. "Effects of age on elastic moduli of human lungs" *J Appl Physiol* 89: 163-168

- [75] Ryan, S. F. 1969 "The structure of the interalveolar septum of the mammalian lung" *Anat. Rec.* 165:467-484
- [76] Gil, J. 2006 "Alveolar Wall Relations" *Annals of the New York Academy of Sciences.* 384(1): pp 31-43
- [77] J. Bastacky, C. Y. Lee, J. Goerke, H. Koushafar, D. Yager, L. Kenaga, T. P. Speed, Y. Chen and J. A. Clements, 1995, "Alveolar Lining layer is thin and continuous: low temperature scanning electron microscopy" *J Appl Physiol* 79: pp 1615-1628
- [78] Welling, L.W., and Zupka, M.T., and Welling D.J. 1995 "Mechanical Properties of basement membrane" *Physiology* 10: pp 30-35
- [79] Gefen, A., Elad, D. and Shiner, R.J. 1999 "Analysis of stress distribution in the alveolar septa of normal and simulated emphysematic lungs" *Journal of Biomechanics* 32: pp 891-897
- [80] Ionescu, C.M., and Segers, P., and Keyser, R.D. 2009 "Mechanical properties of the respiratory system derived from morphologic insight" *IEEE Transactions on Biomedical Engineering.* 56(4): pp 949-775
- [81] Deguchi, S., Fukamachi, H., Hashimoto, K., Iio, K., and Tsujioka, K. 2009 "Measurement and finite element modeling of the force balance in the vertical section of adhering vascular endothelial cells" *Journal of the Mechanical Behavior of Biomedical Materials* 2: 173-185.
- [82] Welling, L.W., Zupka, M.T., and Welling, D.J. 1995. "Mechanical Properties of basement Membrane" *Physiology* 10(1): 30-35
- [83] Candiello, J., Balasubramani, M., Schreiber, E.M., Cole, G.J., Mayer, U., Halfter, W., and Lin, H. 2007. "Biomechanical properties of native basement membranes" *FEBS Journal* 274(11): 2897-2908.
- [84] Dailey, H.L., Yalcin, H.C., and Ghadiali, S.N. 2007. "Fluid-structure modeling of flow induced alveolar epithelial cell deformation" *Computers and Structures* 85: 1066-1071.
- [85] Galle, J., Loeffler, M., and Drasdo, D. 2005 "Modeling the Effect of Deregulated Proliferation and Apoptosis on the Growth Dynamics of Epithelial Cell Populations in Vitro" *Biophysical Journal* 88: 62-75

[86] Wunsch, H., and Linde-Zwirble, W.T., Angus, D.C., Hartman, M.E., Milbrandt, E.B., and Kahn, J.M. 2010. "The epidemiology of mechanical ventilation use in the United States" *Crit Care Med* 38(10): 1947-1953.

[87] Kitaoka, H., Tamura, S., and Takaki, R. 2000. "A three-dimensional model of the human pulmonary acinus" *J Appl Physiol* 88: 2260-2268.

[88] <http://emedicine.medscape.com/article/304068-overview#aw2aab6b5>

[89] [http://droualb.faculty.mjc.edu/Course%20Materials/Physiology%20101/Chapter%20Notes/Fall%202011/chapter\\_16%20Fall%202011.htm](http://droualb.faculty.mjc.edu/Course%20Materials/Physiology%20101/Chapter%20Notes/Fall%202011/chapter_16%20Fall%202011.htm)

[90] Malvé, M., del Palomar, A. P., Trabelsi, O., López-Villalobos, J.L., Ginel, A., and Doblaré, M. 2011. "Modeling of the fluid structure interaction of a human trachea under different ventilation conditions" *International Communications in Heat and mass Transfer* 38: 10-15.

[91] Frank, N.R., Mead, J., and Ferris, Jr. B.G. 1957. "The mechanical behavior of the lungs in health elderly persons" *J Clin Invest* 36(12): 1680-1687.

[92] Byrd Jr., R.P. (2013, November 27). *Mechanical Ventilation*. Retrieved from <http://emedicine.medscape.com/article/304068-overview#showall> on April 22, 2014.

[93] Soni, N., and Williams, P. 2008. "Positive pressure ventilation: what is the real cost?" *British Journal of Anaesthesia* 101(4): 446-457.

[94] Pump, K.K. 1969. "Morphology of the Acinus of the Human Lung" *Chest*. 56(2): 126-134.

VITA**TRENICKA K. ROLLE**

**Permanent Address:** 60 Coral Reef Estate, Freeport, Bahamas

**Current Address:** 1304 Grove Avenue, Richmond VA 23220

**Date of Birth:** July 1<sup>st</sup>, 1989

**Citizenship:** The Bahamas

**Email:** trenicka.rolle@gmail.com

---

**EDUCATION***Virginia Commonwealth University, Richmond, Virginia*

- **Master of Science: Mechanical and Nuclear Engineering**  
Concentration: Computational Biological Modeling and Analysis  
Thesis: Lung Alveolar and Tissue Analysis under Mechanical Ventilation  
Expected Graduation Date: May 2014  
Cumulative GPA: 3.37
- **Bachelor of Science in Biomedical Engineering, May 2011**  
Minors: Mathematics and Physics  
Cumulative GPA: 3.21

**PUBLICATIONS/PRESENTATIONS**

- Rolle, Trenicka and Pidaparti, R.M., 2011, "A Study of Tissue Strains Induced in Airways Due to Mechanical Ventilation" Proceedings of the ASME Early Career Technical Conference 10: pp 136-141
- Rolle, Trenicka and Pidaparti, R.M., 2012, "Fluid Dynamic Analysis of Lung Alveoli Under Mechanical Ventilation" Proceedings of the ASME Early Career Technical Conference Proceedings 11: pp 18-23

- “A Study of the Fluid-Structure Interaction in Lung Alveoli under Mechanical Ventilation” presented at the VCU School of Engineering Research Symposium on February 18, 2014, Richmond, Virginia.
- “A Study of Lung Alveolar and Tissue Analysis under Mechanical Ventilation” presented at the National Society of Black Engineers National Convention, Graduate Tech Talk: Engineering for Medical Discovery on March 29, 2014, Nashville, Tennessee.

## **AWARDS**

- Dean’s List - 2009, 2010, 2011
- VCU Graduate Research Assistantship Fellowship 2012-2013, Fall 2013
- National Society of Black Engineers Region II Academic Excellence Scholarship (NSBE)
- Bahamas National Academic Scholarship – 2013

## **LEADERSHIP**

***ReJOYce in Jesus Campus Fellowship***, Positions Held:  
President 2013-2014

***National Society of Black Engineers (NSBE)*** Positions Held:  
Chapter President 2012-2013 ; Finance Chair 2011-2012 ; Vice President 2010-2011 ; PCI Chair 2009-2010

- Raised membership of the chapter by more than 30% as well as a 32% increase of participation at the annual convention
- Increased community service hours within the chapter with a total of 76 hours for the entire school year
- Hosted one of NSBE’s biggest community service programs called A Walk for Education, for the first time in 3 years
- Obtained approximately \$9000 in sponsorship for the entire year a 200% increase from the year prior.

***Student Government Association***, Positions Held:  
Senator 2010-2011

- Served as member on the appropriations committee and assisted in the management of \$60,000 allocated for student organization budgets and spending
- Voted on bill to remove landline phones in freshmen dorms that helped the university student housing to save tens of thousands of dollars per year
- Helped to establish the first VCU Qatar day that brought students from VCU’s international campus to visit the U.S.



**MENTORSHIP**

- National Society of Black Engineers (NSBE), VCU Chapter 2013-2014
- Society of Women Engineers (SWE), VCU Chapter 2013-2014
- Baker Elementary School, Henrico, Virginia : Jan – May, 2013

**COMMUNITY SERVICE**

Richmond Technical Center - 2014

Engineering Ingenuity Day at the Science Museum of Virginia - 2013

Math Tutoring at Baker Elementary School - 2013

Paint the Town Green – 2011